Diss. ETH No. 13967

Reconstruction and Analysis of Mesoscale Precipitation in the Alps for the 20th Century

A dissertation submitted to the
SWISS FEDERAL INSTITUTE OF TECHNOLOGY (ETH)
ZÜRICH

for the degree of
DOCTOR OF NATURAL SCIENCE

presented by
JÜRG SCHMIDLI
Dipl. Natw. ETH
born 13 December 1971
citizen of Zürich (ZH)

accepted on the recommendation of
Prof. Dr. C. Schär, examiner
Prof. Dr. P. Jones, co-examiner
Prof. Dr. H. Davies co-examiner
Dr. C. Frei, co-examiner

2000

Preface

Alpine precipitation is undergoing strong interannual and inter-decadal variations. The importance of such variations for the inhabitants of the Alpine region has been painfully demonstrated during the recent years: in the winter 1998/99, above normal snowfall led to dramatic avalanche conditions in much of the Alpine region, with more than 100'000 inhabitants and tourists being cut off from the Alpine foreland for several weeks. In May 1999, the associated snowmelt and additional heavy precipitation events caused flooding in many Swiss, Austrian and German catchments, among them the Thur and the Aare. Finally, in October 2000, a long-lasting episode of precipitation on the southern flanks of the Alps was responsible for one of the worst Alpine flooding events of this century, with partly devastating damage in the Ticino, Valais and Piedmont regions.

From a scientific point of view, these events demonstrate the importance of an appropriate analysis of precipitation variability over a time span which is sufficient to cover the variations on interannual, interdecadal and longer-term time scales. In the past, investigations of this type were difficult or even impossible due to the lack of coverage with homogenized long-term precipitation records. This context provides the prime motivation for the Ph. D. thesis of Jürg Schmidli. In his thesis, which was successfully defended last December, a century-scale reanalysis of Alpine precipitation variability is undertaken. Monthly precipitation fields in the period 1901-1990 are reconstructed from two sources of data: a dense data set of short-term precipitation records covering the last decades, and a sparse data set of long-term homogenized records covering the last century. The derived monthly precipitation maps are analysed using modern statistical tools. Even in regions with little or no coverage, the results are shown to be of sufficient reliability. As a key result, the study corroborates the presence of substantial secular precipitation trends in the Alpine region. Indeed, it is of great interest to note that the precipitation trends of the last century are substantially stronger than the precipitation changes anticipated for the future! For illustration, about 10 years ago, climate change scenarios were conducted within the Swiss National Research Programme NFP31, stipulating a winter precipitation increase of 10% (to occur within the next 100 years). Jürg Schmidli's trend analysis shows that this level of change has already been exceeded within the past 100 years (up to 30% increase since 1900).

The study was funded by the Swiss National Science Foundation in the form of a collaborative project between ETH Zürich and the University of Berne. A key element provided by the Ph. D. thesis of Christoph Schmutz from the University of Berne were the carefully compiled and scrutinized long-term homogenized precipitation records. It is a pleasure for us to continue this collaboration under the umbrella of the newly established NCCR Climate.

Christoph Schär, April 2001

Acknowledgements

Abstract

Precipitation is a key-element of the hydrological cycle and one of the most important parameters in the event of global climate change, particularly in regions of complex topography such as the Alps. Changes in its frequency, intensity and distribution could have wide-reaching consequences for the Alpine ecosystems and societies. Therefore, an accurate description of the present and past Alpine precipitation climate and its interannual and interdecadal variability is highly desirable. So far, the investigation of these issues has been restricted by the limited spatial resolution and/or areal extent of the datasets available over a centennial time scale. The aim of this thesis is to develop a method for precipitation reconstruction which makes optimal use of the available data, and to provide a mesoscale analysis of precipitation variability for the 20th century, covering the entire Alpine region.

The reconstruction is conducted with mesoscale gridded analyses as the predictor (resolution 25 km, ~1000 grid points, monthly resolution, available 1971–90) and sparse samples of long-term station records as the predictands (25–150 stations). Sensitivity experiments are undertaken to define the statistical setup, assess the data requirements, and describe the error statistics. The reconstruction method of reduced-space optimal interpolation is employed. It combines data reduction by truncation to the leading empirical orthogonal functions (EOFs), and a subsequent least-squares optimal estimation of the temporal evolution of the respective EOF coefficients. In addition, a covariance-guided station selection procedure which exploits the observed space-time variability is proposed for deriving "representative" station samples for the reconstruction.

In the first part of the thesis, the feasibility of a statistical reconstruction of mesoscale monthly precipitation from sparse observations in a mountainous area such as the Alps is examined. Using a "representative" test sample of 53 stations, the reconstructions account for about three quarters of the total variance in the mesoscale gridded analyses, and reproduce with good accuracy the pattern and amplitude of multi-year anomalies. For individual months, the reconstructed precipitation patterns closely resemble the observed patterns, and the skill depends primarily on the representation of that month in the reduced data space spanned by the leading EOFs. Examination of subdomain-mean time series demonstrate the superior performance of the present method in comparison to spatial analyses using the coarse station network only. In a series of sensitivity experiments, the spatial distribution of the sparse observations is identified as a critical factor for the reconstruction skill. The experiments show that the "representative" test sample exhibits superior performance compared to randomly distributed samples of the same size.

In the second part, an Alpine-wide dataset of mesoscale monthly precipitation fields is produced using a sparse set of 140 long-term records. The reconstruction extends over the period 1901–90 and encompasses the entire Alpine mountain range and adjacent foreland

areas with a nominal resolution of 25 km, thus resolving the rich mesoscale structure in the area. The reconstruction model is calibrated over the subperiod 1971–90. Special emphasis is given to the temporal homogeneity of the dataset in that the sparse set constists of a constant number of quality-controlled, homogenized records. Cross validation with independent data shows that the reconstructions are of good quality for the major part of the Alpine mountain range.

Subsequently, mesoscale Alpine precipitation during the 20th century, its variability, its trends, and its relation to the North Atlantic Oscillation (NAO) are examined. Several (at the 10% level) statistically significant linear trends are detected. For the period 1901–90, these include an increase of wintertime precipitation by 20–30% per 100 years in the western part of the Alps, and a decrease of autumn precipitation by 20–40% to the south of the Alpine ridge. For the period 1961–90, significant trends are observed also for the spring season, including a precipitation increase of 30% per 30 years in the Ticino region. Investigation of the correlation of the NAO and wintertime Alpine precipitation revealed weak and highly intermittent correlations for the region north of the Alpine ridge, and stronger and more robust correlations for the regions to the south.

The new dataset should be of particular interest for applications such as the evaluation and improvement of climate models, the calibration and validation of statistical downscaling techniques over extended periods, and the investigation of the regional impacts of anticipated climate change. Also, a more detailed analysis of the longer-term precipitation variations and their relation to the large-scale forcings (e.g. the synoptic-scale atmospheric circulation and the sea-surface temperature of the Atlantic and Mediterranean oceans) could serve to improve our understanding of the physical processes which led to the observed 20th century precipitation changes.

Zusammenfassung

Der Niederschlag ist ein Schlüsselelement des Wasserkreislaufes und daher ein wichtiger Faktor im Falle eines globalen Klimawandels. Eine Änderung der Niederschlagshäufigkeit, -intensität und -verteilung könnte für die Alpinen Ökosysteme und Gesellschaften weitreichende Folgen haben. Darum ist eine genaue Beschreibung des heutigen und vergangenen Alpinen Niederschlagsklimas und deren Variabilität höchst wünschenswert. Gegenwärtig ist die Erkundung dieser Fragen nur begrenzt möglich, aufgrund der geringen räumlichen Auflösung und/oder Abdeckung der für das ganze 20. Jahrhundert verfügbaren Datensätze. Das Ziel der vorliegenden Arbeit ist einerseits die Entwicklung einer Methode zur Rekonstruktion von mesoskaligen Niederschlagsfeldern, und andererseits die Analyse der regionalen Niederschlagsvariabilität im Alpenraum während des 20. Jahrhunderts.

Die Niederschlagsrekonstruktion basiert auf einer statistischen Kombination von mesoskaligen Analysen (Gitterweite 25 km, ~1000 Gitterpunkte) und einer geringen Anzahl von langen Niederschlagszeitreihen (25–150 Stationen). Die statistische Rekonstruktion beinhaltet eine Hauptkomponentenanalyse zur Datenreduktion und eine anschliessende Schätzung der Entwicklungskoeffizienten der Hauptkomponenten mittels der Methode der kleinsten Fehlerquadrate. Eine Reihe von Sensitivitätsanalysen wurden durchgeführt, um die Details des statistischen Modells festzulegen, und um die Fehler des Modells und die Anforderungen an die Daten abzuschätzen. Zusätzlich wird eine Methode zur Bestimmung von "repräsentativen" Stationsverteilungen, basierend auf der Kovarianzstruktur der mesoskaligen Analysen, vorgestellt.

Im ersten Teil der Arbeit wird die Machbarkeit einer Rekonstruktion von mesoskaligen Niederschlagsfeldern mittels einer geringen Anzahl von langen Zeitreihen untersucht. Die Referenzrekonstruktion, welche auf nur 53 "repräsentativen" Stationen beruht, erklärt etwa 75% der totalen Varianz in den mesoskaligen Analysen und gibt mit guter Genauigkeit die räumlichen Muster und Amplituden von mehrjährigen Niederschlagsanomalien wieder. Auch die Niederschlagsmuster einzelner Monate werden generell gut rekonstruiert. Die Güte für einen bestimmten Monat wird dabei hauptsächlich durch die Repräsentation des Monats im reduzierten Phasenraum, der durch die Hauptkomponenten aufgespannt wird, bestimmt. Eine Analyse von Gebietsmitteln illustriert den Vorteil der neuen Methode im Vergleich zu Niederschlagsanalysen die nur auf den spärlichen Langzeitreihen beruhen. In einer Reihe weiterer Sensitivitätsstudien wurde die räumliche Verteilung der Stationen als ein kritischer Faktor identifiziert.

Im zweiten Teil wird ein Alpiner Datensatz von monatlichen, mesoskaligen Niederschlagsfeldern produziert. Die Rekonstruktion wird auf einem 25 km Gitter für die Jahre 1901–90 durchgefüht und deckt den gesamten Alpenraum und die angrenzende Gebiete ab. Die Kalibrierung der statistischen Beziehungen erfolgt über den Zeitraum 1971–90. Um eine möglichst gute Homogenität des Datensatzes sicherzustellen, besteht das Rekonstruktion-

ssample aus einer konstanten Anzahl von qualitätsgeprüften und homogenisierten Niederschlagsreihen (140 Stück). Die Validierung mit unabhängigen Daten bestätigt die gute Qualität der rekonstruierten Felder für den grössten Teil der Alpen.

Anschliessend wird die Variabilität des Alpinen Niederschlags im 20. Jahrhundert, Niederschlagstrends und die Relation zur Nordatlantischen Oszillation untersucht. Es werden mehrere statistisch signifikante (P-Wert 10%) Trends festgestellt. Diese beinhalten insbesondere eine Zunahme der Winterniederschläge um 20–30% in 100 Jahren in den westlichen und nord-westlichen Teilen des Alpenbogens und eine Abnahme der Herbstniederschläge um 20–40% südlich des Alpenhauptkamms. Für den Zeitraum von 1961–90 werden auch im Frühjahr signifikante Trends gefunden, unter anderem eine Niederschlagszunahme von 30% in 30 Jahren im Tessin und den angrenzenden Gebieten. Eine Analyse der Korrelationen zwischen den Alpinen Niederschlagszeitreihen und der Nordatlantischen Oszillation ergab zeitlich stark fluktuierende Korrelationen für die Gebiete nördlich des Alpenhauptkamms, aber ungefähr konstante Korrelationen für die Gebiete südlich der Alpen.

Der neue Datensatz könnte eingesetzt werden zur Evaluation und Verbesserung von Klimamodellen, zur Kalibration und Validierung von statistischen Downscaling-Methoden über längere Zeitperioden, und zur Untersuchung der regionalen Folgen möglicher Klimaänderungen. Ferner könnte eine detailierte Analyse der längerfristigen Niederschlagsänderungen und deren Abhängigkeit vom grossskaligen Antrieb (z.B. der grossskaligen atmosphärischen Zirkulation und der Meeresoberflächentemperatur des Atlantiks und des Mittelmeeres) das Verständnis der physikalischen Prozesse, welche die beobachteten Niederschlagsänderungen verursacht haben, verbessern.

Contents

1 Introduction

The climate in the Alpine region is characterized by large variability both in space and time. At the short-term (day-to-day) end of the spectrum, the variability is associated with the passage of synoptic-scale weather systems and attendant orographic circulations. The longer-term variations are related to changes in the sea-surface temperature of the Atlantic and Mediterranean, to changes of continental-scale circulation and teleconnection patterns, and in general to variations of the global climate system due to natural internal variability or external forcings (variations of solar radiation, volcanic activity, greenhouse gase concentrations).

The interest in the description and understanding of the longer-term (decadal to centennial) variations of the Alpine climate has further increased in the light of anticipated global climate change. According to climate change scenarios of the anthropogenic greenhouse and aerosol effects, the currently observed global warming rate of 0.1°K per decade could accelerate during the 21st century (Houghton et al., 1996). It is expected that the global warming will be accompanied by changes in the planetary-scale flow patterns, in the thermodynamic structure of the atmosphere, in the energy fluxes at the surface, and in the water cycle. The Alpine region is particularly sensitive to these changes due to the potential for regionally enhanced effects. The close adaptation of the ecosystems, agriculture, and tourism to the current climatic conditions makes the region also particularly vulnerable. Thus the assessment of the potential threat to the Alpine region by climate change is highly desirable.

A basic tool for assessing the regional effects, and a prerequisite for local impact studies, are regional climate change scenarios. Several approaches have been pursued to derive such regional scenarios from larger-scale information which usually comes form coupled atmosphere-ocean general circulation models. These "downscaling" techniques employ either statistically derived relationships (e.g. Cubasch et al., 1996; Gyalistras et al., 1994; Wilby et al., 1998; Zorita and von Storch, 1999) or regional climate simulations (e.g. Lüthi et al., 1996; McGregor, 1997; Mearns et al., 1999). However, the predictions of regional climate are uncertain, due to uncertainties in the emission scenarios, in the general circulation models (GCMs), and in the downscaling techniques (Houghton et al., 1996). Thus there is a pressing need to validate and improve the downscaling techniques in order to better understand the underlying physical processes. For this, detailed climatological data is required. However, the available datasets are often not in a gridded format, too coarse to adequately resolve the regional features, or too short for adequate calibration of the longer-term variations.

One of the most important climatological parameters is precipitation. It is a key-element of the hydrological cycle and thus of central importance for the Alpine ecosystems and civilizations: Water erosion has formed our landscape, the availability of precipita-

tion and soil-moisture governs the distribution of vegetation and agriculture, runoff from precipitation and snow-melt provides freshwater resources for large areas, and heavy precipitation events are responsible for a range of natural disasters such as flash floods, landslides, avalanches, and hail damage. Neither, the causes which determine the longer-term variations of the Alpine precipitation climate, nor even its current climatic state are accurately known. A major reason for this limited understanding is the lack of comprehensive precipitation data — with sufficient spatial resolution to resolve the major subridge precipitation patterns, with sufficient temporal coverage to portray decadal to centennial variations, with sufficient areal coverage to provide a unified view for the entire Alpine region.

A geographically differentiated precipitation analysis covering the whole Alpine region with monthly resolution, and its annual to multidecadal variations during the 20th century, will form the centerpiece of this thesis. As a background to the research issues addressed in this study, selected aspects of the Alpine precipitation climate, precipitation measurement, analysis, and reconstruction are discussed in the following sections. The introduction is concluded by a presentation of the aims of the present study.

1.1   Alpine precipitation

The precipitation distribution in Europe is to a high degree governed by the moisture transport from the Atlantic Ocean by the westerlies. Thus on the continental scale, mean annual precipitation decreases from the north west to the south east, from over 1000 mm along the western coast of the continent and of the British Isles (note the maxima of more than 2200 mm in north-western Scotland) to less than 600 mm in parts of eastern and south-eastern Europe and most of Spain (Fig. 1.1). This precipitation decrease is associated with a transition from maritime to continental climates, and from subarctic to semi-arid and subtropical climates. The Alpine mountain range is located within this transition zone and is characterized by a pronounced regional precipitation surplus much of which is caused by summertime convection. In the coarse resolution of Fig. 1.1, this surplus consists of a single precipitation maxima of more than 2000 mm. In reality, however, the precipitation distribution in the Alpine region is much more complex. The following more detailed discussion is partly based upon Schär et al. (1998).

On the interannual to multidecadal time scales, the variability in the Alpine region and in western Europe is related to changes of continental-scale circulation patterns and the natural variability of the global climate system (cf. Wanner et al., 1997; Schär et al., 1998). A substantial fraction of this variability is associated with the North Atlantic Oscillation (e.g. Hurrell, 1995; Hurrell and van Loon, 1997; Bresch and Davies, 2000). The NAO relates to changes in the strength and location of the Icelandic Low and the Azores High on interannual and multidecadal time scales (Rogers, 1984). Its north-south dipolar anomaly signal is present in the sea surface pressure in all seasons, but it is most pronounced during the winter (Glowienka-Hense, 1990). The NAO modifies the European climate by shifts of the Atlantic storm track (Rogers, 1997), and it is linked to changes in precipitation patterns in western and central Europe (Hurrell and van Loon, 1997; Wanner et al., 1997), see Fig. 1.2. Further factors which may potentially influence the Alpine climate include the Quasi-Biennial Oscillation (QBO), the El Niño/Southern Oscillation (ENSO), and the Pacific North American (PNA) pattern (Wanner et al., 1997).
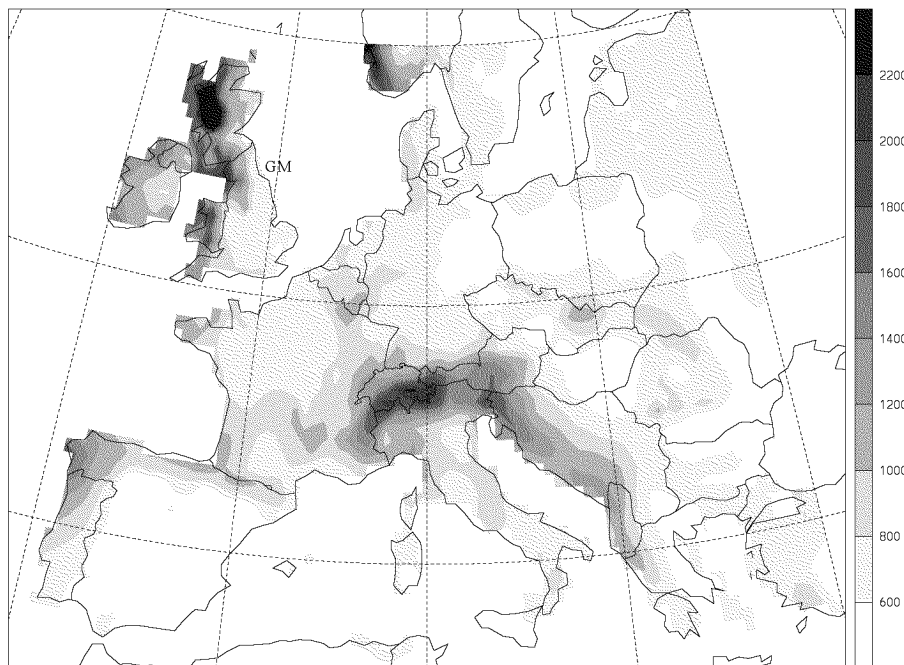
FIG. 1.1: Mean annual precipitation [mm] in Europe for the 1961–90 period (from New et al. 1999, 2000).

On the shorter time scales, much of the variability is related to the passage of synoptic weather systems and associated orographic effects. Even for the analysis of the longer-term variations, it is important to consider these orographic processes and their variability, since they act directly on the time scale of the underlying physical processes. In the Alps, these processes include the interaction of cyclones and frontal systems with the topography (cf. Egger and Hoinka, 1992; Schneidereit and Schär, 2000), the formation of lee cyclones (Tibaldi et al., 1990; Aebischer and Schär, 1998), the modification and lifting of ambient airflow by the Alpine topography (e.g. Foehn, Mistral, Bora, gap flow), the triggering of convection (Cacciamani et al., 1995; Huntrieser, 1995), and cloud-dynamic processes such as the seeder-feeder mechanism (Browning, 1985). A description of prototypes of many orographic precipitation mechanisms is given in Smith (1979). Together these interactions contribute to the high spatial and temporal variability of precipitation in the Alpine region. The basic characteristics of the long-term mean and its seasonal variation have been documented by Fliri (1974) and Frei and Schär (1998). A more recent climatology by Schwarb (2000) is portrayed in Fig. 1.3.

On the scale of the entire mountain range, the main features of the mean annual precipitation distribution are two high-precipitation bands extending along the northern and southern Alpine rim, and drier conditions in the interior of the mountain range and over the adjacent flatland. The maximum along the southern rim is diveded into two major wet zones: the one centered over southern Switzerland and northern Italy, the other over eastern Italy and Slovenia. Several smaller-scale maxima are associated with the hill ranges remote from the main ridge. On the scale of individual valleys and ridges, the driest spots are located in the Aosta valley with mean annual values below 550 mm, in the Venosta valley and the Valais with values around 600 mm, and in the dry northern

FIG. 1.2: Changes in precipitation [mm day^{-1}] corresponding to a unit deviation of the
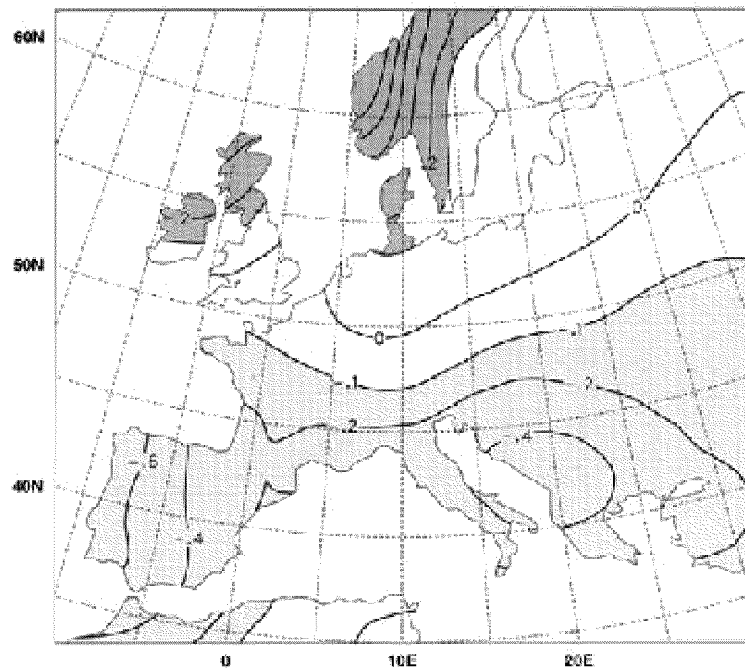NAO index computed over the winters (December–March) from 1900 through 1994 (from
Hurrell and van Loon, 1997).
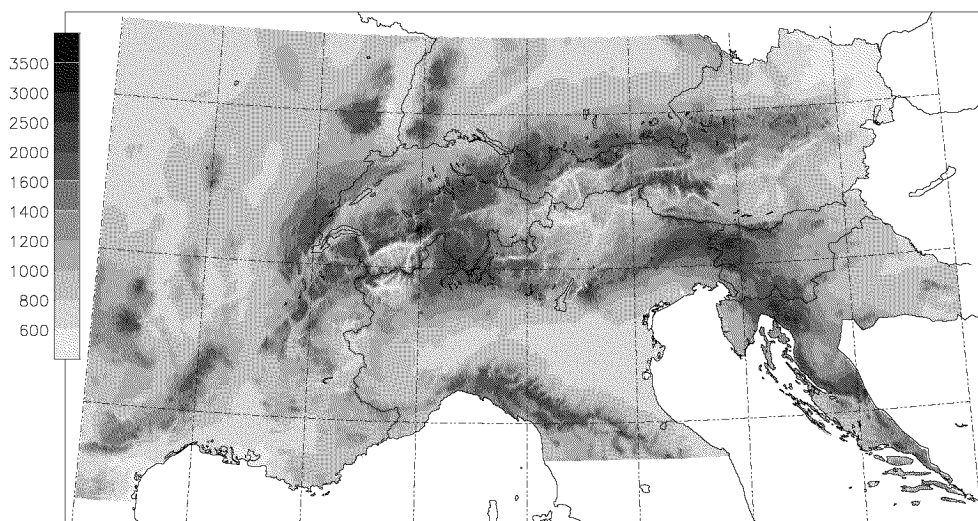
FIG. 1.3: Mean annual precipitation [mm] in the Alpine region for the 1971–90 period
(from Schwarb, 2000). The map is based on normals from over 6000 rain gauge stations
analyzed onto a 2 km grid using PRISM (Daly et al., 1994).
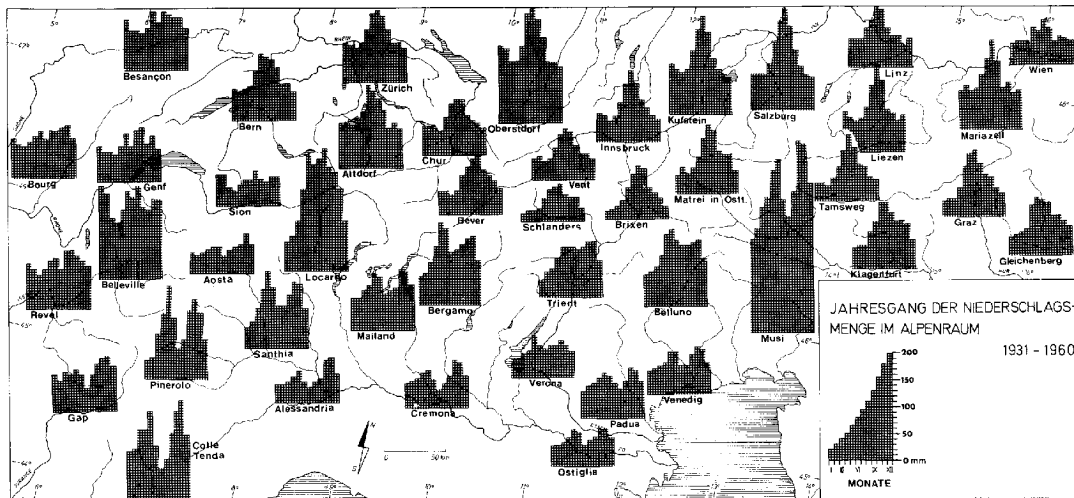
FIG. 1.4: Mean monthly precipitation in the years 1931–1960 at selected sites (from Fliri 1974).

valleys of the Grisons and north Tirol. In the northern wet zone annual means exceed 2000 mm at several locations, in the southern wet zone in the Friuli region precipitation values reach 3000 mm at a few spots, and 2500 mm is observed in the Centovalli in Ticino. Note that the variations in mean annual precipitation in the Alpine region span the range of the values encountered across entire Europe.

The annual cycle and its spatial variability is indicated in Fig. 1.4. In the northeastern Alps there is one maximum in summer related to thermally induced convection, while in the northern and north-western Alps there is a second, weaker maximum in winter related to a southward shift of the Atlantic storm track. In the southern regions two maxima arise in spring and autumn due to a higher frequency of days with a southerly flow component. Further information on the annual cycle can be found in Frei and Schär (1998). Clearly the dominant precipitation-producing processes vary from region to region and from season to season. Therefore, analyses of the Alpine precipitation climate and its long-term variability should be carried out on a seasonal basis and with sufficient spatial resolution.

Long-term precipitation variability with respect to the occurrence of trends has been analyzed by many authors for parts of the Alpine region. For instance, Widmann and Schär (1997) found a 30% increase in winter precipitation for western Switzerland during the 20th century; Buffoni et al. (1999) describe a decreasing trend in autumn precipitation for northern Italy during the period 1833–1996; and Auer and Böhm (1994), based on the last 150 years (1846–1991), observe an increase of wet conditions for the western parts of Austria, and a decrease for the eastern parts. These regional studies differ in the extent and density of the station data base, in the homogeneity standards, and in the analysis procedures (e.g. station-based versus area-mean trends), and the results are therefore difficult to compare. A trend analysis covering all of Europe is provided by Schönwiese and Rapp (1997) in their climate trend atlas of Europe. In the Alpine region, they observe some weakly significant precipitation trends. These include, for the centennial period 1891–1990, an increase of winter precipitation over the whole Alpine region with trends up to 20% per 100 years, and decrease by a similar amount in autumn. However,

the spatial resolution of their analysis is not sufficient to distinguish between the main Alpine precipitation climates. Hence a uniform and regionally differentiated analysis of long-term precipitation trends covering the entire Alpine region is currently not available.

In summary, our knowledge of long-term precipitation variations in the Alpine region, their regional characteristics, and their relation to the larger-scale circulation patterns is limited by the lack of comprehensive precipitation data. An improvement of our understanding of these issues requires long time series of gridded mesoscale precipitation analyses.

1.2   Derivation of precipitation analyses

Here we review important aspects related to the derivation of gridded precipitation analyses from a network of irregularly distributed rain gauge stations. Biases related to precipitation measurement are summarized, followed by some comments on spatial analysis and reconstruction of precipitation data, and by a short description of the gridded analyses available for the Alpine region.

Precipitation measurement

Measuring precipitation can be quite difficult due to biases associated with the gauge measurement process, inhomogeneities in the precipitation time series, and insufficient spatial coverage. All three of these problems are critical to obtaining accurate estimates of precipitation variability and temporal trends (Groisman and Legates, 1995).

The main sources of systematic biases of the gauge measurement can be attributed to the effect of the wind (deviation of precipitation particle trajectories due to wind field deformation around the gauge), wetting losses on the inner walls, and the evaporation of water accumulated in the gauge (Groisman and Legates, 1994). All these biases lead to a systematic undercatch of precipitation. For the most important component, the wind-induced error, the undercatch for monthly totals in the Alpine region (Switzerland) is on average 3–10% for rain and 10–50% for snow (e.g. Sevruk, 1985). According to Legates (1987) the wind-induced error accounts for a negative bias in the annually-averaged, global precipitation of about eight percent. Since precipitation gauges vary in size, shape and design as well as in the elevation above ground level, the effect of the wind is gauge-dependent (e.g. Nespor and Sevruk, 1999). This has significant implications for climate studies as gauge designs have been changed in many countries throughout the 20th century (e.g. Switzerland partly changed to automatic gauges in the 1980's, Gutermann 1986).

Inhomogeneities in the precipitation time series occur either as a gradual trend, or as an abrupt discontinuity (jump) in the time series. Discontinuities may occur for a number of reasons such as changes in instrumentation and recording practices, siting characteristics (e.g. location of surrounding buildings), and station relocations. For example, the decrease of the height above ground of the standard gauge for the national precipitation networks in both the Netherlands and China led to an apparent increase in the actual precipitation, since, due to the reduced height, the wind-induced error was reduced (Groisman and Legates, 1995). On the other hand, trend inhomogeneities may occur for reasons such as the slow growth of vegetation around the gauge, urbanization, or as result of a (real) trend in another climate variable such as temperature or wind speed. Various methods
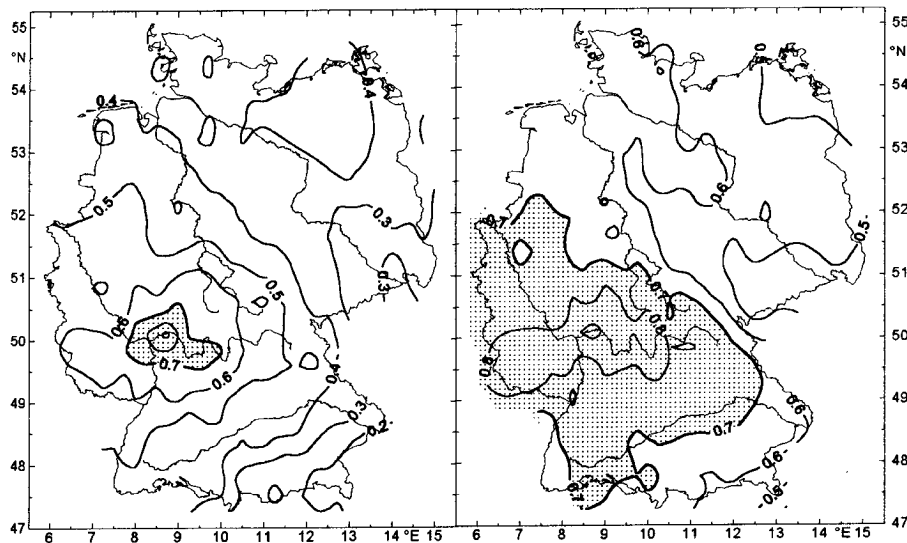
FIG. 1.5: Spatial correlation of (a) summer and (b) winter precipitation in Germany relative to the reference station Frankfurt (from Schönwiese and Rapp, 1997).

have been developed to detect and correct these inhomogeneities, a review is given in Peterson and et al. (1998).

Insufficient spatial coverage is related to the large spatial variability of precipitation which limits the spatial representativity of a single gauge measurement. For a single storm, two identical gauges located 100 meters apart may differ by a factor of two in total precipitation (Golubev, 1975). For monthly precipitation, the situation is less dramatic. Correlation distances (the e-folding distance for the correlation between two time series) vary from several hundred kilometers over level terrain to only a few 10 km in mountainous terrain (Huff and Shipp, 1969; Gandin et al., 1976; Groisman and Legates, 1994). Also, the correlations may vary strongly depending on the season. In central Europe, for instance, the summertime correlation distances are substantially smaller than the corresponding wintertime correlations (cf. Fig. 1.5), due to the more convective nature of the summer precipitation. As a result, if we want to draw conclusions that are indeed representative for the precipitation climate of a region (regions, continent, or the globe), a much denser network is required than for surface temperature or sea-level pressure.

Spatial analysis

The limited spatial representativity of a gauge measurement has also important implications for the analysis of irregularly distributed station data onto a regular grid. To achieve the same accuracy of the analyzed data in level and mountainous terrain, the latter has to be covered by a much denser station network. In other words, a significant correlation of the time series of neighbouring stations is an important prerequisite for the analysis. For accurate results, traditional analysis schemes such as kriging (Matheron, 1971) or inverse-distance weighting (Shepard, 1984; Willmott et al., 1985) not only require sufficiently high station-station correlations, but also that the field varies smoothly on the scale of the typical interstation distance. If the interstation distance is larger, other methods which use additional sources of information may provide more accurate results. For example, the inclusion of a digital elevation model as a covariate has been shown to be

beneficial for the analysis of precipitation in mountainous terrain (e.g. Kirchhofer, 1993; Daly et al., 1994; Schwarb, 2000). Another source of information are spatially detailed observations from a short time period.

The combination of dense observations from a short period, with sparse observations covering a long period, is the central idea of various methods proposed for the reconstruction of time-varying surface climate fields. The "anomaly method", widely applied for centennial temperature and precipitation reconstructions (e.g. Jones, 1994; Dai et al., 1997; New et al., 1999) combines a (monthly) mean climatology with anomaly fields analyzed from sparse station networks. The reconstructions retain the finer-scale variations associated with local orography, despite the poor resolution of the long-term dataset. A large group of EOF-based methods exploit the space-time covariability observed during the short period of dense observations by means of empirical orthogonal functions (EOFs). These methods objectively take into account the heterogeneous pattern of spatial covariability expected in complex terrain. These covariability patterns (EOFs) span a reduced data space, in which the time evolution is subsequently determined from the sparse observations. This thesis is based on the EOF-based methods proposed for the reconstruction of global sea surface temperature (Smith et al., 1996, 1998; Kaplan et al., 1997, 1998). The application of these methods for the analysis of mesoscale climate variability is new. It is not clear whether the methods can be successfully used for the analysis of precipitation, due to the much higher spatial variability and lower correlation distances of precipitation. A further question is, which of the various methods gives the best results, that is, which method optimally exploits the station-station correlations in the dense dataset.

Gridded datasets covering the Alpine region

For the region of the European Alps two types of gridded precipitation analyses exist. First, there are the Alpine sections from global and continental-scale precipitation analyses with a nominal resolution of 50–250 km (e.g. Xie et al., 1996; Dai et al., 1997; New et al., 1999, 2000). Although the nominal resolution is quite high for some of these global analyses, the station density is too small for an accurate representation of the major, let alone the smaller-scale, subridge precipitation patterns (cf. Fig. 1.1). Second, there is the regional analysis of Frei and Schär (1998) which has an effective resolution close to 25 km. It is available for the period 1971–90, which is too short for the study of decadal and longer-term precipitation variability.

1.3   Aims of this study

The aim of this thesis is to develop a new dataset of the observed precipitation variability and to undertake a detailed analysis of past Alpine precipitation trends and variations. The specific issues are

- to develop a statistical method for the reconstruction of monthly mesoscale Alpine precipitation fields, which makes optimal use of the available data, i.e. a sparse set of long-term precipitation records and a dense set of short-term records

- to derive a new Alpine-wide dataset of mesoscale precipitation fields for the 20th century, suitable for studies of regional climate variability and regional climate change

- to provide a geographically differentiated (i.e. 25–200 km scale) analysis of long-term precipitation trends, and variations in the interannual to interdecadal range during the 20th century, for the entire Alpine region

These issues are addressed in the two papers which form the core of this thesis, and which have recently been submitted for publication. The first issue is addressed in the first paper (part B of this thesis), the following two issues are pursued in the second paper (part C). Each paper is accompanied by its own introduction where the specific issues under consideration are addressed in more detail. The thesis is complemented by a summary and several appendices.

2 Reconstruction of mesoscale precipitation fields from sparse observations in complex terrain

JÜRG SCHMIDLI,CHRISTOPH FREI AND CHRISTOPH SCHÄR

Climate Research, ETH Zürich, Switzerland[†]

ABSTRACT

The feasibility of a statistical reconstruction of mesoscale precipitation fields over complex topography from a sparse rain-gauge network is examined. Reconstructions of gridded monthly precipitation for the European Alps (resolution 25 km, 1202 grid points) are derived from rain-gauge samples (70–200 km inter-station distance, 25–150 stations). The statistical model is calibrated over a 15-year period and the reconstructed fields are evaluated for the remaining 5 years of the period 1971–90. The experiments are used to define the statistical setup of, to assess the data requirements for, and to describe the error statistics of a centennial reconstruction to be used in a forthcoming study. Reduced-space optimal interpolation is employed as the reconstruction method, involving data reduction by empirical orthogonal functions (EOFs), and least-squares optimal estimation of EOF coefficients. Also, a procedure to define covariance-guided station samples with a "representative" spatial distribution for the reconstruction is proposed.

Using a covariance-guided reference sample of 53 stations, the reconstruction accounts for 77% of the total variance. For individual grid points the relative reconstruction error (error variance divided by data variance) varies between 10–40%, while this value drops to 2–10% when considering subdomain-means of $100{\times}100\,\mathrm{km}^2$. The mesoscale patterns of the fields and multi-year precipitation anomalies are accurately reproduced. The EOF truncation is identified as the major limitation of the reconstruction skill, but is necessary to avoid overfitting. Reconstructions from covariance-guided representative samples exhibit superior skill compared to those from randomly distributed stations. The skill of the reconstruction was found to depend marginally on the choice of the calibration period within the 20 years, even when months with exclusively positive or negative values of the North Atlantic Oscillation Index where selected for calibration. This indicates that the reconstruction model provides appreciable temporal stationarity.

2.1   Introduction

The variability of the climate system and its possible change due to anthropogenic factors has stimulated numerous observational studies of climate variations during the past decades and centuries (e.g. Houghton et al., 1996). Spatiotemporal analyses of surface observations provide a primary source of information for such studies. For the recent decades such analyses are conveniently derived using data from dense instrumental networks (e.g. Xie et al., 1996; Frei and Schär, 1998). For earlier periods, however, spatial analyses are complicated by the sparsity of available observations, and special reconstruction techniques were developed for the analysis of sparse instrumental and proxy records (e.g. Cook et al., 1994; Smith et al., 1996).

So far, objective analyses over centennial time-scales have mostly focussed on global to sub-continental scales. Recent long-term reconstructions include: gridded time series analyses of monthly land-surface temperature (Jones, 1994; Mann et al., 1998), sea surface temperature (Smith et al., 1996; Kaplan et al., 1998), sea level pressure (Jones and et al., 1999) and monthly precipitation (Dai et al., 1997; New et al., 1999, 2000). The resolution (50–200 km) of these analyses is limited by the sparsity of available station data. Yet, considerable variations on these only marginally resolved scales can be expected in areas of complex topography or land-sea contrast. In these regions, analyses at higher spatial resolution and extending over many decades to one century are desirable for the study of regional climate variability and the development of statistical models for downscaling climate change scenarios from global climate models.

In this study we investigate the feasibility of reconstructing precipitation fields at mesoscale resolution (25–500 km) for a region of complex topography. The reconstruction study is conducted for monthly precipitation in the region of the European Alps. The aim is to evaluate an established reconstruction technique and to assess the data requirements for a reconstruction of 20th century precipitation fields. Our feasibility study is based upon the time period 1971–90. Digitization and homogenization of long-term records is currently underway, and the reconstruction of monthly precipitation fields since 1900 will follow in a subsequent study.

Different methods have been proposed for the reconstruction of time-varying surface climate fields from sparse observations (instrumental or paleoclimate data). Common to these methods is the combination of spatially detailed climate observations from a short period with sparse records (the reconstruction sample) from a long period. The "anomaly method", widely applied for centennial temperature and precipitation reconstructions (e.g. Jones, 1994; Dai et al., 1997; New et al., 1999), combines a mean climatology with anomaly fields interpolated from sparse reconstruction samples (absolute or relative, see also Jones and Hulme, 1996). The reconstructions retain the fine-scale variations associated with local orography, despite the poor resolution of the long-term dataset. More sophisticated methods exploit the space-time covariability observed during the short period of dense observations. This can be achieved by means of an EOF decomposition (e.g. Preisendorfer, 1988) and the calibration of a statistical relation between EOF scores and the long-term reconstruction records. Methods of this type include orthogonal spatial regression and canonical regression (Fritts et al., 1971; Cook et al., 1994), both frequently used for tree-ring reconstructions (e.g. Briffa et al., 1992; Haston and Michaelsen, 1997) and also applied to sparse instrumental records (e.g. Jones and et al., 1999). Related EOF-based methods have been proposed for optimal estimation of mean global surface

temperature from station data (Shen et al., 1994), the reconstruction of sea surface temperature (Smith et al., 1996; Shen et al., 1998), and, adding a linear regression calibration, for the reconstruction of global surface temperature from proxy data (Mann et al., 1998). Recently, these methods have been extended to exploit the temporal autocovariance in the data (Kaplan et al., 1997, 1998; Smith et al., 1998), and they have been demonstrated to improve the reconstruction skill, if the sampling interval is shorter than the autocorrelation time-scale. Further improvements were obtained by adapting the methods to include estimates of observational error of the reconstruction records (Kaplan et al., 1997).

The Alpine mountain range poses both challenges and potentials for the reconstruction of mesoscale precipitation. On the one hand, the region is influenced by a range of synoptic and mesoscale weather systems which imprint complex spatial patterns in the Alpine precipitation climate (Fliri, 1986; Frei and Schär, 1998; Schär et al., 1998) and its interannual and long-term variations (Schönwiese et al., 1994; Widmann and Schär, 1997; Frei and Schär, 2001). As a consequence, precipitation anomalies exhibit a short correlation decay length (50–150 km for annual precipitation; Gutermann, 1974). Therefore, it is to be expected that a skillful reconstruction requires a large number of suitably distributed long-term series and an optimal use of the sparse information. On the other hand, the Alpine region offers a unique observational coverage. Modern operational rain gauge networks, embracing many thousand stations with an inter-station distance of 10–15 km (Frei and Schär, 1998), provide an accurate reference for the calibration and validation of a mesoscale reconstruction. Also, a large number of long-term observations are available for the region. For example, Switzerland's country-wide rain gauge network started in 1864 with an average spacing of 25 km (80 stations, Benteli, 1870). Considerable effort has been expended to verify the quality of the long-term observations and to adjust for inhomogeneities (e.g. Auer et al., 1993; SMI (Eds.), 1996; Buffoni et al., 1999), but still many more documented series await digitization and laborious quality processing. The Alpine region constitutes an ideal test-ground for examining the feasibility of mesoscale reconstructions: the covariability patterns are well observed during the modern instrumental period, and the numerous long-term records already available today or which may be processed in the near future should allow for skillful reconstructions.

The purpose of this paper is to examine the reconstruction of mesoscale precipitation using the reduced-space optimal interpolation technique of Kaplan et al. (1998). Conceptionally this method is promising, as it objectively takes into account the heterogeneous pattern of spatial covariability expected in complex topography. The high-resolution data used is based on an objective analysis of many thousand station records onto a regular grid (25 km resolution) covering the time period 1971–90 (Frei and Schär, 1998). The covariability patterns (EOFs) span a reduced data space, in which the time evolution is subsequently determined from the sparse reconstruction records, using a least-squares optimal estimation procedure. The results are validated against the original 25 km analysis for independent periods.

Special consideration will be given to the sensitivity of the reconstruction skill with respect to the density and distribution of the sparse reconstruction sample. Several questions pertinent to a centennial-scale reconstruction in the Alps are addressed: 1) What is the expected skill from a reconstruction sample available today, and how can this skill be improved if additional long-term series could be made accessible? 2) How can *a priori* information about space-time covariability be used to assemble reconstruction samples with a higher representativity than randomly distributed samples? 3) Which are the
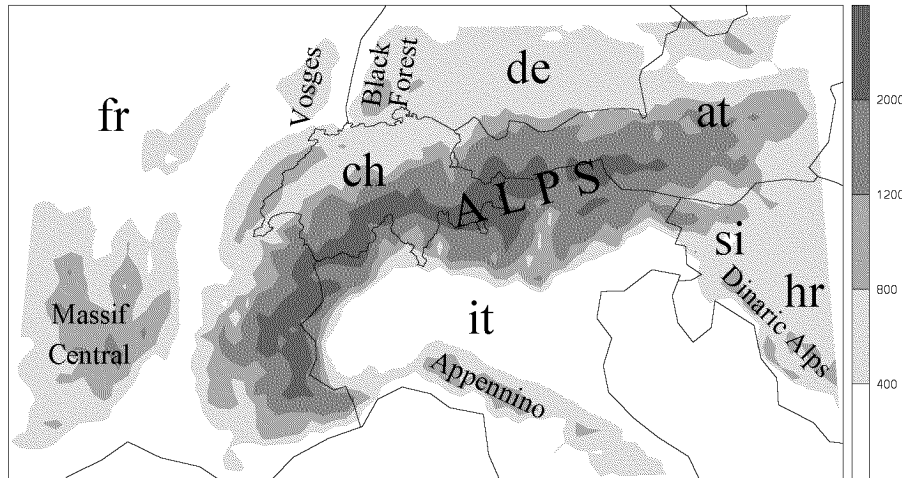
FIG. 2.1:   Map of the study region showing the European Alps and the surrounding
foreland area. Depicted is the height [m] above MSL (shading) and the political boundaries
(fr: France, ch: Switzerland, it: Italy, de: Germany, at: Austria, si: Slovenia, hr: Croatia).

dominant error components and their characteristics? Consideration of these topics is
not only helpful in establishing a suitable reconstruction framework, but it also provides
valuable information for ongoing work on digitization and quality processing of long-term
data records.

The paper proceeds with an introduction to the data sources used (section 2). Section
3 describes the reconstruction technique and the associated skill measures. In section 4,
a procedure to define "representative" reconstruction samples is proposed and used for
defining a reference sample. A detailed validation of reconstructions from the reference
sample is presented in section 5. Sensitivities of the proposed technique are examined in
section 6, and a summary of results and conclusions are given in section 7.

2.2   Study region and data

The reconstruction of monthly precipitation fields from sparse observations is examined
in the region of the European Alps (geographical area defined by 2.1°–16.2°E, 43.28°–
49.0°N). The topographic structure of the study region is displayed in Fig. 2.1. Its main
feature is the arc-shaped mountain range of the Alps, extending in a west-east direction
over a distance of 800 km across five countries. The ridge has a width of 100 to 300 km
and a typical crest height of 2500 m. The adjacent lowland regions are interspersed by
various hill ranges with spatial scales of 50–200 km and typical elevations of 1000 m.

The primary database for this study is a gridded, objective analysis of Alpine pre-
cipitation derived from comprehensive rain gauge data. Monthly precipitation fields over
the 20 year period 1971–90 are used for calibration and validation, and will be referred
to hereafter as ANALYSIS. The ANALYSIS has a grid spacing of 0.22° lat × 0.3° long,
corresponding to a resolution of 25 km. It is based on a high-resolution Alpine rain
gauge dataset that comprises 6800 station records from operational high-resolution sur-
face networks in the Alpine region (Fig. 2.2a, Frei and Schär 1998). The network density
corresponds to a typical inter-station distance of 10–15 km over most parts of the study

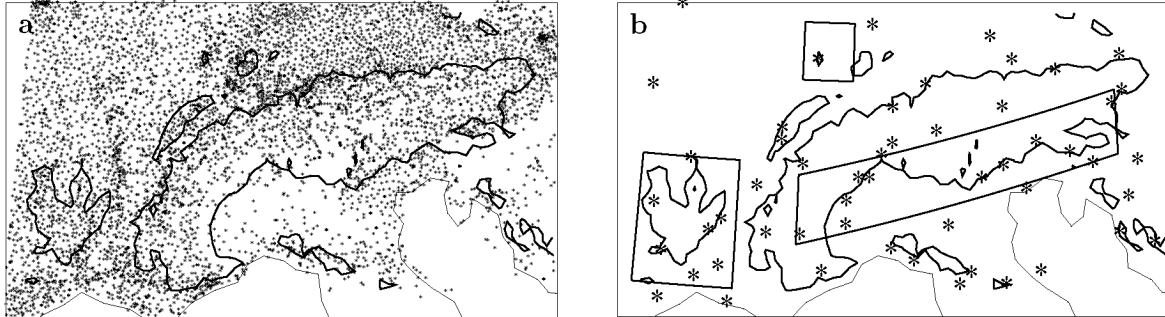FIG. 2.2: (a) Observation sites of rain gauge stations used to produce the Alpine precipitation analyses (ANALYSIS), and (b) location of the 53 stations used for the reference reconstruction (SPARSE-REF). Thick lines (800 m MSL contour) depict the main topographic features. The boxes indicate the subregions used for validation purposes (Massif Central: left, Vosges: top, Mediterranean Alps: right).

domain. The spatial analysis represents area-averages in the surrounding of each of the 1202 land grid points and was calculated from monthly station values using a modified version of the SYMAP algorithm (Shepard, 1984; Willmott et al., 1985). Details of the rain gauge dataset and the analysis procedure are given in Frei and Schär (1998).

The ANALYSIS dataset represents mesoscale precipitation variability as observed by current-day dense operational networks. In this paper, the term mesoscale is used for spatial scales resolved by the ANALYSIS grid. Over most parts of the domain, the effective resolution of the ANALYSIS is close to the nominal grid resolution of 25 km. For some parts of northern Italy, however, the effective resolution may be slightly inferior due to poorer data coverage (Fig. 2.2a, see also Frei and Schär 1998).

Fig. 2.3 displays the mean climatology and the monthly standard deviation of Alpine precipitation, as represented by the ANALYSIS. Mean annual values vary between 1.5–8 mm day^{-1}. The main features of the spatial distribution are two high-precipitation bands extending along the northern and southern rim of the Alpine ridge, and drier conditions in the interior of the mountain range and over the adjacent flatland. The maximum along the southern rim is divided into two major wet zones: the one centered over southern Switzerland and northern Italy, the other over eastern Italy and Slovenia. Several smaller-scale maxima are associated with the hill ranges remote from the main ridge. The monthly precipitation pattern exhibits pronounced seasonal and interannual variations, as reflected in the standard deviation (Fig. 2.3b).

For the purpose of our feasibility study, sparse reconstruction samples are taken from the same high-resolution Alpine rain gauge dataset (Frei and Schär, 1998) that constitutes the basis for the ANALYSIS. Subsets of 25–150 records are selected and serve as surrogates for centennial records. The sparse samples vary in station number and distribution: This allows the assessment of sampling sensitivities. A selected reconstruction sample, which consists of 53 stations, is displayed in Fig. 2.2b. It was chosen to be "representative" in sampling the phase space of Alpine precipitation anomalies, and it will constitute a reference sample (hereafter SPARSE-REF, see section 4). Further sets of sparse station samples will be introduced in section 6.

The reconstructions derived in this study will also be compared to the Alpine section of the Climate Research Unit global climate analysis (New et al. 1999, 2000; hereafter
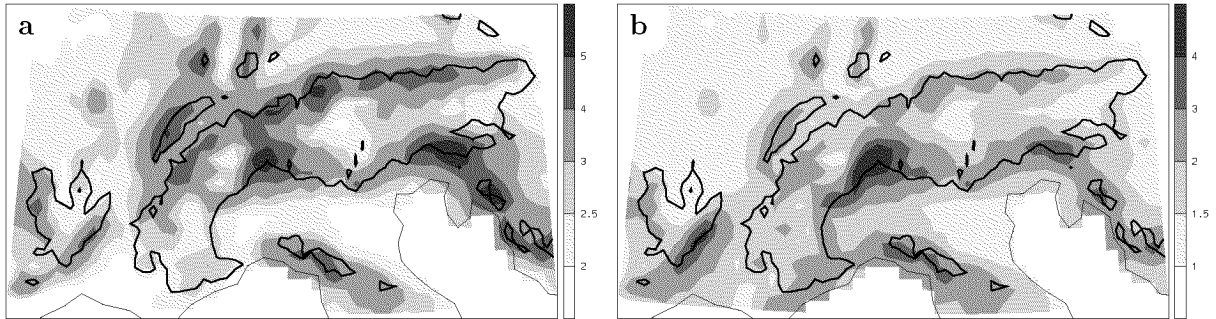
FIG. 2.3: (a) Mean annual precipitation and (b) standard deviation of mesoscale monthly precipitation for the period 1976–90 [mm day^{-1}]. The bold line represents the 800 m topographic contour.

CRU05). CRU05 has a grid resolution of 0.5 degrees and was derived from monthly station data using the "anomaly method" (see New et al., 2000). For the Alpine window of CRU05, 320 climate normals and about 100 station records were available for the period under consideration (M. New, personal communication). Therefore, CRU05 can be considered as an alternative reconstruction from a sparse station sample in the region. However, unlike the method presented in this paper, mesoscale information from a calibration period could not be exploited in the derivation of CRU05, except for some aspects of the mean climatological distribution.

2.3   Reconstruction method and validation measures

The objective of the reconstruction is to derive precipitation fields on a regular mesoscale grid using sparse observations from irregularly distributed rain gauge stations. The method applied here is based on the reduced-space optimal interpolation (OI) technique described by Kaplan et al. (1997), which combines data reduction and least-squares optimal estimation. The procedure involves the computation of empirical orthogonal functions (EOFs) and subsequent truncation to a set of leading modes (a), the assignment of grid points to the reconstruction sample (b), and the reconstruction of EOF scores using least-squares optimal estimation (c). Finally (d) we describe the skill measures used for the subsequent validations.

2.3.a   EOFs and data reduction

An EOF decomposition (e.g. Jolliffe, 1986; von Storch and Zwiers, 1999) was conducted to arrive at a low-dimensional description of the spatiotemporal variability of mesoscale Alpine precipitation. Let the set $\mathbf{s}_n$ be the ANALYSIS fields, where $\mathbf{s}_n$ denotes the analysis at time n (the month of the period, $1 \leq n \leq N$), arranged as column vectors of dimension M (the number of grid points). We can write

$$\mathbf{s}_n = \boldsymbol{\mu} + \mathbf{E}\mathbf{a}_n + \boldsymbol{\epsilon}_n^t \overset{def}{=} \mathbf{s}_n^f + \boldsymbol{\epsilon}_n^t \qquad n = 1, \ldots, N, \qquad (2.1)$$

where $\mathbf{E}$ is an $M \times L$ dimensional matrix comprising the first L EOFs as M dimensional column vectors, $\mathbf{a}_n$ is the L dimensional vector of EOF scores describing the temporal evolution in the reduced-space, $\boldsymbol{\mu}$ is the climatological mean of the field, $\boldsymbol{\epsilon}_n^t$ is the error
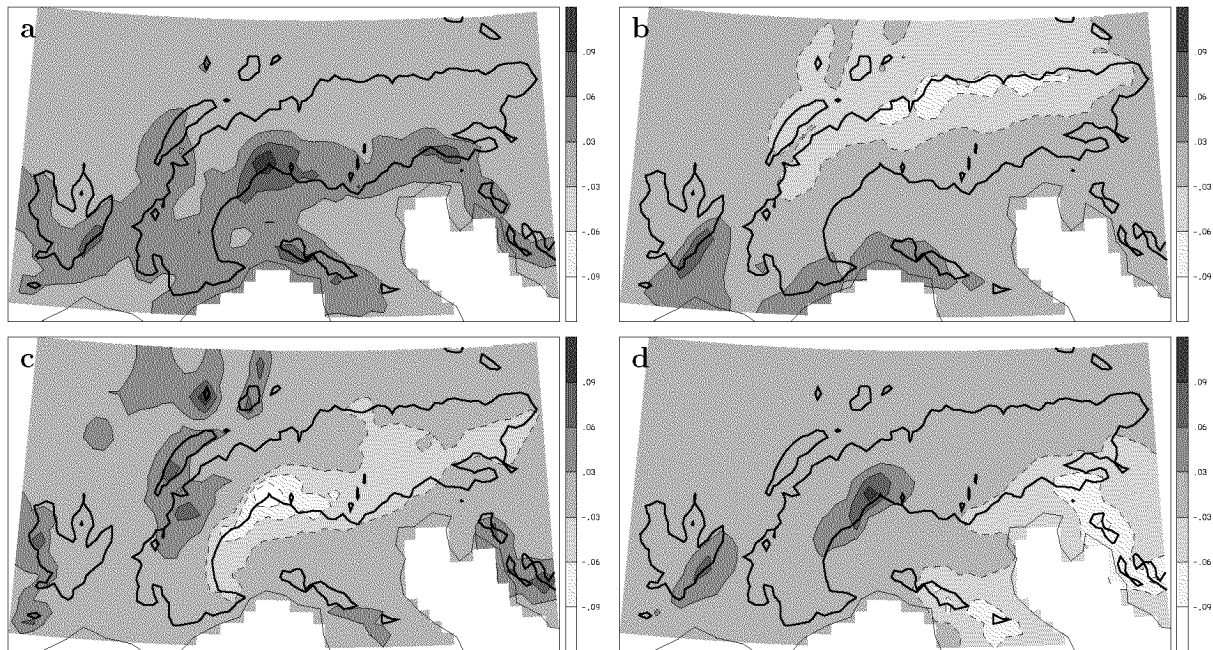
FIG. 2.4: Patterns of the four leading EOFs of monthly precipitation for the years 1976–90. The depicted EOFs explain (a) 37%, (b) 17%, (c) 9%, and (d) 8% of the total variance, respectively. The bold line represents the 800 m topographic contour.

due to EOF truncation (space reduction), and $\mathbf{s}_n^f$ is the "filtered" ANALYSIS field. The spatial EOFs are the eigenvectors of the ANALYSIS covariance matrix with eigenvalues λ_l. The eigenvalues represent the variance of each mode l, and are traditionally ordered so that $\lambda_l \geq \lambda_{l+1}$.

We choose $L \ll \min(N, M)$, that is the complete set of EOFs is truncated to a much smaller subset. In this case, $\mathbf{s}_n^f$ forms a L-dimensional reduced-space representation of $\mathbf{s}_n$. The contribution from higher-order modes is transferred to the residual term $\boldsymbol{\epsilon}_n^t$ and is considered as "noise". Various rules have been proposed to guide the truncation L in an EOF representation (e.g. logarithmic eigenvalue rule: Craddock and Flood 1969; Preisendorfer 1988; truncation between non-degenerate eigenmodes: O'Lenic and Livezey 1988), but from a practical point of view a suitable discrimination of signal from noise often depends on the application under consideration (von Storch, 1995).

Fig. 2.4 displays the first four EOFs of the ANALYSIS fields for the calibration period 1976–90. The EOFs exhibit pronounced large-scale gradients (e.g. EOF 3 with a north-south asymmetry across the ridge), and embedded mesoscale patterns (e.g. EOF 4 with an asymmetry between the regions of prominent precipitation variability to the south of the ridge). The four modes explain 37%, 17%, 9% and 8% of the total variance, respectively. Each of the higher order modes accounts for less than 3% of the total variance. The logarithmic eigenvalue rule suggests a truncation at $L \approx 50$. In this application, the reduced-space dimension is set to $L = 24$, the value being determined from a cross-validation experiment (section 4c). In the reminder of the text, a truncated representation of the ANALYSIS fields using the first L EOFs will be referred to as the filtered ANALYSIS $\mathbf{s}_n^f$, referring to the EOF decomposition as a noise-filtering technique (see also Kaplan et al., 1997).

In the present application, EOFs are calculated from individual monthly fields and

hence the reduced-space representation is optimized towards capturing a combination of the interannual variations and the seasonal cycle. Reconstructions using different EOFs for each season or month resulted in lower skill, due to the non-robust estimation of specific EOF patterns from the short calibration period. Also, a comparison of seasonal and non-stratified EOFs revealed little differences between EOF patterns, suggesting a satisfactory overlap of the phase-space portions characteristic for interannual and seasonal variations.

2.3.b *Assigning point observations to grid points*

The reconstruction method requires assigning a specific grid point of the ANALYSIS to each of the K rain gauge records of the reconstruction sample. This is accomplished by choosing the grid point with the highest correlation from the four ANALYSIS points nearest to the rain gauge. The resolved variance statistic β (see later in section 3d) is chosen as the respective correlation measure. Formally, the assignment can be written as

$$\mathbf{s}_n^\circ = \mathbf{H}^\circ \mathbf{s}_n + \boldsymbol{\epsilon}_n^\circ \qquad n = 1, \dots, N, \tag{2.2}$$

where $\mathbf{s}_n^\circ$ is the K-dimensional vector of rain gauge observations, $\mathbf{H}^\circ$ is a $K \times M$ binary matrix (matrix elements 0 or 1) and $\boldsymbol{\epsilon}_n^\circ$ is a local error term (the observational error in data assimilation). The matrix $\mathbf{H}^\circ$ puts a complete field of the analyses into the format of the reconstruction sample. The local error $\boldsymbol{\epsilon}_n^\circ$ embraces instrumental errors and local sampling errors, the latter arising from differences between the point observation of the rain gauges and the areal precipitation of the grid points.

2.3.c *Reconstruction*

To obtain an estimate of the mesoscale precipitation field at time n, the reduced-space EOF scores $\mathbf{a}_n$ have to be estimated from the observations $\mathbf{s}_n^\circ$ of the reconstruction sample. Combining (2.1) and (2.2), a relation between the observation anomalies $\boldsymbol{\delta s}_n^\circ$ (with respect to the ANALYSIS) and the EOF scores $\mathbf{a}_n$ is obtained:

$$\boldsymbol{\delta s}_n^\circ \overset{def}{=} \mathbf{s}_n^\circ - \mathbf{H}^\circ \boldsymbol{\mu} = \mathbf{H} \mathbf{a}_n + \boldsymbol{\epsilon}_n^r \tag{2.3}$$
$$\text{with } \mathbf{H} = \mathbf{H}^\circ \mathbf{E} \text{ and } \boldsymbol{\epsilon}_n^r = \mathbf{H} \boldsymbol{\epsilon}_n^t + \boldsymbol{\epsilon}_n^\circ.$$

Here $\mathbf{H}$ is a $K \times L$ matrix which is determined from the EOFs and sample locations, and $\boldsymbol{\epsilon}_n^r$ is the combined truncation and local error. The covariance matrix $\mathbf{R}$ of $\boldsymbol{\epsilon}_n^r$ required by the OI procedure (i.e. $\mathbf{R} = \langle \boldsymbol{\epsilon}_n^r \boldsymbol{\epsilon}_n^{r\,T} \rangle$) can be estimated from the calibration period for which $\boldsymbol{\epsilon}_n^r$ is known. (The error $\boldsymbol{\epsilon}_n^r$ is equal to the difference between the observations $\mathbf{s}_n^\circ$ and the filtered ANALYSIS $\mathbf{s}_n^f$ at the corresponding grid points.) The knowledge of $\boldsymbol{\epsilon}_n^r$ allows the computation of the full covariance matrix $\mathbf{R}$, but all off-diagonal elements are set to zero, because use of the full covariance matrix results in overfitting of the statistical model (for the present application). Setting the off-diagonal elements to zero is equal to assuming the errors to be spatially uncorrelated with each other.

The least-squares estimate $\hat{\mathbf{a}}_n$ for the EOF scores $\mathbf{a}_n$ is obtained by minimizing the quadratic cost function

$$S[\mathbf{a}_n] = (\mathbf{H} \mathbf{a}_n - \boldsymbol{\delta s}_n^\circ)^T \mathbf{R}^{-1} (\mathbf{H} \mathbf{a}_n - \boldsymbol{\delta s}_n^\circ) + \mathbf{a}_n^T \mathbf{C}^{-1} \mathbf{a}_n \tag{2.4}$$

(see Kaplan et al., 1997). Here $\mathbf{C}$ is the reduced-space data covariance matrix, a diagonal $L \times L$ matrix containing the eigenvalues λ_l. The first term of (2.4) is the familiar cost term for a weighted least-squares estimate. The second term is a specific feature of the reduced-space OI which constraints the EOF spectrum: the higher the mode, the larger is the cost for deviations of its amplitude. Hence the OI cost function discourages solutions with high energy on features which "historically" had little energy (Kaplan et al., 1997). The amplitudes of higher-order modes are damped in accordance with their larger estimation error.

The reduced-space OI estimate $\hat{\mathbf{a}}_n$ and its error covariance matrix $\mathbf{P}$ are given by (Kaplan et al., 1997):

$$\hat{\mathbf{a}}_n = \mathbf{P}\mathbf{H}^T\mathbf{R}^{-1}\delta\mathbf{s}_n^o \tag{2.5}$$

$$\mathbf{P} = \left(\mathbf{H}^T\mathbf{R}^{-1}\mathbf{H} + \mathbf{C}^{-1}\right)^{-1}.$$

The solution $\hat{\mathbf{a}}_n$ makes the best possible use of the observations and their error estimates. It is an unbiased estimate of the L-dimensional reduced-space field with minimum error variance, under the assumption that the error $\boldsymbol{\epsilon}_n^r$ is random, has zero mean, and is uncorrelated with the retained modes (Kaplan et al., 1997).

A full grid representation of the reconstruction can be obtained from the estimated EOF scores $\hat{\mathbf{a}}_n$ through

$$\hat{\mathbf{s}}_n = \boldsymbol{\mu} + \mathbf{E}\hat{\mathbf{a}}_n \qquad \tilde{\mathbf{P}} = \mathbf{E}\,\mathbf{P}\,\mathbf{E}^T, \tag{2.6}$$

where $\tilde{\mathbf{P}}$ corresponds to the error covariance within the reduced-space. The total reconstruction error includes the error of truncation and can be obtained by

$$\hat{\mathbf{s}}_n - \mathbf{s}_n = (\hat{\mathbf{s}}_n - \mathbf{s}_n^f) + (\mathbf{s}_n^f - \mathbf{s}_n) = \boldsymbol{\epsilon}_n^e + \boldsymbol{\epsilon}_n^t, \tag{2.7}$$

where $\boldsymbol{\epsilon}_n^e$ is the estimation error. The estimation error $\boldsymbol{\epsilon}_n^e$ is the difference between the reconstructed and filtered field, whereas the truncation error $\boldsymbol{\epsilon}_n^t$ is the difference between the filtered field and the ANALYSIS.

It is worth noting that other reconstruction methods can be considered as special forms of the reduced-space OI. For example, the projection method of Smith et al. (1996) is recovered, if the second term in the cost function (2.4) is dropped and $\mathbf{R}$ is set to the identity matrix (i.e. no error-related weighting). The solution becomes:

$$\hat{\mathbf{a}}_n^P = \left(\mathbf{H}^T\mathbf{H}\right)^{-1}\mathbf{H}^T\delta\mathbf{s}_n^o. \tag{2.8}$$

An advantage of the OI method is its ability to provide error estimates for the reconstructed data. An error estimate which is easy to compute and which holds for any single grid point is (Kaplan et al., 1997)

$$\boldsymbol{\Pi} = 2(\tilde{\mathbf{P}} + \mathbf{C}^r), \tag{2.9}$$

where $\mathbf{C}^r$ is the covariance matrix of the truncation error $\boldsymbol{\epsilon}_n^t$. Note that this error estimate is calculated from calibration data only.

In the present application, observation anomalies $\delta\mathbf{s}_n^o$ are obtained by subtracting the climatological mean $\boldsymbol{\mu}$ of the ANALYSIS from the sample observations $\mathbf{s}_n^o$. This approach differs to previous projection and OI reconstructions for SST. Kaplan et al. (1998) removed the seasonal cycle from the observations prior to reconstruction, and Smith et al. (1996,

1998) removed a time-dependent low-frequency anomaly. The application of a stationary μ in our case was found to be advantageous because a robust estimation of the seasonal cycle was not possible, due to the short calibration data and the large month-to-month precipitation variability which generally exceeds the amplitude of the seasonal cycle.

The success of the approach, described above, for the reconstruction of mesoscale precipitation depends on a few fundamental preconditions. 1) Monthly precipitation series at individual rain gauges must be representative on a local scale (the scale of one analysis grid pixel). The sensitivity studies in section 6 suggest that local representativity is not a critical issue for the present application. 2) The sparse reconstruction network must sample the leading degrees of freedom of mesoscale precipitation variability. This "global" representativity condition depends on the size and spatial distribution of the reconstruction sample. It will be examined in section 6. 3) The historical mesoscale precipitation anomalies must lie approximately within the linear subspace spanned by the "signal" EOFs of the calibration period. This assumption represents a weak "stationarity" requirement. The assumption cannot be assessed without detailed historical data. However, cross-validation results and sensitivity experiments conducted in section 6 rule out some potential factors of non-stationarity. Also, split-period checks and seasonal stratification have shown that the linear subspace spanned by the first dozen EOFs is fairly robust (see also Widmann, 1996).

2.3.d Measures of reconstructive skill

Among standard measures of correspondence, such as bias, root-mean-square error (rmse), and anomaly correlation, the resolved variance statistic β (e.g. Murphy and Epstein, 1989; von Storch and Zwiers, 1999) is used as a primary measure for the validation and intercomparison of the reconstructions. Its generic form is

$$\beta = 1 - \frac{\sum (x - x_r)^2}{\sum (x_r - \overline{x}_r)^2},\tag{2.10}$$

where x is the series to evaluate (i.e. the reconstruction), x_r is the reference series (i.e. the ANALYSIS data), and $\overline{x}_r$ is the mean of the reference data over the period of comparison. In our evaluations, β will be determined either for the time series at individual grid points (summation over time) to yield a map of temporal correspondence, or for a reconstructed field at individual time (summation over space) to yield a time series of spatial correspondence.

The resolved variance β is a rigorous measure of the similarity between two variables: It measures their correspondence not only in terms of the relative departures from their means, but also in terms of the means and absolute variances of the two series (Murphy and Epstein, 1989). The expected correspondence between two random series with equal mean and variance is $\beta = -1$; a trivial "climatological" reconstruction results in a skill of $\beta = 0$. Reconstructions with $\beta > 0$ can be considered as skillful. Notice that the difference between the time series is measured relative to the local variance, and this facilitates the comparison of reconstruction skills between regions of differing variance.

A compound measure β_{tot} of the reconstruction skill is obtained when the sum in (2.10) extends over all grid points and time levels. For fields with equal means, β_{tot} is equal to the fraction of total variance explained by the reconstruction.

Accordingly, a measure of the compound relative error can be introduced as

$$e = \frac{\sum (x - x_r)^2}{\sum (x_r - \overline{x}_r)^2},$$ (2.11)

where again the sum extends over all grid points and time levels. Eq. 2.11 is used to quantify the relative reconstruction error e^r ($x \hat{=} \hat{\mathbf{s}}_n$; $x_r \hat{=} \mathbf{s}_n$), the relative truncation error e^t ($x \hat{=} \mathbf{s}_n^f$; $x_r \hat{=} \mathbf{s}_n$), and the relative estimation error e^e ($x \hat{=} \hat{\mathbf{s}}_n$; $x_r \hat{=} \mathbf{s}_n^f$). For easier comparison of the errors, the relative estimation error is also scaled by the variance of the ANALYSIS $\mathbf{s}_n$, and not by the variance of the filtered ANALYSIS $\mathbf{s}_n^f$, as would be indicated by (2.11). Note that e^r is related to β_{tot} by $e^r = 1 - \beta_{\text{tot}}$.

2.4 The reference reconstruction

This section describes the specification of the sparse reconstruction sample SPARSE-REF and its application to reduced-space OI. The sample will be used as a reference for assessing the performance of the reconstruction method (section 5) and for estimating sampling sensitivities (section 6).

2.4.a Covariance-guided selection of sparse reconstruction samples

The application of the reconstruction method will depend on the availability of an accurate and suitable reconstruction sample. Besides the total number of sample stations, their spatial distribution is expected to be of crucial importance, as it determines the overall representativity. Here we describe a procedure for selecting a reconstruction sample of prescribed size, whose spatial distribution can be expected to achieve near-to-optimal overall representativity. Such a sample provides a reference for examining the role of sampling errors. Moreover information on ideal sample distributions can be valuable when observations are abundant, but require costly preprocessing, digitization and homogenization, as is the case for precipitation in the Alps. Evidently, for a real reconstruction all available long-term records would be used, irrespective of their position, provided they are homogenized and available in a digital format.

The idea of the covariance-guided selection procedure is to exploit *a priori* knowledge of the spatiotemporal covariance of the field, as represented by the EOFs of the ANALYSIS data. A station network is selected which — as an entity — samples "evenly" the directions of the reduced signal subspace of the precipitation data. The directions of the subspace are represented by rotated EOFs. The notion "even sampling" describes the attempt of avoiding redundancy in some directions of phase space at the expense of undersampling of others.

The specification of a covariance-guided reconstruction sample consists of the following steps: Firstly, a "suitable" number k of rotated EOFs are determined from the leading EOFs by the "varimax" procedure (e.g. Richman, 1986). The rotation provides loading patterns associated with geographically covariant subregions (Barnston and Livezey, 1987). The truncation point can be chosen according to the desired sample size, while avoiding the splitting of a multiplet (North et al., 1982). Secondly, for each of the rotated EOFs, J grid pixels are selected in the high-loading patch of the mode, resulting in a set of $k \times J$ grid points with an ideal overall representativity of the space-time variability. Thirdly, from the surrounding of each selected grid point the station that exhibits the
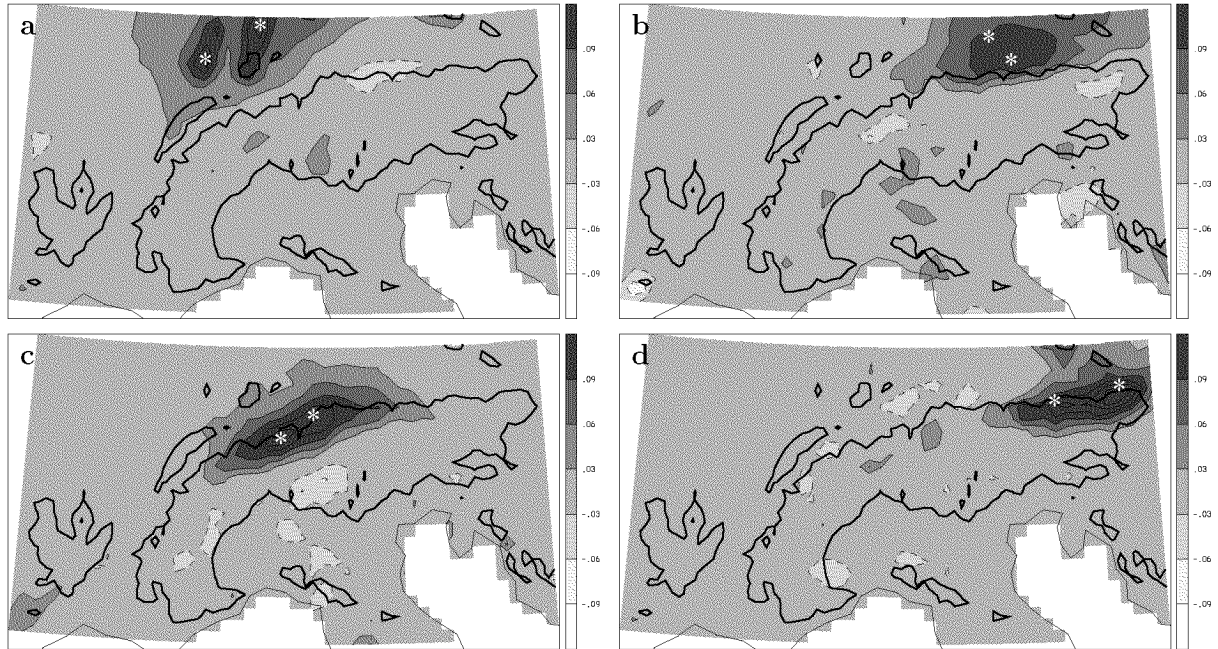
FIG. 2.5: Rotated EOFs (four out of 27) with their main loadings localized to the north of the Alpine ridge. Stars indicate stations of the covariance-guided selection procedure associated with each of the modes.

highest correlation with the gridpoint series is chosen to belong to the sample. If the same stations should be selected more than once, the grid points which lead to the multiple selections are removed from the set. Some elements of the selection procedure in steps 2 and 3 seem ambiguous. However, sensitivity experiments have shown that the reconstruction skill is only weakly dependent on these details, such as the exact positioning of the pixels in the high-loading patch, or the selection of the local station (see later section 6a). It is the location of the stations in the high-loading areas and their distribution among all signal modes which is essential for achieving good overall representativity.

2.4.b   The reference sample

The sample used for the reference reconstruction is derived using the covariance-guided selection procedure with $k = 27$ (dimension of the phase space), and $J = 2$ (number of stations per dimension). This setting was chosen such that the resulting sample SPARSE-REF reflects the expected density of centennial homogenized rain gauge records, likely to become available in the near future for the Alpine region. Note that SPARSE-REF comprises only 53 stations, because one of the grid points had to be omitted because of multiple selection of the same station (see previous subsection).

For illustration, Fig. 2.5 depicts the loading patterns of the rotated EOFs representative for the region north of the Alpine ridge, together with the location of the stations selected for each mode. The loading patterns demark virtually disjunct regions of precipitation variability: the Vosges/Black Forest hills (panel a), the eastern Alpine foreland (b), and the Central (c) and Eastern (d) Alpine rim, respectively.

The entire station network of SPARSE-REF is displayed in Fig. 2.2b. The distribution reflects a balanced representation of all major subregions, with a slightly denser coverage
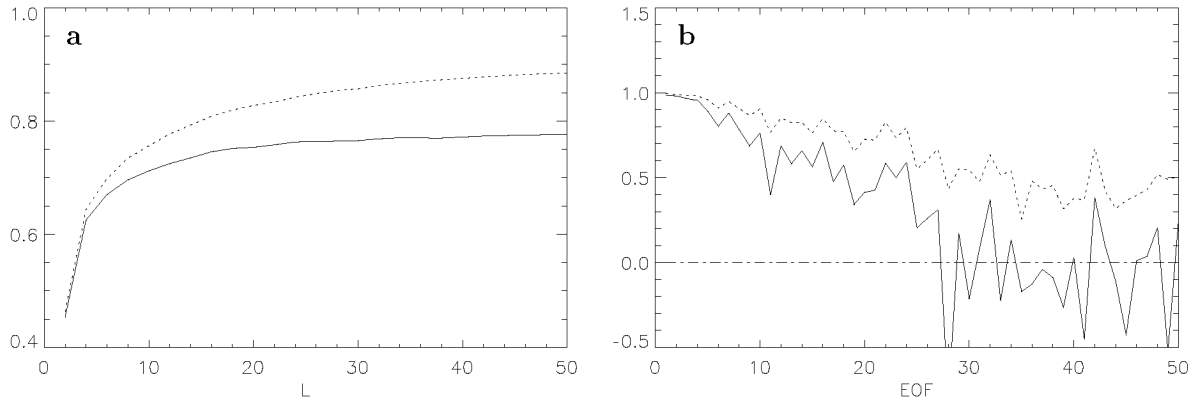
FIG. 2.6: (a) Fraction of total variance β_{tot} as a function of the reduced-space dimension L for the reconstruction (solid) and the filtered ANALYSIS (dashed). (b) Skill β (solid) and correlation skill r (dotted) of individual EOF scores for a reconstruction with $L = 50$. Both panels are for the validation period 1971–75.

over mountainous terrain compared to the flatland regions. For example, the Massif Central (westernmost box) is represented by 7 stations, whereas the flatland region of Central France contributes with 2 stations only. Also, the southern Alpine rim, a region of higher precipitation variability, shows denser sampling than the northern rim. These features corroborate the idea of the covariance-guided station selection to account implicitly for the smaller spatial scales and larger magnitude of precipitation variability in areas of complex topography.

2.4.c   Application of the method

For the reference reconstruction, the model described in section 3c is calibrated over the 15-year period 1976–90 and then evaluated over the independent five-year period 1971–75. (For an operational reconstruction, the calibration period would be extended to the full length of the data period). The calibration involves the calculation of EOFs, and the estimation of the reduced-space data covariance matrix **C** and the error covariance matrix **R** (see section 3c).

The reduced-space dimension L (i.e. EOF truncation point) is determined by examining the reconstruction skill for the independent period (1971–75) with various settings of L. Fig. 2.6a shows the skill β_{tot} (see section 3d) of reconstructions as a function of L using SPARSE-REF. Also shown is the skill of the EOF-filtered ANALYSIS at the corresponding levels of truncation (i.e. a perfect reconstruction). The skill for the filtered ANALYSIS increases over the entire range of truncations, whereas the skill of the reconstruction reaches saturation at $L \approx 25$. The improvement of the skill beyond $L = 25$ is marginal ($\beta_{tot} = 0.77$ for $L = 25$ and $\beta_{tot} = 0.78$ for $L = 50$); this indicates that higher-order modes are only marginally resolved. This is corroborated by Fig. 2.6b, which shows the skill β and anomaly correlation r for the individual EOF scores for $L = 50$. For EOF modes larger than about 24, the skill fluctuates around zero. Thus we choose a reduced-space dimension of $L = 24$ for the reference reconstruction. The same setting of L is chosen for all other reconstruction experiments (see section 6) in order to facilitate the comparison of the results.

2.5 Validation

This section provides a detailed validation of the (mesoscale) monthly precipitation fields, reconstructed with the reference sample SPARSE-REF depicted in Fig. 2.2b and described in section 4, for the independent five-year period 1971–75. We proceed from a visual inspection of example cases (a), to a systematic skill and error analysis (b), the representation of long-term variations (c), and the reconstruction of subdomain-mean variations (d).

2.5.a Example cases

The ability of the reconstruction to reproduce characteristic month-to-month variations in the mesoscale precipitation patterns is illustrated in Figs. 2.7 and 2.8, for two winter and two summer months, respectively. The example cases have been selected from the validation period (1971–75) as the months with highest and lowest reconstruction skill in the corresponding season, respectively. December 1974 (case with high skill, Fig. 2.7a) is dry throughout the Mediterranean region with large maxima located along the northern Alpine rim. In contrast, January 1974 (low skill, Fig. 2.7b) shows widespread wetness with various maxima along the Alpine mountain range and a peak maximum over the southern range of the Massif Central. The reconstruction (Fig. 2.7c, d) reproduces all these characteristic patterns for both cases. Also many of the fine-scale anomalies are accurately retained both in location and magnitude, at least for the December case. The skill β of the two cases is 0.94 and 0.66, respectively. In absolute terms, the differences between the reconstruction and the ANALYSIS (Fig. 2.7e, f) are mostly smaller than $0.5 \, \text{mm day}^{-1}$ for both cases.

The two summer season cases are displayed in Fig. 2.8. In July 1974 (high skill, Fig. 2.8a) a major wet anomaly is located along the northern Alpine flank, and in July 1971 (low skill, Fig. 2.8b) precipitation is lower and more evenly spread. The reconstructed fields (Fig. 2.8c, d) are smoother and lack some of the small-scale variability seen in the ANALYSIS. The skill β of the two cases is 0.85 and 0.35, respectively. The deficiencies of the month with lowest skill are more prominent than in winter, as is reflected, for instance, in the excess precipitation in the French flatland region. Nevertheless, even for this poor month, the observed precipitation bands along the Alpine flanks are reproduced by the reconstruction.

The examination of further cases revealed a tendency of the reconstruction to be less skillful for months with low precipitation values and weak gradients.

2.5.b Systematic skill and error analysis

A systematic evaluation of the spatiotemporal correspondence between the reference reconstruction and the ANALYSIS is shown in Fig. 2.9. Fig. 2.9a shows the spatial pattern of resolved variance β for the validation period. The highest skill, locally $\beta > 0.9$, is found along the Alpine flanks, especially the northern rim, and in the regions of the Massif Central and the Vosges. Low skills, locally $\beta < 0.6$, are found in the flatlands of central France, a region with low precipitation variability (see Fig. 2.3b) and poor coverage in the reconstruction sample SPARSE-REF (cf. Fig. 2.2b). The overall reconstruction skill β_{tot} is 0.77.
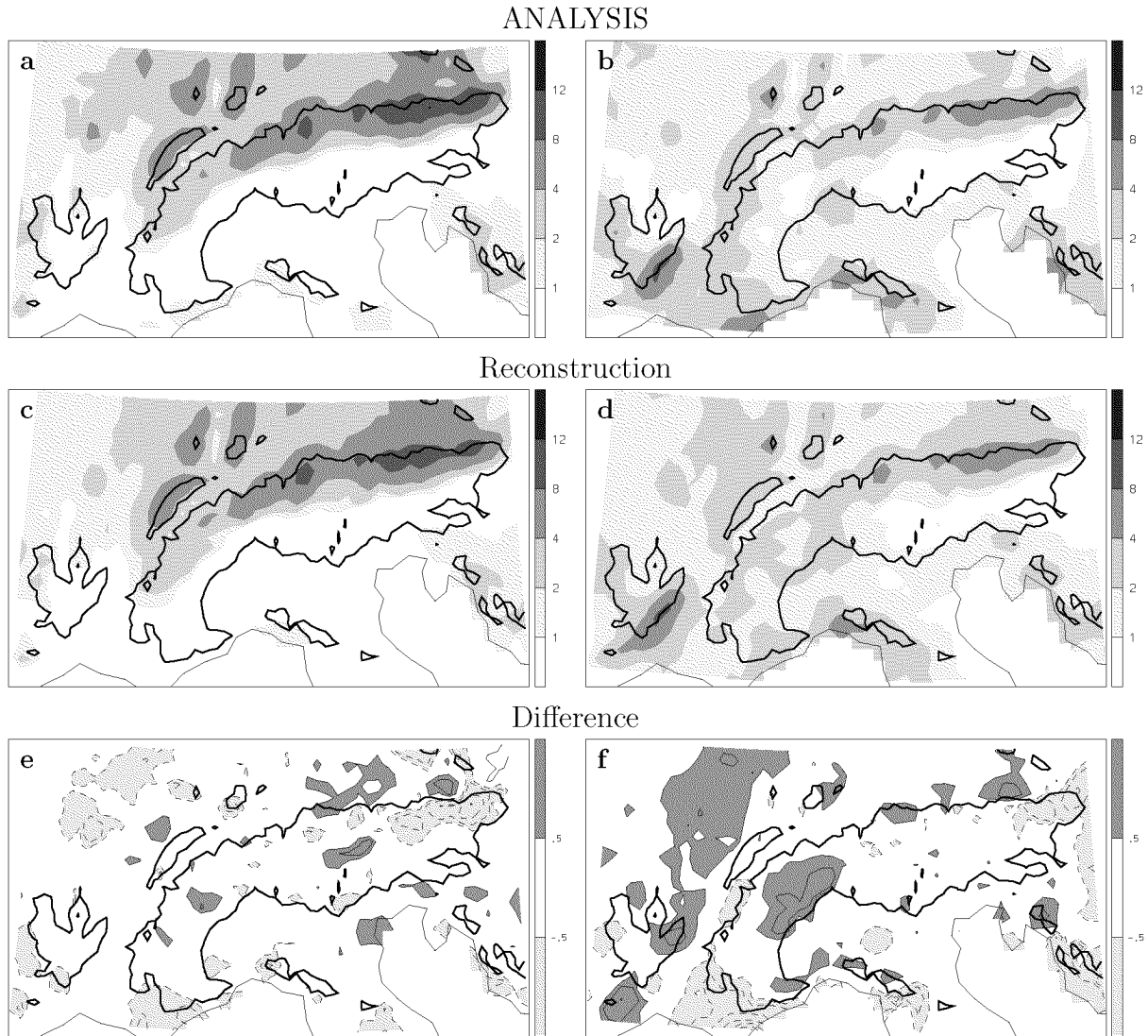
ANALYSIS

FIG. 2.7: Observed (ANALYSIS), reconstructed and difference fields [mm day^{-1}] for the winter months with highest (December 1974, left, $\beta = 0.94$) and lowest skill (January 1974, right, $\beta = 0.66$) within the independent validation period. Reconstruction with the reference sample SPARSE-REF and a reduced-space dimension of $L = 24$. The contour interval for the difference fields is 1 mm day^{-1}, except that the ± 0.5 mm day^{-1} contours are included.

Fig. 2.9b shows the relative reconstruction bias, that is the relative error of the mean precipitation for the validation period. Typically, the bias is less than 10% of the standard deviation of the ANALYSIS. However, in the flatlands of central France, the relative bias is about 20%. This value is still smaller than the critical value for a statistically significant bias, which for the present sample size (60 months) is 26%.

Fig. 2.9c shows the time dependence of the reconstruction skill for the validation period. The Skill-values (solid line) range from 0.35 to 0.94 and are greater than 0.6 for 88% of the months. There is some evidence for a systematic seasonal signal: Cases with particularly low skill occur mainly during summer and autumn. However, the seasonal variation of the mean skill is small: the median and standard deviation (determined from

ANALYSIS

Reconstruction
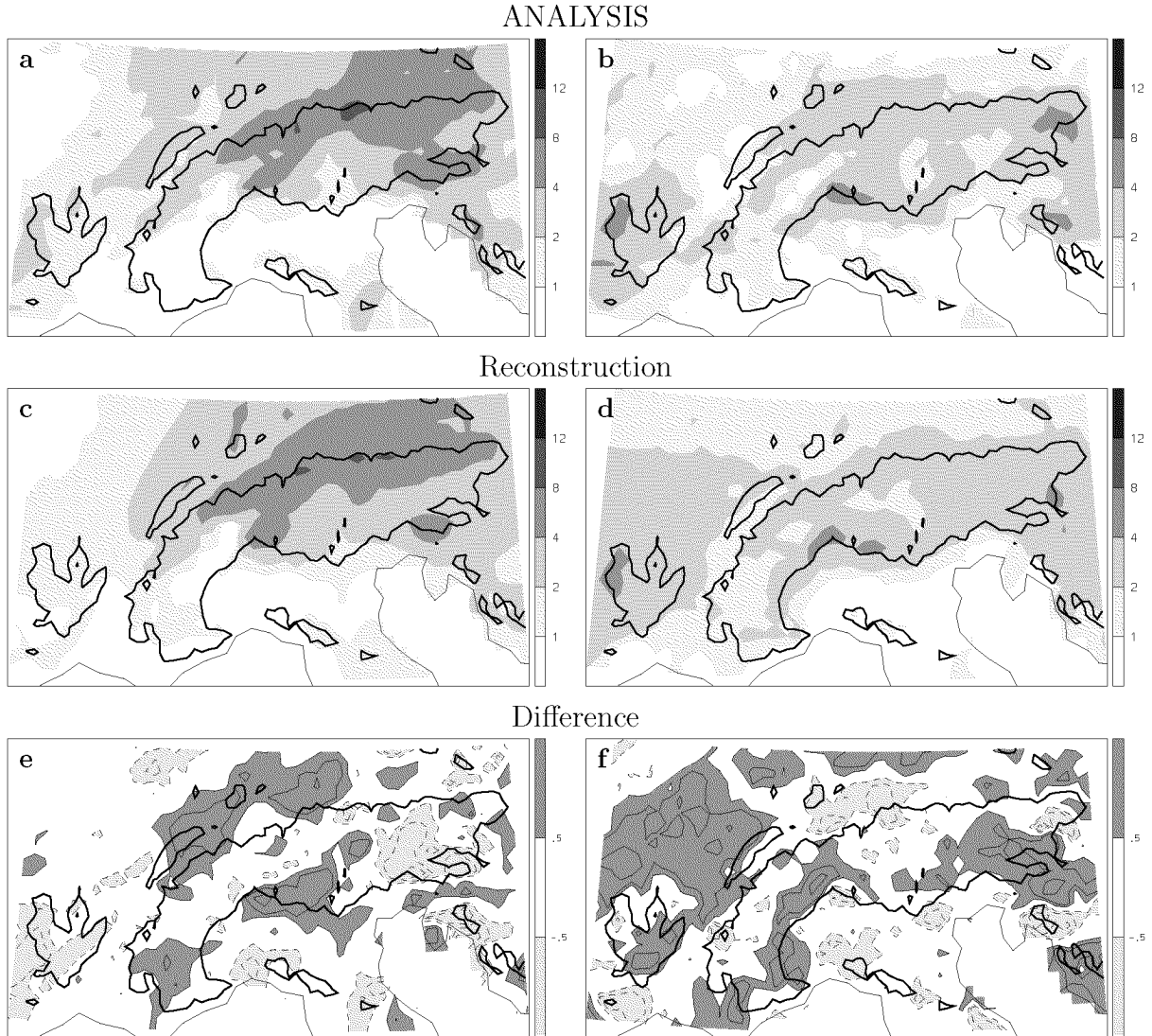
Difference

FIG. 2.8:   As in Fig. 2.7, but for the two summer months with highest (July 1974, left, $\beta = 0.85$) and lowest skill (July 1971, right, $\beta = 0.35$).

the quartile difference) of β is 0.79 ± 0.06 for winter, 0.76 ± 0.10 for spring, 0.74 ± 0.13 for summer, and 0.76 ± 0.11 for autumn. From Fig. 2.9c it is also evident that the temporal variation of the reconstruction skill closely matches that of the filtered ANALYSIS (dashed line). The latter can be considered as a perfect reconstruction with the same EOF truncation. This correlation suggests that the reconstruction performance depends critically on the representation of the monthly precipitation field in the low-dimensional phase space; hence EOF truncation limits the skill for months with an anomalous spatial distribution. Poor phase-space representation occurs mainly in summer and autumn.

Fig. 2.10 shows the root-mean-square error (rmse) of the reconstruction, derived from the validation (panel a), and estimated from the calibration using Eq. 2.9 (panel b). The validation rmse is smaller than $1.0 \, \text{mm} \, \text{day}^{-1}$ for the major part of the domain, with higher values (1.0–$1.5 \, \text{mm} \, \text{day}^{-1}$) along the southern mountain ranges. The values correspond to typically 40–60% of the temporal standard deviation at individual grid points. The theoretical prediction of the error structure (Fig. 2.10b) agrees reasonably well with that
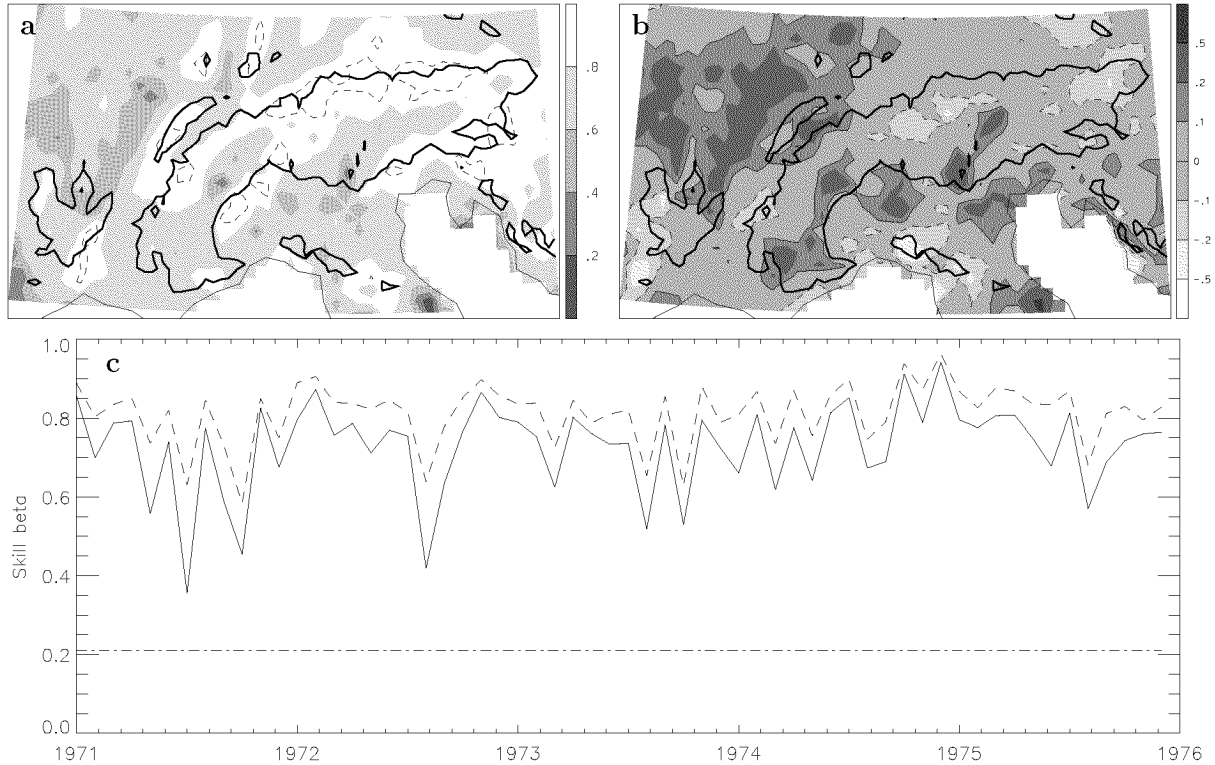
FIG. 2.9: Validation of the reference reconstruction (SPARSE-REF) for 1971–75. (a) Spatial pattern of skill β (dashed 0.9 contour). (b) Spatial pattern of relative bias: difference between reconstructed and observed mean of the validation period, scaled by the standard deviation of ANALYSIS. (c) Time dependence of spatial β for the reconstruction (solid) and the filtered ANALYSIS (dashed). The dash-dot line is the 5% significance level of a one-sided statistical test, based on a temporal randomization procedure. The overall skill β_{tot} is 0.77.

of the validation rmse, and it provides a good upper bound on the error. Hence the OI method was successful in estimating the error structure from calibration data alone, a valuable feature for a real application.

The relative reconstruction error is $e^r = 0.23$, corresponding to a loss of total variance of 23% (see Eq. 2.11). The reconstruction error can be divided into contributions from space truncation and from estimation (see Eq. 2.7). For the reference reconstruction, the relative truncation error $e^t = 0.16$ amounts to roughly twice the relative estimation error $e^e = 0.07$, and hence corroborates the previous finding that the skill of the reference reconstruction is mainly limited by the EOF truncation.

It is worth noting that the lower relative skill and bias of the reconstruction over the poorly sampled flatlands of France (Fig. 2.9) does not contradict the selection procedure for SPARSE-REF. The sample was constructed for overall representativity in terms of resolved variance. The SPARSE-REF sample is therefore adapted to regions of high variance (i.e. mountainous regions) where sampling is more favorable for the overall skill. While this preference is at the expense of the relative performance over the flatlands, it is of no disadvantage to the absolute performance as measured by the rmse (Fig. 2.10).

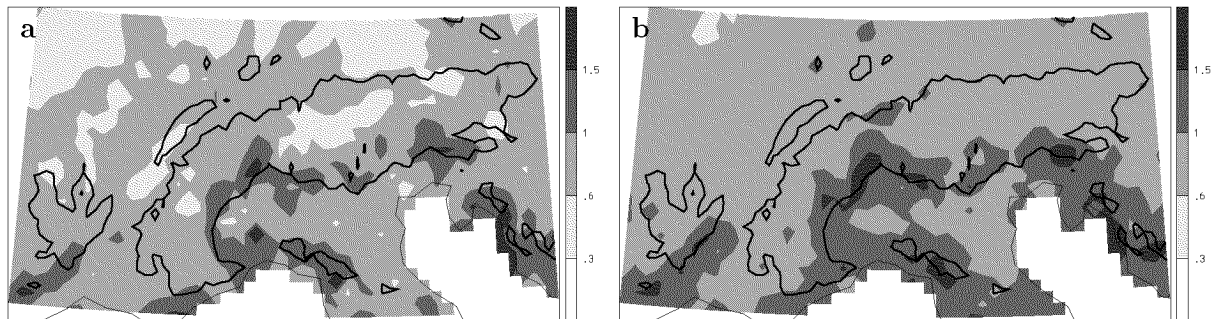FIG. 2.10:   Root mean square error [mm day^{-1}] of the reconstruction for SPARSE-REF. (a) Error from the five-year validation (1971–75), (b) theoretically expected error estimated from the calibration period. The average rmse is 0.68 (a) and 0.95 (b).

2.5.c   Multi-year means and variability

The study of multi-year fluctuations is an obvious application of a long-term dataset. The capability of the reconstruction to reproduce variations over several years is therefore of interest. Fig. 2.11a displays the deviation of the 1971–75 annual mean precipitation of the ANALYSIS from that of the 1976–90 mean. The difference is characterized by a west-east oriented, elongated positive anomaly along the Mediterranean coast and Mediterranean Alps, and a negative anomaly north of the Alps. Within this large scale pattern are many smaller-scale variations. Both large-scale anomalies and many of the smaller-scale features are well reproduced by the reconstruction (Fig 2.11b).

   This result illustrates the capability of the reconstruction method to reproduce comparatively small changes in multi-year climate. However, the suitability of the reconstructed fields for studying even longer-term variations (e.g. centennial trends) will depend critically on the homogeneity of the reconstruction sample, and on the stationarity of the EOF subspace and the local error variances.

2.5.d   Subdomain-mean variations

The validation has so far focussed on the skill at individual grid points. Evidently, a reconstruction on the scale of 25 km (the resolution of the analysis grid) is quite ambitious, and for a number of applications it is the performance on the scale of many grid points that matters most. Time series of domain-mean precipitation determined from the reconstruction are displayed in Fig. 2.12 for four regions (subdomains in Fig. 2.2b), and compared to the ANALYSIS. Also shown are domain-mean precipitation series from the CRU05, an alternative reconstruction (see section 2). All regions exhibit large month-to-month fluctuations, which are accurately reproduced by the reconstruction. The CRU05 is significantly correlated with the ANALYSIS, but shows weaker skill, both in terms of rmse and anomaly correlation (Table 2.1). Several factors can contribute to the difference between the reconstruction and CRU05: (i) The station sample used for CRU05, although more comprehensive (∼ 100 stations), is less representative than SPARSE-REF. (ii) The coarser grid resolution of CRU05 introduces interpolation errors in the estimation of subdomain-mean values. (iii) Our reconstruction profits from the exploitation of the spatial covariability by the EOF-based interpolation method.

ANALYSIS   Reconstruction
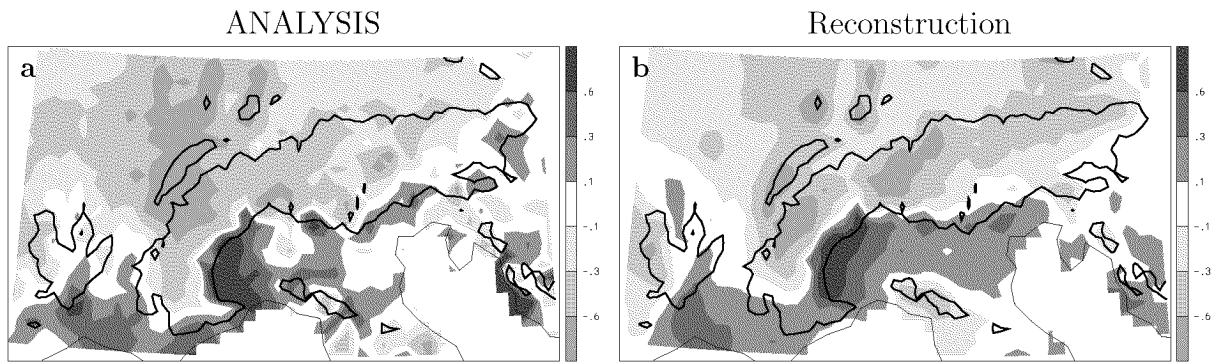
FIG. 2.11: Differences of mean annual precipitation [mm day^{-1}] between the periods 1971–75 and 1976–90: (a) in the ANALYSIS, (b) as reconstructed using the reference sample SPARSE-REF.

Entire domain   Mediterranean Alps

Massif Central   Vosges
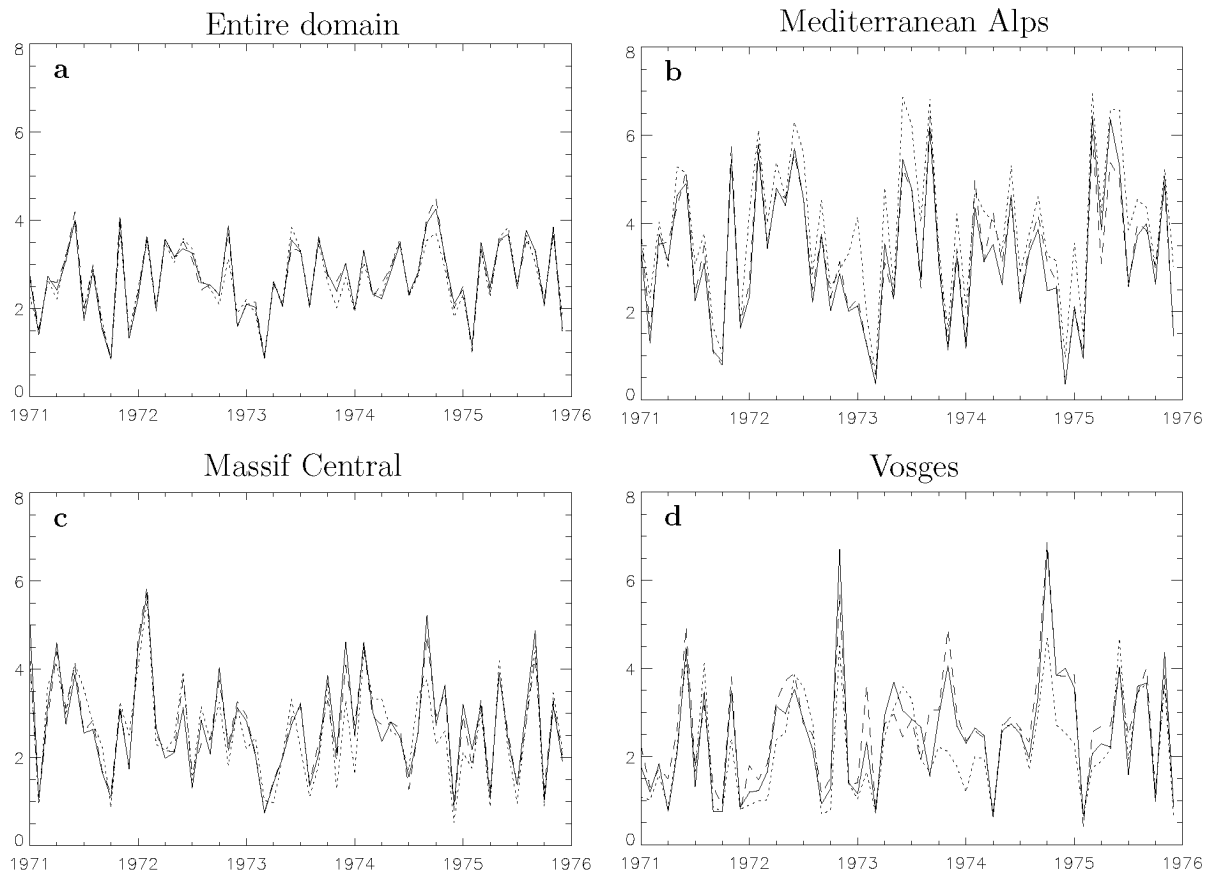
FIG. 2.12: Time series of subdomain-mean precipitation [mm day^{-1}] calculated from observations (ANALYSIS, solid), from the reference reconstruction (SPARSE-REF, dashed), and from a global precipitation dataset (CRU05, dotted); the subdomains are indicated in Fig. 2.2b.

TABLE 2.1: Skill for subdomain-mean precipitation for four characteristic regions calculated from the reference reconstruction and from the CRU05 data, respectively. Correlations r and rms [mm day^{-1}] differences with respect to the ANALYSIS are tabulated

Region	Reconstruction r	Reconstruction rms	CRU05 r	CRU05 rms
Entire domain	0.99	0.10	0.97	0.21
Mediter. Alps	0.99	0.27	0.96	0.83
Massif Central	0.97	0.30	0.89	0.55
Vosges	0.95	0.43	0.88	0.70

2.6   Sensitivity analyses and comparison of methods

The validation of section 5 is for a reconstruction using the objectively chosen sparse station sample SPARSE-REF and predefined calibration and validation periods. In this section, we examine the sensitivity of the reconstruction skill to the choice of the calibration period (a), to local representativity (b), and to the size and spatial distribution of the reconstruction sample, i.e. global representativity (c). Finally, a brief comparison of the OI reconstruction with the projection-type method of Smith et al. (1996) is presented (d). The sensitivity analyses will enable the assessment of the performance of a real reconstruction and identify critical factors for its improvement.

2.6.a   Sensitivity to calibration period

A fundamental precondition for the ability of the reconstruction method (in fact for any statistically based method) to reproduce historical climate variations is the stationarity of the relationship between the mesoscale precipitation pattern and the data of the reconstruction sample. In our case this involves the stationarity of the local error variances and of the phase space spanned by the leading EOFs (not necessarily the patterns of individual EOFs themselves). Proving the long-term stationarity is difficult for the present feasibility study, and even in a real application it can be assessed only from independent long-term data.

   To assess the sensitivity to the choice of the calibration period, the performance of the method was examined for an ensemble of 10 different calibration periods, selected randomly from the full period (1971–90). The length of the calibration and validation periods, as well as the reduced-space dimension and the reconstruction sample (SPARSE-REF) were chosen as in section 5. The mean overall skill and standard deviation for these experiments is $\beta_{tot} = 0.76 \pm 0.02$. Thus the skill for the reference calibration period ($\beta_{tot} = 0.77$, see section 5) is contained within one standard deviation. Further evidence for the stationarity of the reduced subspace is provided by the robustness of the rotated EOF patterns within the ensemble (not shown). These results suggest the absence of serious non-stationarity for the period considered, but they cannot rule out such an effect over a longer time-scale.

   In terms of non-stationarity, a likely important factor for a long-term Alpine reconstruction is the North Atlantic Oscillation, measured in terms of the North Atlantic Oscillation Index (NAOI). The NAOI is a standardized scalar measure of westerly low-level circulation over the Northern Atlantic. It has been shown to be associated with variations
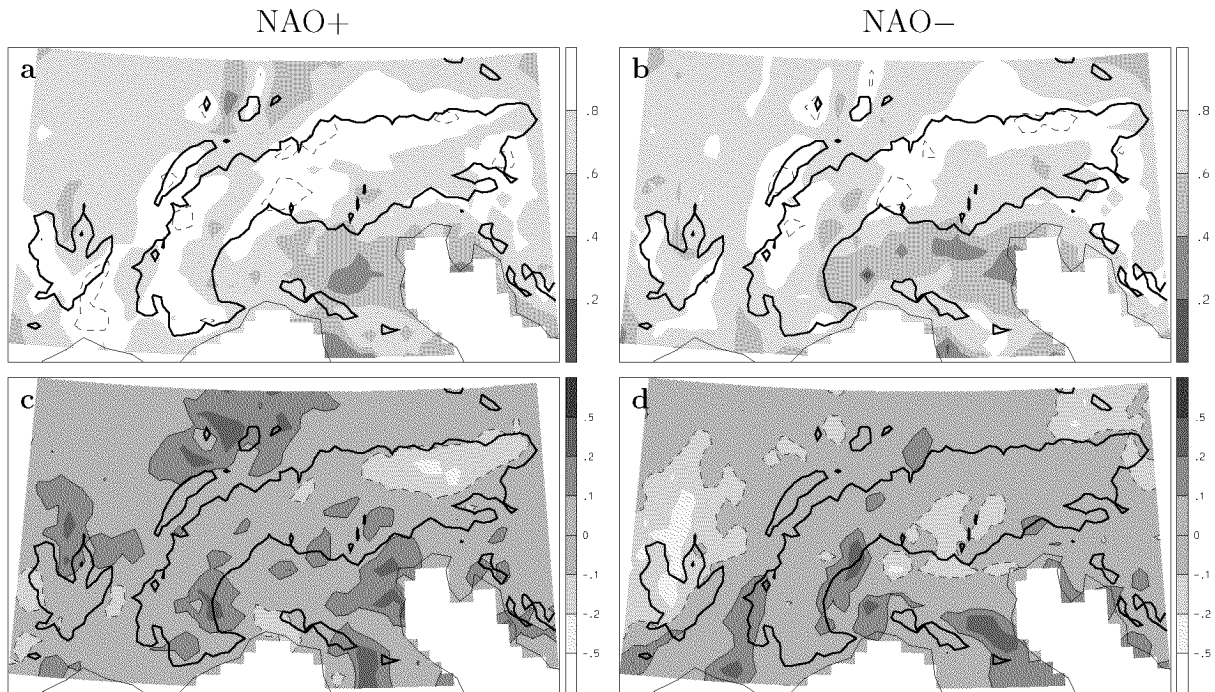
NAO+   NAO−

FIG. 2.13: (a, b) Skill β and (c, d) relative bias for a reconstruction calibrated with positive NAO months (NAO+) and negative NAO months (NAO−), respectively. The skill shown is for the independent validation period. Contours as in Fig. 2.9.

of weather types (e.g. Stefanicki et al., 1998) and the distribution of precipitation (Hurrell and van Loon, 1997) over Central Europe. The NAOI has exhibited a pronounced long-term trend during the 20th century (Hurrell, 1995, 1996). In our context, it is thus of interest to examine the sensitivity of the reconstruction model to the variations of the NAOI.

For this purpose, the reconstruction model is calibrated using months with positive (negative) NAOI and reconstructed for the independent validation period with negative (positive) NAOI. The set of "positive NAOI" months (NAO+) is defined, as those months where the NAOI is above its median for the corresponding month of the year. This results in two independent 10-year sets. Fig. 2.13 shows the β-maps and the biases for the two experiments. The skill patterns are very similar, and they are in agreement with the pattern of the reference reconstruction. Surprisingly, the bias even tends to be smaller than for the reference reconstruction. The overall skill β_{tot} for NAO+ is 0.74, compared to 0.75 for NAO−. These values can be compared to 20 independent reconstructions using 10 years of randomly chosen months with average skill $\beta_{\text{tot}} = 0.74 \pm 0.01$. (Notice the slightly lower average skill compared to the previous cross validation using 15 years for the calibration.) The NAOI-split calibrations perform similar to a random calibration period. Hence, from the short observational period at hand, there is no evidence for a NAO sensitivity of the reconstruction approach.

2.6.b Local representativity

The reconstruction procedure uses rain gauge records to sample area-average precipitation at analysis grid points. (Section 3b describes the procedure for assigning a grid point to

TABLE 2.2: Reconstruction results for four sets of random station samples of size K, each averages over 100 realizations. The columns refer to statistics for the four sets: mean and standard deviation of overall reconstruction skill (β_{totGP}), mean estimation error using grid points (e^e_{GP}), specific estimation error for one particular realization using stations (e^e_{ST}), and estimation error for covariance-guided sample using stations (e^e_{cov}).

K	β_{totGP}	e^e_{GP}	e^e_{ST}	e^a_{cov}
27	0.69 ± 0.02	0.16	0.21	0.12
54	0.75 ± 0.02	0.09	0.13	0.07
100	0.79 ± 0.01	0.05	0.09	–
150	0.810 ± 0.003	0.03	0.07	–

a particular rain gauge station.) It must be expected that the reconstruction quality will depend on the representativity of the selected sample stations. The limitations in local representativity are cast in the local error ϵ^o_n (see Eq. 2.2). The relevance of local representativity is investigated by comparing the reference reconstruction to results from a "perfectly representative" (SPARSE-PR) and a "non-representative" (SPARSE-NR) reconstruction sample. Both samples are based on the same gridpoint distribution as SPARSE-REF, but the gridpoint series themselves (rather than station series) are used for SPARSE-PR, and the stations with the lowest correlation with the grid points are used for SPARSE-NR.

The overall reconstruction skill β_{tot} for the three samples is 0.79 (SPARSE-PR), 0.77 (SPARSE-REF), and 0.75 (SPARSE-NR). All three reconstructions are subject to the same truncation error $e^t = 0.16$, due to identical reduced-space dimension ($L = 24$). The differences between the samples are the sole consequence of a different estimation error e^e, which is 0.05 for SPARSE-PR, 0.07 for SPARSE-REF, and 0.09 for SPARSE-NR. Hence the local representativity is of minor importance for the overall skill, provided the station sample has good global representativity, as is the case for our covariance-guided samples.

2.6.c   Global representativity

The sensitivity of the reconstruction performance to size and spatial distribution of the sample is assessed by comparing the results of section 5 with results obtained using samples of 27, 54, 100 and 150 records, with random spatial distributions. For each sample size, an ensemble of 100 distributions was constructed. For this exercise, sample records were taken directly from the analysis grid points, rather than rain gauge stations, in order to isolate the influence of global representativity. The comparison of results is facilitated by setting the reduced space dimension to a fixed value ($L = 24$) for all reconstructions. Table 2.2 summarizes the results of these experiments.

The mean overall reconstruction skill (β_{totGP}) increases from 0.69 for sample size 27 to 0.81 for sample size 150, indicating a substantial improvement of the performance for denser reconstruction samples. At the same time, the standard deviation of the skill decreases from 0.02 to 0.003, showing that the reconstruction becomes less sensitive to the spatial distribution if a large number of stations are available (at least within the range of random distributions). The mean estimation error e^e_{GP} decreases from 0.16 to 0.03.

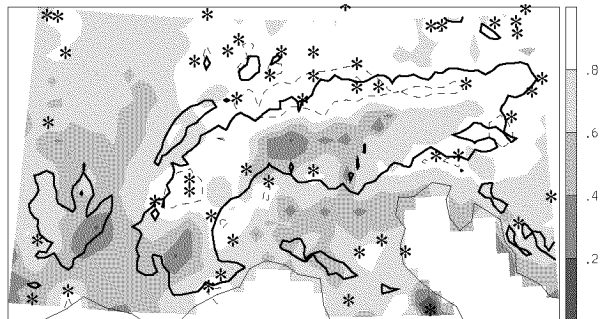For comparison of the random samples with the covariance-guided station samples, an

FIG. 2.14: Reconstruction skill β for a random (SPARSE-RAN, 51 stations) station sample (see text for details). The overall skill β_{tot} is 0.71. Contours as in Fig. 2.9.

additional reconstruction is undertaken using station data adjacent to the selected grid points for the realization with average performance in each of the ensembles. The resulting estimation error (see column e^e_{ST} of Table 2.2) increases by typically 0.04 with respect to the gridpoint reconstruction. These values represent expected values of the skill from reconstructions with a random station sample. Comparison with the covariance-guided station samples (produced for $K = 27$ and $K = 54$, e^e_{cov} in Table 2.2) indicates the benefit of a globally representative station distribution. The representative samples reduce the estimation error by about 50%, an improvement which is well beyond the band-width obtained for the random distributions.

Fig. 2.14 displays the station distribution and the β-map for a sample that produced average overall performance in the ensemble with $K = 54$ random stations (SPARSE-RAN). Compared to SPARSE-REF (Fig. 2.9a), SPARSE-RAN shows slightly higher skill north of the Alps, where many of the stations are clustered. Some regions, however, exhibit particularly low skill ($\beta < 0.4$), such as parts of southern France and the central part of the southern rim (south-eastern Switzerland). In the latter region the skill is low despite the presence of three stations nearby. The overall skill β_{tot} is equal to 0.71, compared to 0.77 for SPARSE-REF.

This example illustrates the possible outcome of a reconstruction with typically 50 long-term records if important parts of the spatiotemporal precipitation variability are unsufficiently sampled by the reconstruction network. It shows that for small samples the performance depends critically upon the spatial distribution of the network. The benefits from a *suitably* located station may well recompense the efforts required for data digitization, homogenization, and quality processing; whereas the same efforts may result in marginal benefit in cases of ill-positioned stations. The set of rotated EOFs provides a direct guide to the critical sampling locations. The covariance-guided network described in section 4 assures some sort of global representativity by avoiding excessive sampling in some areas at the expense of others.

Any forthcoming Alpine reconstruction will inevitably be confronted with a highly variable density of the centennial networks between individual countries. For example, for Switzerland there are more than hundred records available at present, but many less for the other countries. It is not clear, if such a high station density in Switzerland would result in lower reconstruction skill in the poorly-sampled areas. However, further tests (not shown) indicate that this is not a problem, provided there is a good primary representation of the entire domain by the sample. In this case, a regionally denser network is beneficial and there is no need to exclude any stations.
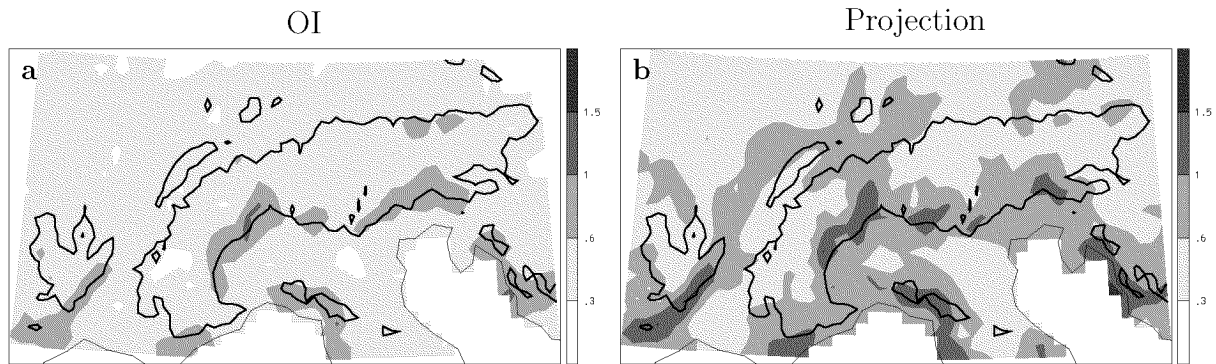
OI   Projection

FIG. 2.15:   Root mean square error [mm day^{-1}] of the estimation error for the OI- and projection method. Reconstruction with the reference sample SPARSE-REF and reduced-space dimension $L = 24$.

2.6.d   Comparison of the OI and projection method

The OI reconstruction applied here and the projection method of Smith et al. (1996) are related in terms of their reduced-space representation, but differ in the details of the least-squares estimation (see Eq. 2.8 in section 3). Fig. 2.15 compares the rms estimation error of the OI and projection solution. (Both reconstructions were carried out with a reduced-space dimension $L = 24$ and the same reconstruction sample SPARSE-REF.) The general pattern of rmse is very similar, but the OI solution produces notably lower values. The overall estimation error of the projection method is $e^e = 0.17$, compared to $e^e = 0.07$ for the OI. A comparison of reconstruction skills for individual EOF modes (not shown) showed that the projection method generates excessive variance in the higher-order modes (small scales). The better performance of the OI method is due to its inherent damping of the high-order modes. This finding is in agreement with the results of Kaplan et al. (1997) for their comparison of the same methods for SST reconstruction.

2.7   Conclusion

This study has examined the feasibility of reconstructing mesoscale precipitation fields from sparse long-term rain gauge records, using an EOF-based statistical method. To our knowledge this is the first reconstruction attempted for a climate parameter with pronounced variability on spatial scales of a few 10 kilometers. The region of the Alpine mountain range has provided a rigorous test ground considering its complex physiography and spatiotemporal precipitation variability.

Using a specific test sample of 53 stations, which was chosen to be "representative" for the observed precipitation variability in the region, the reconstructed monthly precipitation fields explain 77% of the total variance of a mesoscale analyses (obtained from about 6000 rain gauge stations). Months with a comparatively poor skill (60% explained variance) are found mostly in summer, but the seasonal variation of the mean skill is small. Reconstructed gridpoint time series account for typically 60–90% of the observed variance. When considering subdomain-means of $100 \times 100\,\text{km}^2$ or larger, the resolved variance increases to 90–98%. The reconstruction reproduced, with good accuracy, the pattern and magnitude of the long-term precipitation anomaly of an independent five-year

validation period. Theoretical estimates of the error from calibration data alone have been shown to provide a good estimate of the true error (i.e. that seen in an independent cross validation).

The skill of the reconstruction was found to be close to that expected from a perfect reconstruction using the same phase-space truncation. For sample sizes between 50 and 100 stations, the error component attributable to the truncation is typically twice as large as that from the reconstruction step. Less stringent truncation does not improve the overall performance, because the sampling of higher-order modes is limited by the low-density of the reconstruction records. However, a reduction of the truncation error can be expected if a sample with well above 100 stations would be available.

The spatial distribution of a reconstruction sample was identified as a critical factor for samples with less than 100 stations. "Representative" samples, obtained by a covariance-guided station selection procedure which exploits the observed space-time variability, showed superior performance compared to randomly distributed samples of the same size. The reference sample (53 stations), for instance, had the same overall skill as that expected for a random sample with 150 stations. In contrast to the domain-wide distribution, the details of station location (local representativity) did not have a big influence on the reconstruction results.

A priori knowledge about sampling locations providing good overall representativity can be valuable, even if in practice the distribution of long-term records for a reconstruction cannot be chosen to match ideal sampling locations. The information allows ranking of costly digitization, quality control and homogenization efforts aimed at processing additional long-term series. This is especially valuable in the Alpine region, where probably more than 150 centennial series are available, but in many cases require costly preparation from printed records, and generation of station histories for homogenization purposes.

An elementary assumption of the reconstruction method is the stationarity of the spatial covariance structure and its representation by the sample network. A proof of this assumption for the centennial time-scale cannot be given from this feasibility study. In fact, it will be even difficult to achieve when long-term data is included. However, the results of the reconstruction experiments (section 6) show only very minor dependence on the calibration period, even when the calibration is restricted to a single phase of the North Atlantic Oscillation.

This study affirms the feasibility of reconstructing mesoscale precipitation in the Alpine region. The results show the potential of EOF-based reconstruction methods for regional applications and for spatial resolutions that were not the primary focus of such methods in the past. The promising results motivate the use of these techniques for other parameters and regions where the physiography imposes complex patterns of variability. As a next step, we plan to apply this methodology to Alpine precipitation covering a centennial period, a task that requires a comprehensive effort to acquire, digitize, validate and homogenize long-term precipitation records.

of the Environment Contract EPG 1/1/16) on behalf of the Climatic Research Unit, University of East Anglia.

3 Mesoscale precipitation variability in the region of the European Alps during the 20th century

JÜRG SCHMIDLI[1], CHRISTOPH SCHMUTZ[2], CHRISTOPH FREI[1], HEINZ WANNER[2], AND CHRISTOPH SCHÄR[1]

[1]*Atmospheric and Climate Science, ETH Zürich, Switzerland*
[2]*Geography, University of Berne, Switzerland*[†]

Abstract

The purpose of this study is to construct and evaluate a new gridded analysis of precipitation that covers the entire region of the European Alps (3.2°–16.2°E, 43.2°–48.8°N), resolves the most prominent mesoscale variations (grid spacing 25 km) and extends with a monthly time-resolution over most of the 20th century (1901–90). The analysis is based on a reconstruction using the reduced-space optimal interpolation technique. It combines data from a high-resolution network over a restricted time period (1971–90) with homogeneous centennial records from a sparse sample of stations. The reconstructed fields account for 78% of the total variance in a cross-validation with independent data. The explained variance for individual grid points varies between 60–95% with lower skills over the southern and western parts of the domain. For averages over 100×100 km² subdomains, the explained variance increases to 90–99%. Comparison of the reconstruction with the CRU05 global analysis reveals good agreement with respect to the interannual variations of large subdomain averages (10000-50000 km²), some differences in decadal variations, especially for recent decades, and physically more plausible spatial patterns in the present analysis.

The new dataset is exploited to depict the 20th-century precipitation variations and the correlations with the North Atlantic Oscillation. A linear trend analysis (1901–90) reveals an increase of winter precipitation by 20–30% per 100 years in the western part of the Alps, and a decrease of autumn precipitation by 20–40% to the south of the main ridge. Correlations with the North Atlantic Oscillation Index (NAOI) are weak and highly intermittent to the north and weak and more robust to the south of the main Alpine crest, indicating that changes in the NAOI in recent decades are not of primary importance in explaining observed precipitation changes.

3.1   Introduction

Precipitation is a key-element of the hydrological cycle. Accurate quantification of its observed variability on interannual to centennial time-scales is required for a number of purposes. These include the assessment of present and past climate variability (e.g. Groisman and Legates, 1995); the validation of numerical weather predicition models (e.g. Mladek et al., 2000), general circulation models (GCMs) (e.g. Airey and Hulme, 1995; Murphy, 1999; Widmann and Bretherton, 2000), and regional climate models (RCMs) (e.g. Jones et al., 1995; Lüthi et al., 1996; Fukutome et al., 1997; Murphy, 1999); the use for ecosystem and hydrological impact modelling; and the construction of regional climate change scenarios by statistical downscaling techniques (e.g. Cubasch et al., 1996; Wanner et al., 1997; Wilby et al., 1998; Zorita and von Storch, 1999; Widmann and Bretherton, 2000).

Current knowledge on precipitation variability in the region of the Alpine mountain range in Central Europe stems from numerous studies that were devoted to specific subregions. As regards the analysis of long-term trends, the studies by Auer and Böhm (1994), Widmann and Schär (1997), and Buffoni et al. (1999), for example, have considered observational records from Austria, Switzerland, and Italy, respectively. Their results provide evidence for regionally varying trends of mean seasonal precipitation. However, a direct comparison of the results is complicated by differences in the temporal extent and spatial density of the underlying standards and differences in the analysis procedure (e.g. station-based versus area-mean trends). Consistent Alpine-wide precipitation analyses are in principal available but they suffer from other drawbacks. The Alpine section of global and continental-scale analyses (e.g. Xie et al., 1996; Dai et al., 1997; New et al., 1999, 2000), for example, exhibit a grid spacing between 50–250 km, but their effective resolution (Grasso, 2000) is considerably coarser, especially in mountainous terrain where precipitation varies over short distances and the availability of station data was limited for these analyses. Similar limitations in spatial resolution are to be expected for the supraregional trend analysis of Schönwiese et al. (1994) and Schönwiese and Rapp (1997). The 25 km-resolution objective analysis of Frei and Schär (1998) covers the entire mountain range and resolves the major mesoscale patterns, but it is restricted to a 20-year time period.

The aim of the present study is to establish and evaluate a new gridded analysis of precipitation that covers the entire region of the European Alps, resolves the most prominent mesoscale variations (grid spacing 25 km) and extends with a monthly time-resolution over most of the 20th century (1901–90). The new gridded dataset is exploited to derive an Alpine-wide picture of precipitation variations and centennial trends, and to examine the relationship between winter-time precipitation and the North Atlantic Oscillation (NAO).

The reconstruction of the mesoscale precipitation fields is based on the reduced-space optimal interpolation method of Kaplan et al. (1997), which was originally used for reconstructions of sea surface temperature. The method has been adapted and tested for the reconstruction of Alpine precipitation in a preceding feasibility study (Schmidli et al., 2001). The basic idea of the method is to combine spatially dense observations from a short period with sparse observations over a long period. The dense short-term component consists of gridded monthly precipitation fields derived from high-resolution surface networks (6800 rain-gauge stations, 1971–90) and the sparse long-term component comprises
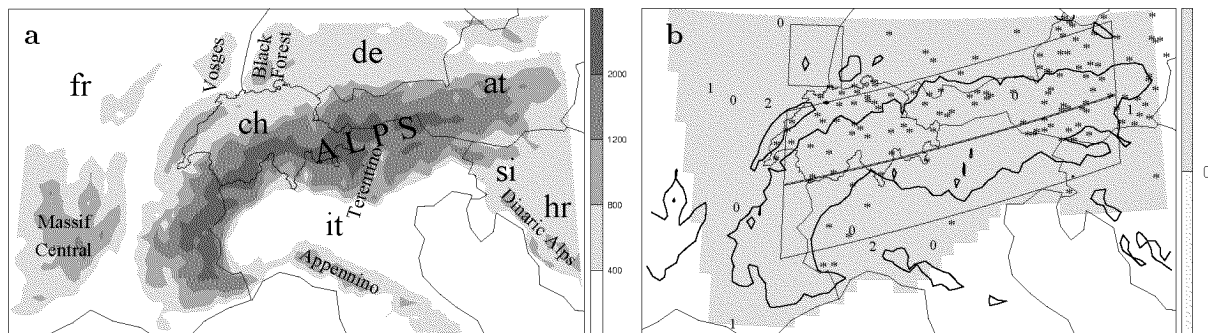
FIG. 3.1: (a) Map of the study region showing the Alps and the surrounding foreland area. Depicted is the height above MSL (shading) and the political boundaries (fr: France, ch: Switzerland, it: Italy, ge: Germany, at: Austria, si: Slovenia, hr: Croatia). (b) Location of the 140 stations (stars and numbers) used for the reconstruction. Thick lines (800 m MSL contour) depict the main topographic features. The boxes indicate the subregions used for validation: Vosges (top), N-Alps (middle), and S-Alps (bottom). The numbers indicate stations with some missing data in the period 1986–90 (0), the period 1901–85 (1), and with more than ten missing monthly values prior to 1985 (2).

140 homogeneous station records extending back to the beginning of the 20th century. The statistical combination of the two datasets involves a decomposition of the dense component into a set of dominant modes of space-time variability using Principal Component Analysis and the estimation of the coefficients of the modes from the sparse component using least-squares optimal estimation. Particular benefits of this reconstruction method are the reproduction of spatial variations beyond the scale resolved by the sparse network alone, and a high level of temporal homogeneity due to the use of a time-constant reconstruction network and rigorous testing of its original data.

Section 2 presents the data used for the reconstruction and is followed by a description of the reconstruction method in section 3. The reconstructed fields are then validated in section 4. Results on long-term Alpine precipitation variability and trends as well as the relationship with the NAO are discussed in section 5. Section 6 finally provides a comparison of the new reconstruction with the Alpine section of a global dataset, followed by concluding remarks in section 7.

3.2   Data

The reconstruction of mesoscale precipitation fields is carried out for the region of the European Alps (3.2°–16.2°E, 43.2°–48.8°N). The topographic structure of the study region is displayed in Fig. 3.1a. The main feature is the arc-shaped mountain range of the Alps extending in west-east direction over a distance of 800 km across five countries. The reconstruction and analysis of centennial precipitation variations in this region proceeds from two datasets: a high-resolution gridded monthly precipitation analysis for the recent decades, and a comparatively sparse sample of homogenized station records extending back to the beginning of the 20th century. These two datasets are described in subsections (a) and (b), respectively. For comparative purposes, this study also makes use of the Alpine window from a global precipitation analysis, which is discussed in subsection (c).
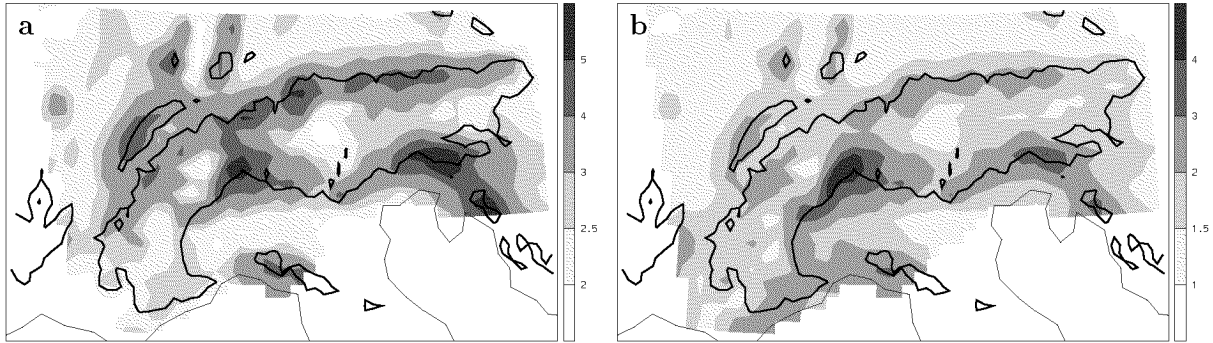
FIG. 3.2: (a) Mean annual precipitation and (b) standard deviation of monthly precipitation for the period 1971–90 [mm day^{-1}], as inferred from the ANALYSIS dataset. The bold line represents the 800 m topographic contour.

3.2.a   Gridded data

The high-resolution gridded dataset, hereafter referred to as ANALYSIS, consists of monthly precipitation fields for the period 1971–90 with a grid spacing of 25 km (0.22° lat × 0.3° long). It was derived from 6800 station records of the operational high-resolution rain-gauge networks in the Alpine region (Frei and Schär, 1998). The spatial analysis was derived using a modified version of the SYMAP algorithm (Shepard, 1984; Willmott et al., 1985) and represents area-average precipitation in the surrounding of each of the 928 land grid points. The original rain-gauge network exhibits a typical inter-station distance of 10–15 km and hence the effective resolution of the ANALYSIS is close to 25 km over most parts of the study domain. For some parts of northern Italy, the effective resolution may however be slightly inferior to the grid spacing. Details of the rain-gauge dataset and the analysis procedure are given in Frei and Schär (1998).

Fig. 3.2 displays the mean annual climatology and the monthly standard deviation of Alpine precipitation, as represented by the ANALYSIS. Mean annual values vary between 1.5–8 mm day^{-1}. The main features of the spatial distribution are two high-precipitation bands extending along the northern and southern rim of the Alpine ridge, and drier conditions in the interior of the mountain range and over the adjacent flatland. The maximum along the southern rim is divided into two major wet zones, centered over southern Switzerland/northern Italy and over eastern Italy/Slovenia, respectively. The monthly precipitation patterns exhibit pronounced seasonal and interannual variations, as reflected in the standard deviation (Fig. 3.2b). Regions with high standard deviation coincide with regions of high annual means.

3.2.b   Long-term station records

The sparse dataset comprises 140 long-term station records covering the period 1901–90.[1] Fig. 3.1b displays the distribution of stations. The network exhibits the densest coverage over the northern and eastern parts of the domain, while lower coverage is obtained for the southern Alps, the French flatlands, Slovenia, and Croatia. The south-western tip of the Alpine ridge is not sampled at all. The partition between the countries is: Austria 76 stations, Switzerland 37, Italy 12, southern Germany 8, France 6, Croatia 1.

---

[1]see Appendix H

The substantial inhomogeneity of the station coverage is a particular challenge for the reconstruction of area-covering fields. In terms of temporal coverage the sparse dataset is near to complete: For the period 1901–85, six stations have incomplete data, and only two of those have more than 10 missing monthly values, but still less than 1% (see special marks in Fig. 3.1b). For the period 1985–90, eight stations have missing data, two of which miss more than 50%. The station coverage during the last five years is therefore not representative for the rest of the century.

Long-term station records can be affected by station relocations, changes in local environment, instrumentation changes, and observation practices (see e.g. Groisman and Legates, 1995). To alleviate the temporal inhomogeneities in the long-term records, the dataset was subjected to a rigorous homogenization procedure. In fact, the final station sample was selected from a database of 478 records, based on criteria of a multi-step homogeneity test. For this purpose, the Alexandersson test (Alexandersson, 1986) has been employed which has been shown to be particularly powerful in identifying undocumented shifts in monthly time series (Easterling and Peterson, 1995), especially for precipitation (Aschwanden et al., 1996).

The homogeneity test consists of four steps: In the first step, using all stations, the homogeneous records to be used for building the reference time series are determined. A station record is considered homogeneous if it passes the test at a probability level of 5%. In the second step, all stations are tested using the previously determined homogeneous records to build the reference series. The reference time series are determined by a correlation-weighted mean of the five homogeneous records with the highest correlation with the candidate series. Again, a station is considered homogeneous if it passes the test at the 5% level. In the third step, records considered non-homogeneous in the first two steps are adjusted according to the ratio method of Alexandersson (1986). In the final step, the adjusted and non-adjusted station records are subjected to a final test, and those that pass the test at the 5% level are considered homogeneous, except those which failed one of the first two steps at the 0.1% level. Details of the homogenization procedure for this particular dataset are described in Schmutz (2001).

Homogenization via reference time series can be expected to account for changes at individual stations but may be less effective in identifying changes that affect the entire station sample simultaneously. To obtain a complete overview of network-wide changes is difficult due to the lack of meta-data information for our long-term records. In Austria, several systematic changes have occurred due to variations in rain-gauge orifice and shielding (Auer et al., 2001). In contrast, the principal observing practice in Switzerland has been largely consistent and stable throughout the 20th century, the principal measuring device beeing the Hellmann gauge (Müller and Joss, 1985). Of the Swiss records, only very few have been affected by automatization (in the 1980's) and these were only considered if they passed the homogeneity test.

From the complete original dataset (478 records) the homogenization procedure classified 79 records as homogeneous without adjustment and 61 records as adjustable, leading to the 140-station sample depicted in Fig. 3.1b. It is important to notice that the exclusions from the original dataset have mainly occurred in areas with dense coverage in Austria and Switzerland (283 out of 313 excluded records). Hence the application of less rigorous criteria would not improve substantially the poor coverage in France and Northern Italy.

It is interesting to compare the present long-term dataset with the reference station

sample (53 stations) introduced by Schmidli et al. (2001) with the objective of optimal overall representativity. The coverage of the present station network is denser in the northern Alps, but lower within the Alpine ridge, north-eastern Italy, along the Mediterranean coast, and in the south-western Alps.

3.2.c   Dataset for comparison (CRU05)

The reconstruction derived in this study will be compared against the Alpine section of the Climate Research Unit global climate analysis (New et al., 1999, 2000, hereafter CRU05). CRU05 has a grid spacing of 0.5 degrees and was derived from monthly station data using the "anomaly method" (see New et al., 2000). In this technique, grids of monthly anomalies relative to a standard normal period (e.g. 1961–90) are first derived, and then combined with a mean monthly climatology to arrive at fields of estimated mean monthly precipitation. For the Alpine window of CRU05, the mean climatology is based on 320 stations, and the monthly anomalies are estimated using 50–110 stations, the higher values being valid for the period 1951–1980 (M. New, personal communication).

3.3   Reconstruction method

The reconstruction is based on the reduced-space optimal interpolation technique of Kaplan et al. (1997). The basic idea of the method is to extract the modes of spatio-temporal variability from high-resolution observations over a limited time period and to subsequently estimate the coefficients of these modes from sparser long-term data. The method has been adapted and extensively tested for the reconstruction of mesoscale Alpine precipitation in Schmidli et al. (2001). It comprises three main steps: a principal component analysis (PCA) of the gridded fields, the assignment of each station record to a specific grid point, and the reconstruction of reduced-space principal components (PCs, the temporal EOF coefficients) from the sparse station data. Here we provide a brief summary of each of these steps as required for the discussion of the results in the later sections. A more detailed description of the method is given in Schmidli et al. (2001).

Step 1: A PCA of the high-resolution gridded fields (ANALYSIS) is conducted to arrive at a set of basis functions, the empirical orthogonal functions (EOFs). The EOFs are determined from the covariance matrix. They represent the spatial patterns of the dominant modes of precipitation variability in order of decreasing importance. Together with their corresponding PC time series, they provide a compact description of the original data. Next, the complete set of EOFs is truncated to a subset which captures the main signal of variability and discards unwanted noise. Some general rules have been proposed as to define a theoretically meaningful truncation point L, that is the number of modes to retain (see Preisendorfer, 1988, for a review of various rules), however, a suitable choice of the truncation level L often depends on the application under consideration (von Storch, 1995). In this study, the truncation point is determined by optimizing the reconstruction skill over an independent validation period (see below). The truncated representation of the ANALYSIS data using the first L EOFs will be referred to as the filtered ANALYSIS. It represents the best possible reconstruction that can be obtained by the method.

Step 2: Each station of the long-term network is considered as a predictor for a particular grid point of the ANALYSIS grid and is therefore assigned to one of the four nearest

grid points on the basis of the best explained variance. The station observations s° are subsequently linked to the respective gridpoint values by means of a linear transformation

$$s^\circ(t_j) = \hat{a} + \hat{b}\, s(t_j). \tag{3.1}$$

The coefficients $\hat{a}$ and $\hat{b}$ are estimated from a linear regression analysis between the station records and corresponding gridpoint records over the period 1971–90. This transformation has been newly introduced in this version of the reconstruction and is not included in Schmidli et al. (2001). Its purpose is to alleviate for systematic differences between the station and gridpoint records emanating, for example, from a non-representative exposure of the station compared to mean conditions in the grid pixel. In order to avoid overcalibration, the linear transformation is applied exclusively to stations where the null hypothesis $b = 1$ is rejected with an error probability of $p < 0.001$. This was the case for 21 out of the 140 stations.

Step 3: The final reconstruction step involves the estimation of the reduced-space PCs from the sparse station records using a least-squares estimation procedure (see Kaplan et al., 1997). The implementation of this step is similar to Schmidli et al. (2001). The result of the least-squares estimation procedure is a set of linear equations relating the estimates $\hat{pc}_l$ of the PCs to the K station records

$$\hat{pc}_l(t_j) = \sum_{k=1}^{K} w_{lk}\, \delta\tilde{s}_k^\circ(t_j) \qquad l = 1, \ldots, L, \tag{3.2}$$

where w_{lk} are the weights describing the linear relation, and $\delta\tilde{s}_k^\circ$ are the (transformed) station anomalies with respect to the mean of the corresponding ANALYSIS grid point. The reconstructed field $\hat{\mathbf{s}}$ at time t_j is then obtained from

$$\hat{\mathbf{s}}(t_j) = \overline{\mathbf{s}} + \sum_{l=1}^{L} \hat{pc}_l(t_j) \times \mathbf{eof}_l, \tag{3.3}$$

where $\overline{\mathbf{s}}$ is the mean field of the calibration period, and $\mathbf{eof}_l$ are the EOFs determined from the calibration. An advantage of the optimal interpolation method used in this study over other EOF-based methods (e.g. Smith et al., 1996; Mann et al., 1998) is the implicit damping of energy (i.e. the variance) for higher-order PCs in accordance with their estimation uncertainty. This results in substantially smaller reconstruction errors (Schmidli et al., 2001; Kaplan et al., 1997).

Missing data in the long-term station sample can be treated in two ways: either the weights w_{kl} are recalculated for each variation in the coverage of the station sample, or the anomalies $\delta\tilde{s}_k^\circ$ are set to zero for stations with missing data. The former method is preferable for highly variable station networks, while the latter, which is used here, is more practicable for almost constant networks with only few missing data.

Skill measures: The following evaluations of the reconstruction against the high-resolution ANALYSIS are based on standard skill measures such as the anomaly correlation and the root-mean-square error (rmse). In addition, the explained variance statistic β (e.g. Murphy and Epstein, 1989; von Storch and Zwiers, 1999) is used. Its generic form is

$$\beta = 1 - \frac{\sum (x - x_r)^2}{\sum (x_r - \overline{x}_r)^2}, \tag{3.4}$$
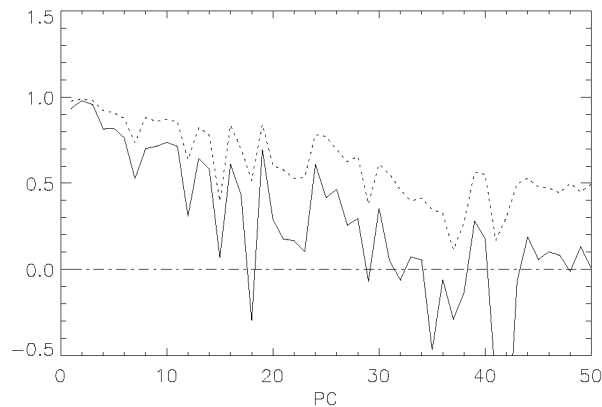
FIG. 3.3: Skill β (solid) and correlation skill r (dotted) of individual PCs for a reconstruction with reduced space dimension $L = 50$ for the validation period 1971–75.

where x is the series to evaluate (i.e. the reconstruction), x_r is the reference series (i.e. the ANALYSIS data), and $\bar{x}_r$ is the mean of the reference data over the period of comparison. In our evaluations, β will be determined either for the time series at individual grid points (summation over time) to yield a map of temporal correspondence, or for a reconstructed field at individual time (summation over space) to yield a time series of spatial correspondence.

The explained variance β is a rigorous measure of the similarity between two variables: It measures their correspondence not only in terms of the relative departures from their means, but also in terms of the means and absolute variances of the two series (Murphy and Epstein, 1989). The expected correspondence between two random series with equal variance is $\beta = -1$; a trivial "climatological" reconstruction results in a skill of $\beta = 0$. Reconstructions with $\beta > 0$ can be considered as skillful. Notice that the difference between the time series is measured relative to the local variance, and this facilitates the intercomparison of reconstruction skills between regions of differing variance.

Truncation: An appropriate selection of the EOF truncation point L depends critically on the number and distribution of the sparse stations. Here, we determined a suitable value of L by inspecting the reconstruction skill as a function of the number of PCs. For this purpose, reconstructions were calibrated for the period 1976–90, and validated over the independent period 1971–75. Fig. 3.3 shows the skill β and the anomaly correlation r for individual PCs using a truncation of $L = 50$. It is evident that for PCs larger than about 28, the skill β fluctuates around zero. In fact, a comparison of the overall skill as a function of L revealed minor improvements of the reconstruction with truncations beyond 30 (see also Schmidli et al., 2001). This result was robust upon other selections of calibration and validation periods. For the reconstruction of this study, the truncation point was chosen at $L = 28$.

3.4   Validation of reconstructed fields

In this section, the performance of the reconstruction is assessed by crossvalidation with the high-resolution ANALYSIS. The 20-year period (1971–90) is divided into five-year periods where the reconstruction is calibrated over 15 years and validated over the remaining five years. The results were found to be qualitatively similar between each set of calibration and validation, therefore only the validation for 1971–75 is discussed in full

TABLE 3.1: Overall performance for four independent validation periods. Tabulated are the total variance σ^2 [mm^2 day^{-2}] and the explained variance β. The latter is listed for the filtered (filt) and reconstructed (rec) fields, for a reconstruction with 28 (β) and 5 (β_5) EOFs, respectively. The values for the 1986–90 period (italics) are not representative for the centennial reconstruction, because there are many more missing station values in that period.

period	σ^2	β [%] filt	β [%] rec	β_5 [%] filt	β_5 [%] rec
1971–75	2811	89	77	73	68
1976–80	3327	89	78	74	70
1981–85	3255	90	79	78	74
1986–90	2954	88	*72*	75	*68*

detail.[2] The performance is assessed in several ways:

1. Overall performance: This is the fraction of total space-time variance of the ANALY-SIS explained by the reconstruction. It is calculated for each of the four independent periods.

2. Spatial performance: The skill in reproducing the temporal variations as a function of space is assessed by maps of explained variance β and root-mean-square error (rmse). The rmse is a measure of the absolute error, whereas $1 - \beta$ represents the error relative to the local variance. Additionally, the quality of reconstructed multi-year anomalies is assessed.

3. Temporal performance: The skill in reproducing the spatial pattern of precipitation expressed in terms of β is depicted as a function of time.

The above validations are complemented by an illustration of the model performance for a typical winter and summer month, by the analysis of time series of subdomain-mean precipitation, and by a discussion of possible improvements.

3.4.a   Overall performance

The overall performance β, that is the fraction of total variance explained by the reconstruction, is listed in Table 3.1 for the four independent validation periods. In spite of the substantial variations of the total variance σ^2 between the periods, the explained variance β remains at a similar level (77–79%). The lower value of 72% for the period 1986–90 is due to many missing data for that period. The average result for the three periods, $\beta = 78\%$, provides a conservative estimate of the overall performance of the final, centennial reconstruction. The true overall performance is expected to be slightly higher due to the longer calibration period for the centennial reconstruction — 20 instead of 15 years.

What causes the observed loss in variance? The reconstruction error can be separated into the error of space truncation, that is discarding the higher-order PCs, and the error in estimating the PCs from the sparse station data. The two error sources can be quantified

---

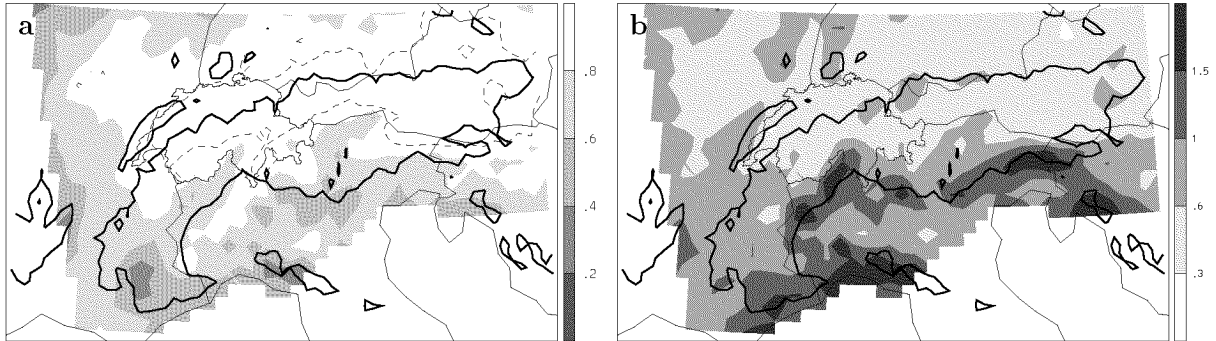[2]The results for all four periods are given in Appendix G.

FIG. 3.4:   Spatial performance for the years 1971–75. (a) Explained variance β (dashed the 0.9 contour), and (b) root-mean-square error [mm day^{-1}].

by $1 - \beta_{filt}$ and by $\beta_{filt} - \beta_{rec}$, respectively. For $L = 28$ they obtain a similar magnitude, amounting to a reduction of explained variance by about 11% each (see Table 3.1). For illustration, the explained variance is also reproduced for a reconstruction using only 5 EOFs (β_5). In this case the truncation error amounts to about 25% of the total variance and dominates the estimation error which is in the order of 5%. It is also illustrative to compare the overall performance of this reconstruction with that achieved from the smaller, but more evenly distributed and globally representative, reference station sample (53 stations) of Schmidli et al. (2001). While the overall performance is similar, the estimation error for the reference sample is smaller (c.f. Table 2 of Schmidli et al. 2001). This indicates that the uneven distribution of stations available for the present study is a limiting factor for the reconstruction skill and improved performance could be achieved by improving the data coverage over poorly sampled areas.

3.4.b   Spatial performance

Fig. 3.4 depicts a map of explained variance β, determined for each grid point. The spatial pattern of β is characterized by high skill ($\beta > 0.9$) along the northern Alpine flank and low skill ($\beta \approx 0.6$) in the southern- and western-most part of the domain. Areas of low skill correspond to regions with low to very low station density in the reconstruction sample (Fig. 3.1b).

   The absolute error measure, the rmse, is shown in Fig. 3.4b. North of the Alpine crest the rmse is generally smaller than 0.6 mm day^{-1}, whereas to the south and along the western boundary of the domain it is larger than 0.6 mm day^{-1}. The highest values, locally above 1.5 mm day^{-1}, are found in regions with very high precipitation amounts and variability along the southern Alpine rim (c.f. Fig. 3.2), and in regions with very poor station coverage along the Mediterranean coast. Relative to the local standard deviation, the error for individual grid points is typically 10–30% for the Alpine ridge, and 30–60% for the Terentino and Po valley, the south-western tip of the Alps, and along the western boundary of the domain (cf. Fig. 3.4a). In comparison to the reconstruction from the reference sample of Schmidli et al. (2001), the skill of the present reconstruction is higher north of the Alpine ridge, but lower to the south of the ridge.

   The capability of the reconstruction to represent multi-year variations is assessed by comparing observed (ANALYSIS) and reconstructed five-year means. Fig. 3.5 displays the
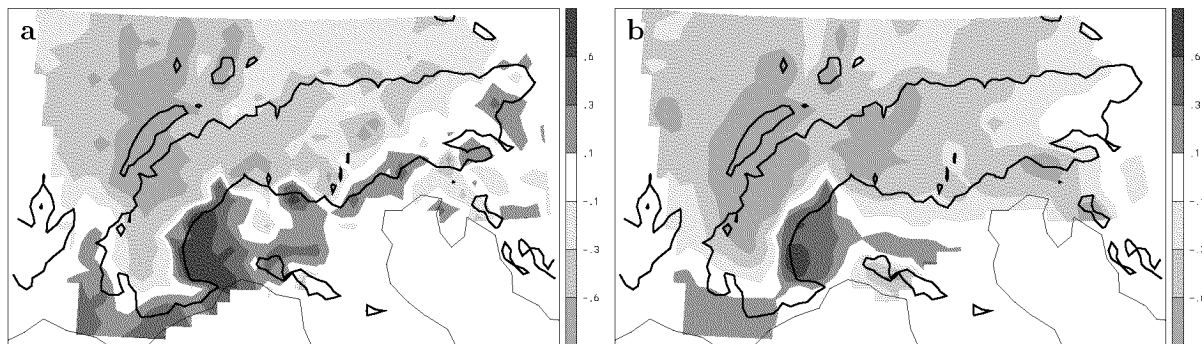
FIG. 3.5: Differences of mean annual precipitation [mm day^{-1}] between the periods 1971–75 and 1976–90: (a) in the ANALYSIS, (b) in the reconstruction.

deviation of the 1971–75 mean precipitation from that of the 1976–90 mean. The observed (i.e. ANALYSIS) difference is characterized by a west-east oriented, elongated positive anomaly along the Mediterranean coast and Southern Alps, and a negative anomaly north of the Alps. Within this large scale pattern are many smaller-scale variations. Both the large-scale anomalies and many of the smaller-scale features are well reproduced by the reconstruction (Fig. 3.5b). Note the evidence of the truncation in the smoother appearance of the reconstructed field, and the good representation of the structure located at the south-western tip of the Alps, an area not sampled directly (see Fig. 3.1b). This illustrates the capability of the reconstruction method to reproduce comparatively small changes in multi-year climate, also in areas not sampled.

3.4.c   Temporal performance

Fig. 3.6 shows the spatial correspondence of precipitation fields (as measured by spatial β) for the period 1971–75. There are large month-to-month variations; the lower and upper quartiles of β are 0.67 and 0.80, respectively. The reconstruction skill is statistically significant for all months. Months with particularly low skill seem to occur mainly in summer. However, the seasonal variation of the mean skill is small compared to the month-to-month variations: The median (inter-quartile range) of β is 0.76 (0.14) for winter, 0.74 (0.13) for spring, 0.71 (0.19) for summer, and 0.71 (0.21) for autumn. Comparison with the filtered ANALYSIS shows that the temporal variation is largely determined by the representation of a particular month in the reduced-space spanned by the leading L EOFs.

3.4.d   Illustration: Two typical months

Fig. 3.7 compares reconstructed fields and original analyses for two selected months (February 1981, June 1983). The spatial β for these cases is equal to the average skill and hence the two months are representative for reconstructions in winter and summer, respectively. The winter month, February 1981 (Fig. 3.7a), is dry throughout the Mediterranean and northern Italy, whereas moderate precipitation, interspersed with various maxima, occurs to the north of the Alpine ridge and in Slovenia. The reconstruction (Fig. 3.7c) reproduces accurately the large-scale pattern and also the location and magnitude of many of the fine-scale anomalies. However, the precipitation along the Ligurian coast, a region
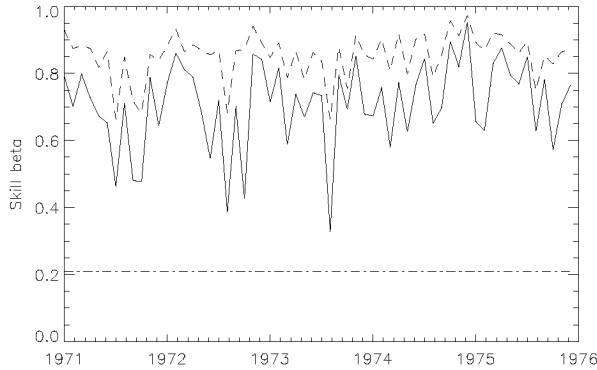
FIG. 3.6: Time dependence of spatial β for the reconstruction (solid) and the filtered ANALYSIS (dashed). The dash-dotted line is the 5% significance level of a one-sided statistical test based on a temporal randomization procedure.

not covered by the station sample, is overestimated. The differences between the reconstruction and the analysis (Fig. 3.7e) are mostly smaller than $0.5\,\mathrm{mm\,day^{-1}}$. In contrast, the summer months, June 1983 (Fig. 3.7b), shows widespread wetness with maxima along the northern Alpine flank, the south-eastern Alpine tip, and in Slovenia. Also for this case, the large-scale pattern is accurately reproduced (Fig. 3.7d). However, the reconstructed field is smoother and lacks some of the small-scale variability seen in the ANALYSIS. The lower performance for this summer month is also evident in the difference (Fig. 3.7f) which exceeds $0.5\,\mathrm{mm\,day^{-1}}$ over large parts of the domain. The large-scale patterns are also accurately reproduced for most individual months (Schmidli et al., 2001).

The smoother appearance of the reconstructed field reflects the effect of the applied phase-space truncation. Notice also that the reconstruction has successfully reproduced the pattern of change across the south-western Alps despite that this area is not sampled directly by the station network. The reconstruction for this area is entirely based on the correlation with remote stations, taken into account by the combination of dense short-term and coarse long-term data.

3.4.e Regional means

The validation has so far focussed on the skill at individual grid points, but for a number of applications it is the performance on the scale of many grid points that matters most. Time series of subdomain averages, calculated from the reconstruction and from the ANALYSIS are presented in Fig. 3.8 for four regions: the entire domain, the northern Alps (N-Alps), the southern Alps (S-Alps), and the Vosges (see Fig. 3.1b). The large month-to-month fluctuations, observed in all four regions, are accurately reproduced by the reconstruction. The skill measures for the reconstructed subdomain time series are listed in Table 3.2. The reconstruction explains between 89% and 99% of the variance in subdomain-mean precipitation. These values are substantially better than typical values for individual grid points in the respective subdomain ($\overline{\beta}_{GP}$ in Table 3.8). Even though the smallest of the domains (Vosges) does not contain any station in the reconstruction sample, its precipitation variations are captured surprisingly well (see Fig. 3.8). The subdomain-mean β is higher than $\overline{\beta}_{GP}$ for all regions, as it would be expected from the reduced variability of subdomain-means The rmse varies from $0.14\,\mathrm{mm\,day^{-1}}$for the northern Alps to $0.43\,\mathrm{mm\,day^{-1}}$for the Vosges region.
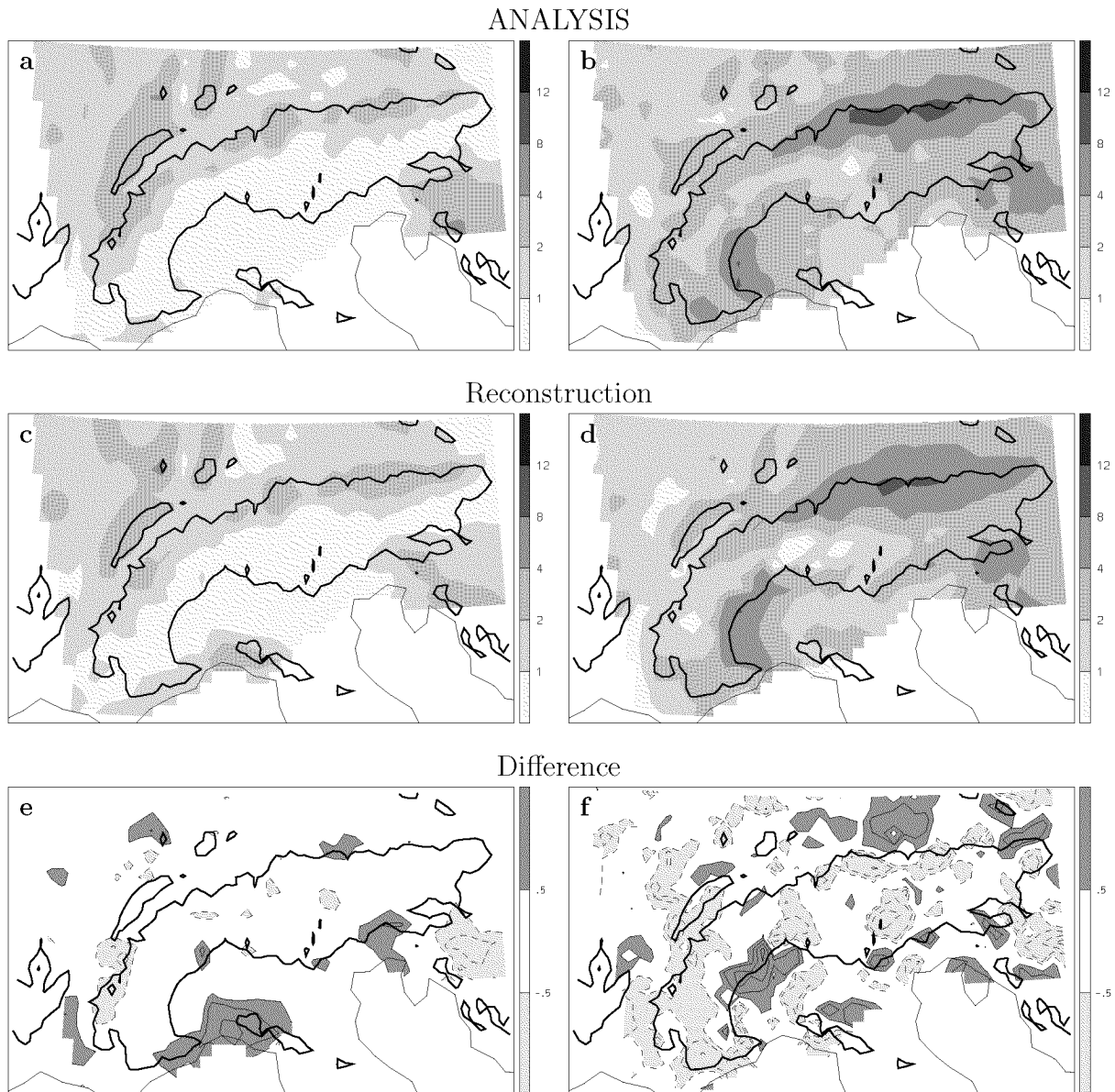
ANALYSIS

Reconstruction

Difference

FIG. 3.7: Observed (ANALYSIS), reconstructed and difference fields [mm day^{-1}] for a winter month (February 1981, left, $\beta = 0.75$) and a summer month (June 1983, right, $\beta = 0.70$). Reduced space dimension $L = 28$. The contour interval for the difference fields is 1 mm day^{-1}, including the ± 0.5 mm day^{-1} contours.

3.4.f Possible improvements

Several measures could lead to a further improvement of the reconstructed fields. (i) Processing and inclusion of additional long-term station records: Poor representation over the southern and western areas of the Alps has enforced a moderate choice of the phase-space truncation L and hence has prevented the reconstruction of modes with small spatial scales even though the station network was dense enough to resolve these modes over parts of the domain. Inclusion of additional station records for poorly sampled areas can therefore be expected to improve, at the same time, the skill over closeby areas and the spatial detail over remote areas from a better exploitation of available records by

TABLE 3.2:   Skill for subdomain-mean precipitation of four regions (see Fig. 3.1b) cal-
culated from the reconstruction for 1971–75. Explained variance β and the rmse [mm
day^{-1}] with respect to the ANALYSIS are tabulated. $\overline{\beta}_{GP}$ is the average skill for a single
gridpoint time series within the corresponding region (cf. Fig. 3.4a). The last two columns
refer to the number of grid points and reconstruction stations in each of the subdomains.

Region	β	rmse	$\overline{\beta}_{GP}$	No$_{GP}$	No$_{St}$
Entire	0.95	0.20	0.76	928	140
N-Alps	0.99	0.14	0.91	153	61
S-Alps	0.93	0.40	0.76	153	22
Vosges	0.89	0.43	0.80	25	0

the methodology. (ii) Temporal extension of the ANALYSIS dataset (currently restricted
to 1971–90): This measure would allow for a more robust calibration of the reconstruc-
tion relationships, and eventually a seasonally stratified application of the reconstruction
technique. While an extension of the ANALYSIS dataset into the 1990's seems feasible,
a backward extension would require that some of the high-resolution Alpine rain-gauge
datasets are digitized at the original data providers for the pre-1970's. (iii) Optimizing
the balance between temporal homogeneity and spatial sampling density: In the present
study, the long-term records were selected from a rigorous homogeneity test. Relaxing
the homogeneity requirements would result in a larger reconstruction sample. The cost
and benefit of such a measure would have to be explored by experimenting with various
sets of station samples. In the present situation improvements would be marginal as the
homogeneity requirements have led to the exclusion of records primarily from densely
sampled areas.

3.5   Centennial precipitation variability

In this section we discuss selected results of 20th century precipitation variations in the
region of the European Alps as revealed in the mesoscale dataset. The final reconstruction
was obtained by calibration over the full 20 year period 1971–90 and using truncation at
$L = 28$. The presentation of the results proceeds from the multi-year variability of
seasonal precipitation, to the observed long-term trends, the role of snow undercatch for
the trends, and the correlation of Alpine precipitation with the North Atlantic Oscillation
Index (NAOI).[3]

3.5.a   Interannual to interdecadal variability

A compact description of the interannual to interdecadal precipitation variations is given
in this section in terms of the leading rotated principal components (RPCs). This is
achieved by subjecting the leading EOFs (and PCs) of the 90-year reconstruction to a
linear transformation (VARIMAX EOF-rotation, Richman 1986). The resulting rotated
empirical orthogonal functions (REOFs) exhibit loading patterns confined essentially to
contiguous parts of the domain, and the rotated principal components (RPCs) represent

---

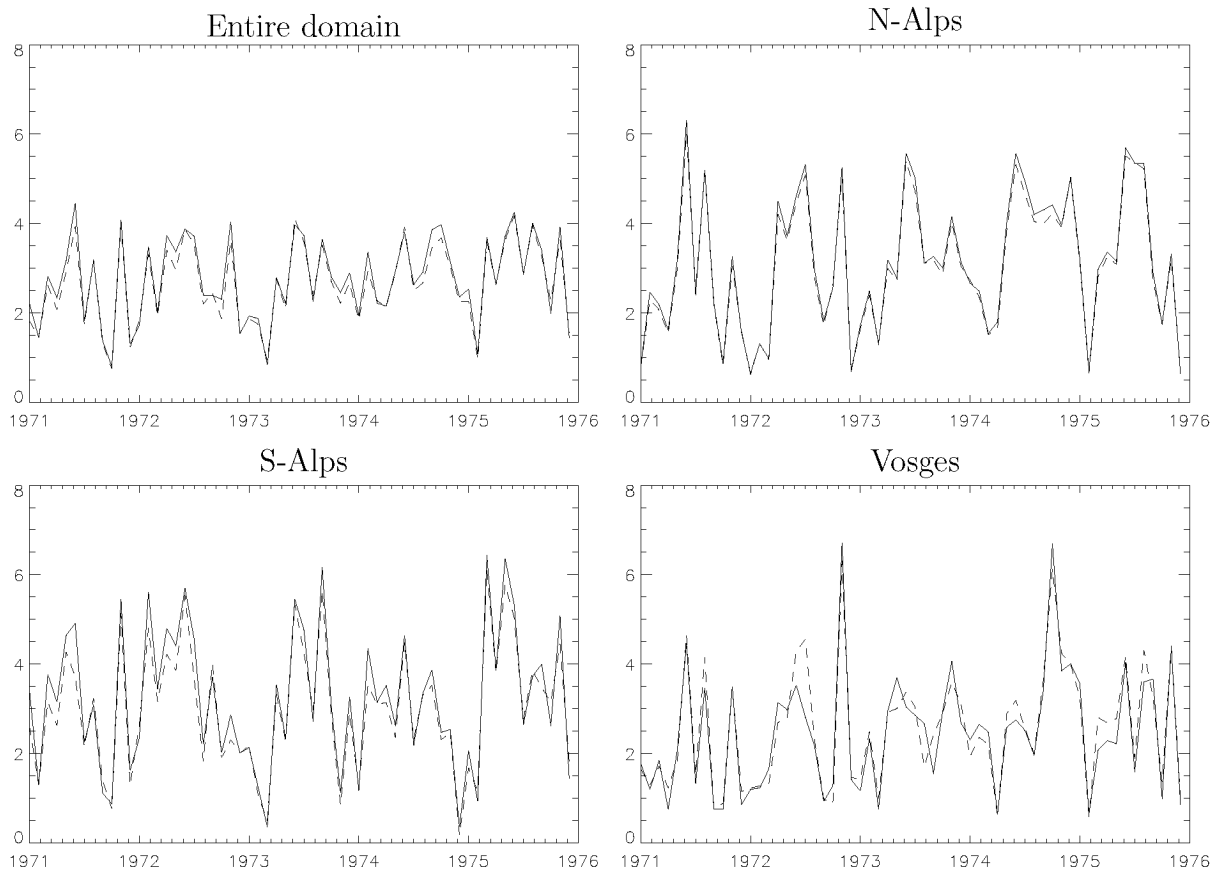[3]Additional results are shown in Appendices A, B, and C.

FIG. 3.8: Time series of subdomain-mean precipitation calculated from observations (ANALYSIS, solid) and from the reconstruction (dashed). The subdomains are indicated by the boxes in Fig. 3.1b.

estimates of area mean precipitation anomalies in the area of the REOF loadings (see also Richman and Lamb 1987).

The loadings patterns of the five REOFs are shown in Fig. 3.9.[4] The patterns are characterized by nearly contiguous areas of positive loadings. Hereafter, these regions will be referred to as: western Alps (WEA), northern Alps (NOA), Ticino (TIC), Mediterranean (MED), and south-eastern Alps (SEA). For the period 1971–90, the five reconstructed RPCs explain 70% of the total variance of the ANALYSIS, compared to the 77% explained by the leading 28 PCs. Thus the leading five modes explain 90% of the total variance of the reconstruction.

The RPC time series for mean seasonal precipitation are displayed in Fig. 3.10.[5] Large variability on annual to multi-decadal time-scales is evident. The magnitude of the interannual variability varies considerably between the regions and the seasons. For instance, in autumn the coefficient of variation (i.e. the standard deviation divided by the mean) is 0.58 for the Ticino area (TIC), but only 0.28 for the western Alps (WEA). Also the variability in the south-eastern Alps (SEA) is considerably larger in autumn compared to summer.

In winter, most of the regions exhibit pronounced variability on decadal time-scales.

---

[4]See Appendix D for the REOFs of the leading 28 PCs.

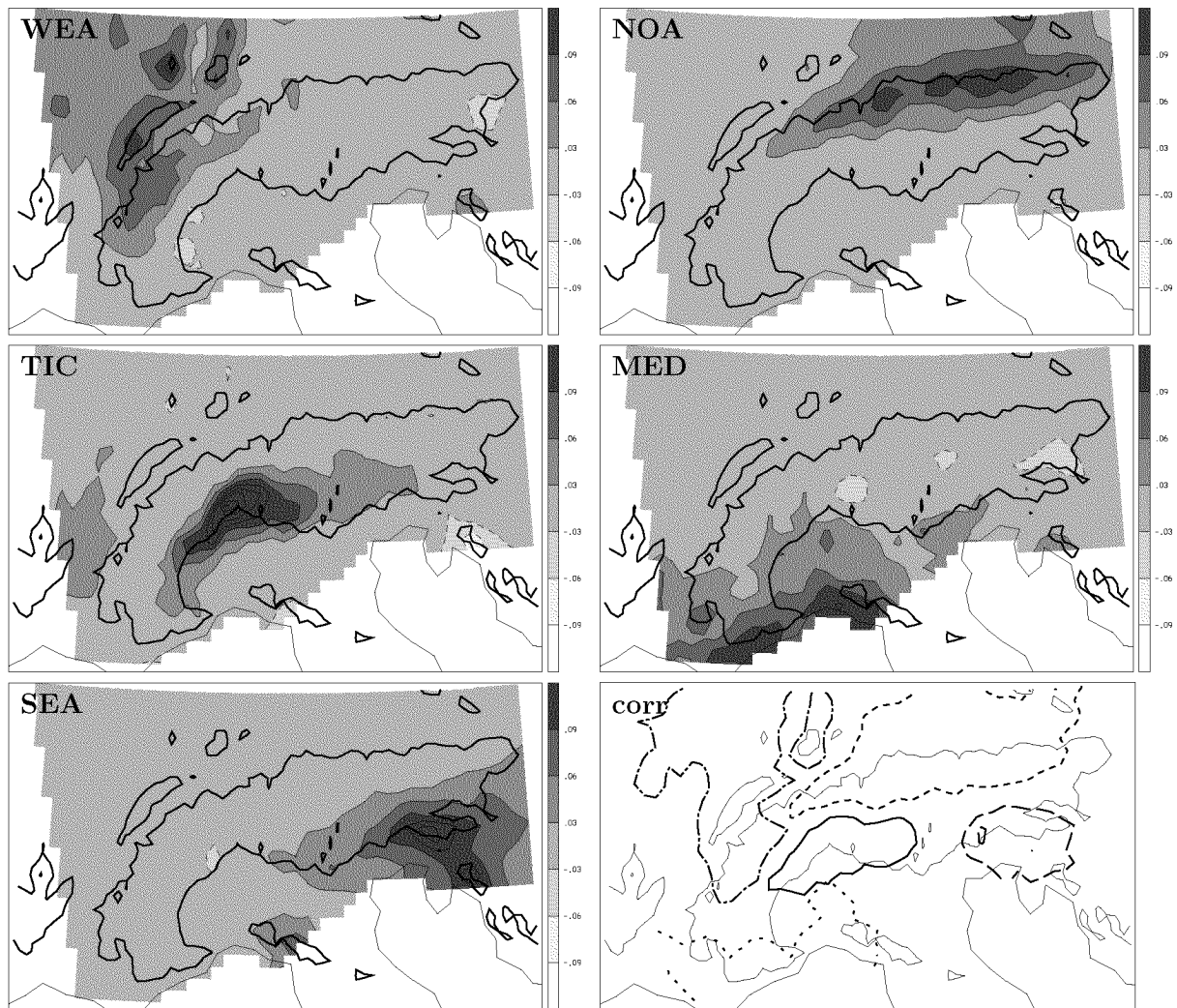[5]The annual cycle of the RPCs is given in Appendix E.

FIG. 3.9: Loading patterns of the five leading RPCs of monthly precipitation for the years 1971–90. The RPCs and their explained variance fraction are: WEA, 16%; NOA, 16%; TIC, 17%; MED, 16%; and SEA, 14%. The lower right panel indicates the regions with a correlation larger than 0.8 with the five RPCs.

In the western Alps, an increase of precipitation is evident after a minimum in 1930. Note that there is substantial correspondence between the western and northern Alps on the one hand, and between the three southern areas on the other hand. Various of the decadal-scale extrema and also some of the annual peaks are common between the corresponding PCs. There are a few interesting features in the spring precipitation series. The Ticino area exhibits a pronounced multi-decadal variability, characterized by a precipitation decrease from 1915 to 1955 and a strong increase in the following 30 years. A similar trend pattern is also visible for the western Alps. A further large anomaly is the decadal minimum in the south-eastern Alps PC in the period 1940–50. An interesting feature of the summer precipitation series is the correlation between the Ticino PC and the two northern PCs. For instance, for the years 1950–60 all three PCs have a distinct decadal maximum. A notable aspect of autumn precipitation is the marked decrease since 1960 in the Mediterranean, south-eastern Alps, and Ticino; and the remarkable interannual variability in the Ticino area. The autumn precipitation total varies between

Winter (DJF)   Spring (MAM)
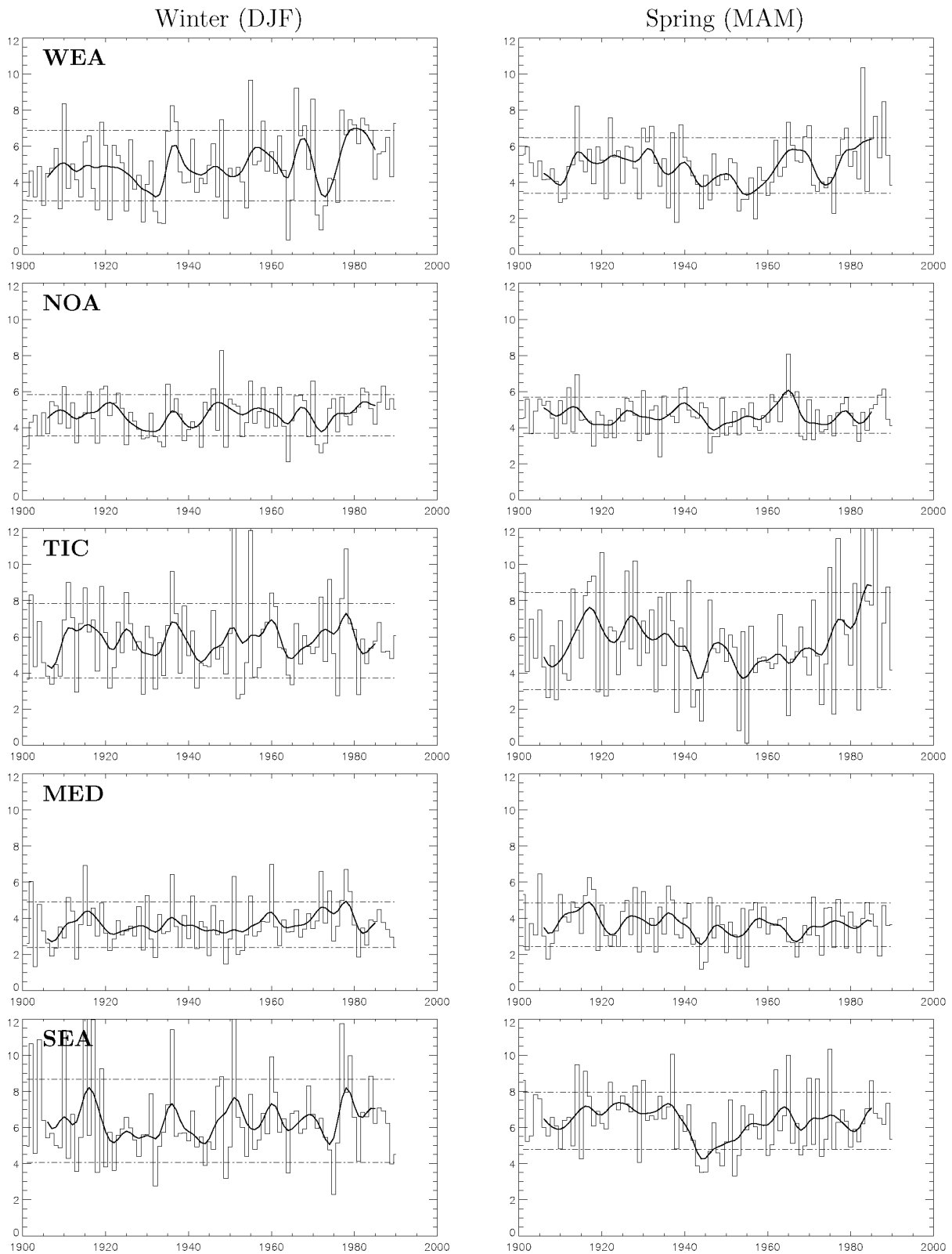

FIG. 3.10: Time reconstructions of seasonal means of the five leading RPCs for the period 1901–90. Shown are seasonal (steps) and lowpass filtered values (11 point binomial filter, solid). Also indicated is the standard deviation of the seasonal RPCs (dash-dotted line). The units are in [mm day^{-1}] at the grid point with maximal loading of the respective REOF.
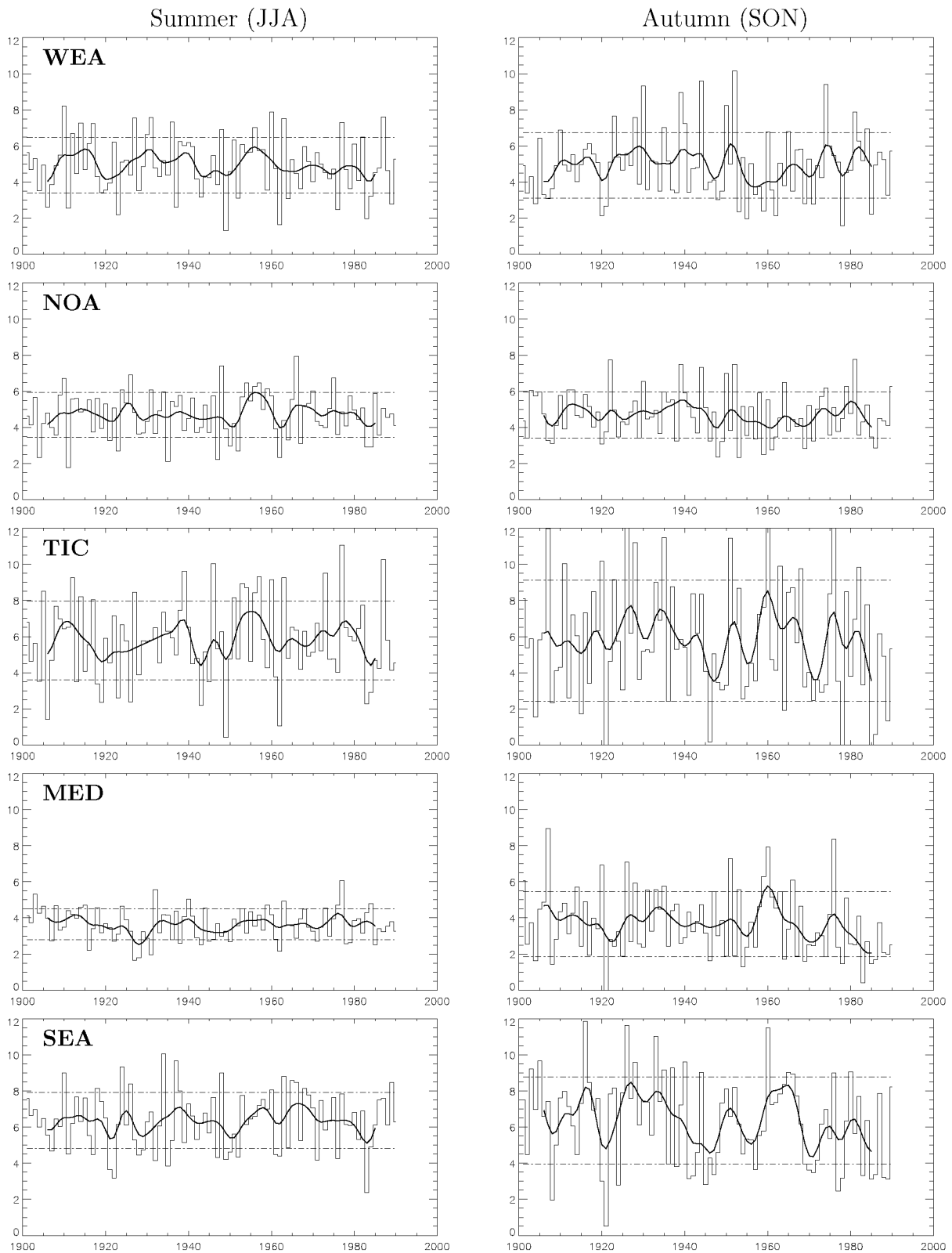
FIG. 3.10:   (cont.)

TABLE 3.3: Linear trends of seasonal precipitation. The trends are given in percent change per 100 (1901–90) and 30 (1961–90) years, respectively, of the mean seasonal precipitation at the grid point with maximum loading of the PC. Significance levels are 5% (bold), 10% (normal), 20% (italics). Empty entries denote values not significant at the 20% level.

	1901–90				1961–90			
PC	Aut	Win	Spr	Sum	Aut	Win	Spr	Sum
WEA		**37**				*24*		
NOA								
TIC							62	
MED	−35				**−57**			
SEA	−28				**−42**			

almost 0 mm and more than 1500 mm. This high variability could be associated with the occurrence of heavy precipitation events, which are particularly frequent in this time of the year, but can also be completely absent in some years.

3.5.b Long-term trends

So far, we have looked at the variability of the mesoscale precipitation in the Alps in terms of the five leading RPCs. In this section the spatial distribution of linear trends of seasonal precipitation is presented for the complete reconstruction (28 PCs), and compared to linear trends in the five leading RPCs.

Fig. 3.11 depicts linear precipitation trends for the period 1901–90, obtained from a linear regressions for each grid point and using the full (i.e. non-truncated) reconstruction dataset. The trends are given as percentage change over 100 years of the seasonal mean. Only winter and autumn precipitation exhibit well-established areas of significant (at 10% level) trends. In winter, significant positive trends of 20–30% per 100 years are found for a region extending from southern Germany, through Switzerland, to the south-western tip of the Alps; and non-significant negative trends of 20–30% are observed in the south-eastern part of the Alps. In autumn, significant negative trends of 20–40% per 100 years occur in southern France, parts of northern Italy, and in the eastern Alps. While the negative trend along the Mediterranean coast should be considered with caution (only a few stations, Fig. 3.1b), the negative trend in the eastern Alps is trustworthy as it is supported by a few dozen stations. For both seasons the trend signal is corroborated by a trend analysis of the RPCs (Table 3.3). The western Alps PC shows a highly significant increase (at the 5% level) by 37% per 100 years in winter, and the Mediterranean and south-eastern Alps PCs show a significant decrease by −35% and −28% per 100 years, respectively, in autumn. Note that these trends are normalized according to the grid point with maximal loading in the corresponding REOF.

Fig. 3.12 provides gridpoint-based precipitation trends for the last climate normal (1961–90). Significant trends are found in winter, spring, and autumn. In winter, positive trends of more than 20% per 30 years are observed for most regions north of the Alpine crest, and also for the central Alps. Although the trends are three times larger than for 1901–90 (20–40% per 30 years), they are only significant in southern Germany (small sample size). In spring, positive trends of 20–40% are observed in the Ticino and Piedmont
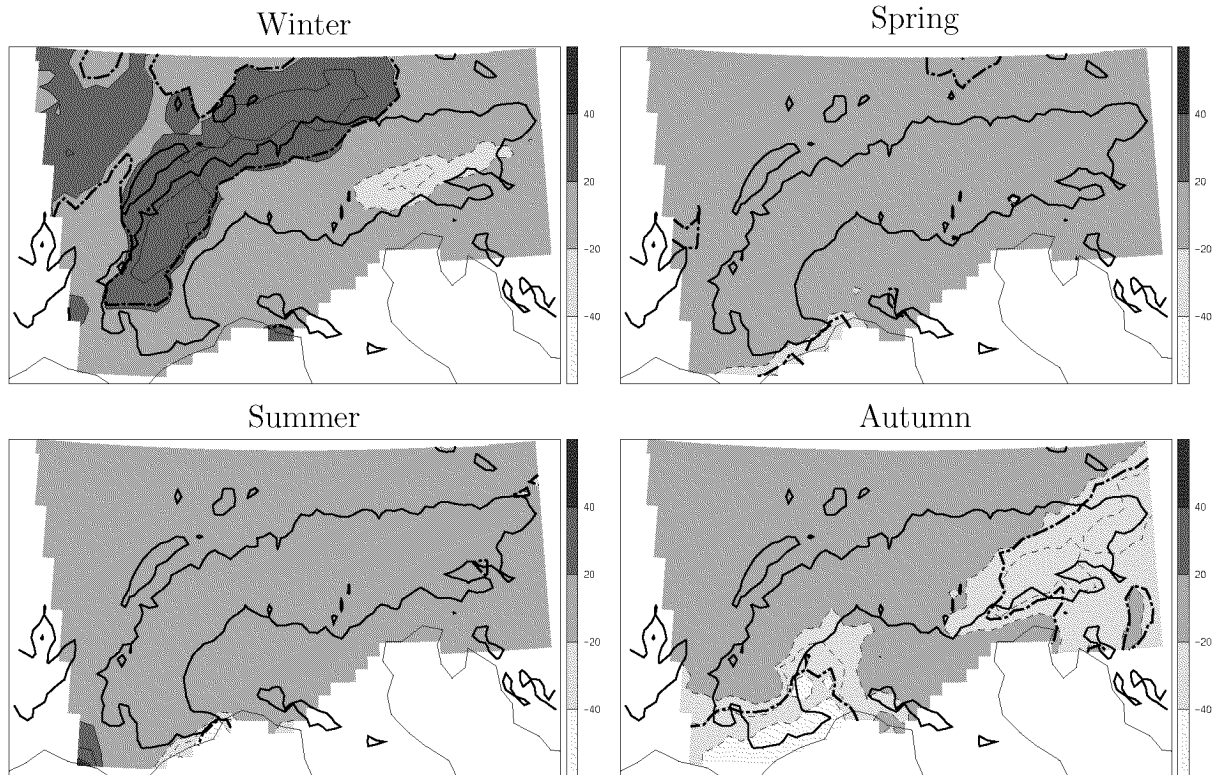
FIG. 3.11:   Linear trends of seasonal precipitation means for the period 1901–90. The trends are given in percents of mean seasonal precipitation (1971–90) at the corresponding grid point per 100 years. The bold dashed line is the 10% significance level. The contour interval is 10, except the 0 and ±10 contours are excluded.

region, south-western Alps, and along the western boundary of the domain; significant negative trends of 20–30% per 30 years are found in a small region along the northern Alpine rim. In autumn, a precipitation decrease of up to 40% per 30 years and more is found south of the Alps, in southern France and in most of northern Italy. Again the gridpoint-based trend patterns are consistent with the trends inferred from the RPCs (Table 3.3). Moreover the pattern of the trend was found to be consistent but smoother than the pattern resulting from a station-by-station trend analysis (Fig.3.13).

The present trend results agree qualitatively well with the findings of previous studies (e.g. Auer and Böhm, 1994; Schönwiese and Rapp, 1997; Widmann and Schär, 1997; Buffoni et al., 1999). A direct, quantitative comparison is complicated by the different time periods, homogeneity standards, and analysis procedures, for example, station versus gridpoint-based trends, and by the coarser resolution of most other studies. On the large scale our results are similar to those of Schönwiese and Rapp (1997) who, for the period 1891–1990, also observed the largest trends in winter, 20–30% increase in the northern and western part of the Alps, and autumn, 10–20% decrease south of the Alps. Our high-resolution trend maps, however, allow a more accurate demarcation of the regions with significant trends. One feature not captured by the analysis of Schönwiese and Rapp (1997) is, for instance, the strong localized precipitation decrease of 30% in winter in the south-eastern Alps (see Fig. 3.11). For the region of Switzerland, Widmann and Schär (1997) provide high-resolution trend maps for the same periods as in the present

FIG. 3.12:   Linear trends of seasonal precipitation means for the period 1961–90. The trends are given in percents of mean seasonal precipitation at the corresponding grid point per 30 years. Bold dashed line and contour interval as in Fig. 3.11.
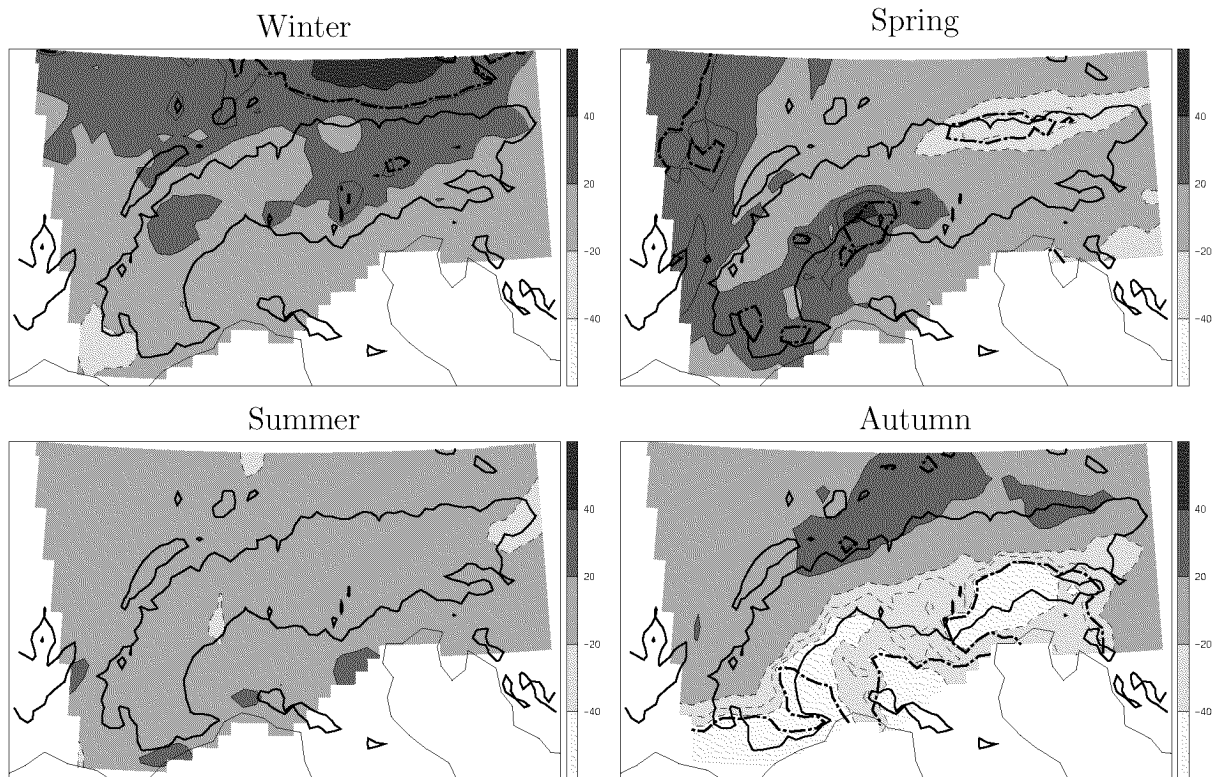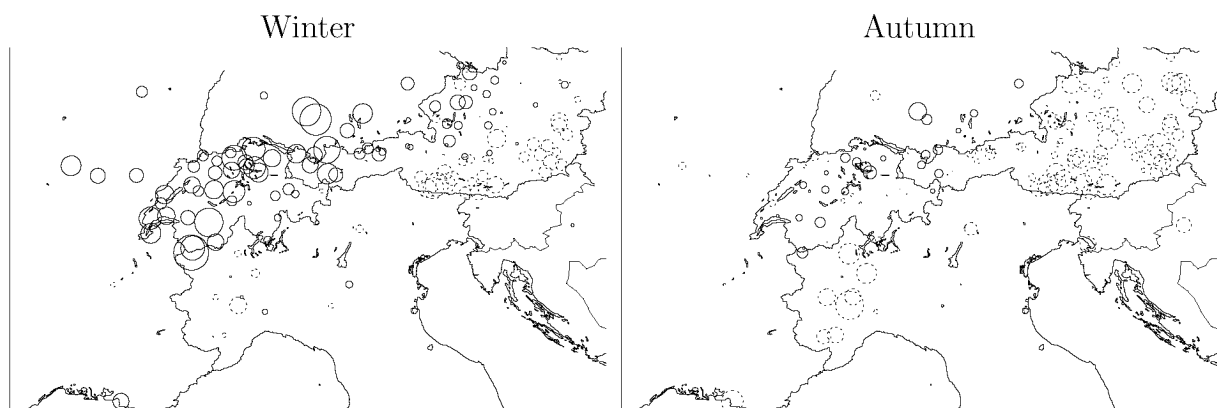

FIG. 3.13:   Station-based linear trends of seasonal precipitation means for the period 1901–90. The trends are given in percents of the mean seasonal precipitation per 100 years. Positive (negative) trends are depicted by solid (dashed) circles. The trends are proportional to the circle radius (the largest circle corresponds to an increase of 67%).

TABLE 3.4: Station-based linear trends of seasonal precipitation means for six Swiss stations. The trends are given in percent change of mean seasonal precipitation per 100 years. Tabulated are the linear trends calculated from the homogenized station time series (hsta), from station time series with an ad-hoc correction for snow undercatch (csta), and from the reconstructed gridpoint time series (gp). The trends are for the period 1901–90 (normal) and 1931–90 (italics), respectively.

Station	°E	°N	h[m]	hsta	csta	gp
Arosa	9.68	46.78	1847	*41*	*42*	15
Basel-Binningen	7.58	47.54	317	21	23	20
Zürich-SMA	8.57	47.38	556	29	31	31
Engelberg	8.41	46.82	1018	*-9*	*-12*	21
Bern-Liebefeld	7.42	46.93	570	21	21	29
Lugano	8.96	46.01	276	16	13	5

study. Generally, the trends agree well in magnitude as well as in their distribution. For the winter season, the season with the largest trends, the magnitude of our trends lies between the magnitude of the station-based and the PC filtered trend of Widmann and Schär (1997). Surprisingly, the present trend patterns are closer to the station-based analysis of Widmann and Schär (1997), than to their PC filtered trend patterns. The present study shows how these trends seen in Switzerland fit into the larger-scale picture of Alpine-wide trends.

3.5.c   Role of snow undercatch

Wind-induced measurement biases are particularly large for snowfall (e.g. Sevruk, 1985). Here we briefly test to what extent the centennial increase of mean winter-time precipitation, emerging from our analysis of bias-uncorrected records, could be related to a decreasing fraction of snowfall, expected with the 20th century warming in the region (e.g. Jungo and Beniston, 2001). For this purpose, we consider six Swiss station records, colocated with the pattern of increasing trends, by adopting an approximate ad-hoc correction for snow undercatch. This is accomplished on a daily basis, assuming a snow-related undercatch of 40% for a daily mean temperature below 0°C, and a linear reduction of this value in the temperature range 0°C–4°C. Note that this procedure considers only the bias due to snowfall and neglects wind-induced measurement biases of rain. The actual value of the snow bias depends on wind conditions. For this ad-hoc correction, we have chosen a bias value which is at the upper end of the bias range estimated in gauge comparison studies in the Alps (e.g. Sevruk, 1985).

The results in Table 3.4 show that the possible effect of snow undercatch on the trend is marginal, even for the rather large bias assumed here. For some stations the trend decreases slightly while for other stations it even increases slightly. The robustness of the trend with respect to snow undercatch and the uniform picture of the station-based trends indicates that the observed trend is not purely an artefact of warming-induced reduction of measurement biases.

3.5.d   Correlation with the NAO index

The new gridded long-term dataset offers the possibility to study the relationship between variations of the continental-scale circulation and the Alpine precipitation. Here we discuss an example of such an application, by examining the correlation between Alpine precipitation and the North Atlantic Oscillation (NAO). The NAO is one of the major factors influencing the Central European climate (e.g. Wanner et al., 1997, 2001). It has been associated with variations of weather types (e.g. Stefanicki et al., 1998), local Alpine climate (Beniston et al., 1994), and the distribution of precipitation over Central Europe (Hurrell and van Loon, 1997). The strength of the NAO is conventionally measured by the NAO index (NAOI), which is a standardized scalar measure of westerly low-level flow over the Northern Atlantic (Hurrell, 1995, 1996; Jones et al., 1997). For the present study, values of monthly NAOI were taken from Hurrell (2000). The correlation study is undertaken for several independent time periods to examine the stationarity of the NAOI-Alpine precipitation link.

Fig. 3.14 displays correlation maps of the NAOI with winter-season (JFM) precipitation means for the last three 30-year climate normals and for the full period 1901–90. For the 1901–30 period, the correlation is between 0.2 and 0.4 north of the Alpine crest, and between -0.2 and -0.4 to the south of the Alps along the Mediterranean coast. The correlation is significant (at the 10% level) only in a small region along the northern Alpine rim and in some isolated patches to the south. In contrast, for the 1931–60 period, no significant positive anomalies are visible. Instead, large parts of the domain show significant negative correlations of -0.3 to -0.5. For the 1961–90 period, the area with significant negative correlations is again smaller, essentially confined to the south-eastern part of the domain, and there are no significant correlations north of the Alpine divide. For the full period 1901–90, negative correlations prevail south of the Alps, whereas no significant correlations are found to the north. In summary, the correlations are relatively stationary for the analysis grid points in the Mediterranean region, whereas they are comparatively weaker and intermittent for the regions north of the Alpine crest. A analysis of the correlations between the NAOI and the leading five RPCs confirms these findings. For the 90-year period 1901–90, only the Mediterranean (MED)- and the south-eastern Alps (SEA) PCs exhibit significant (at the 5% level) correlations with values of -0.28 and -0.35, respectively. For the remaining PCs the correlations are not significant, even at the 20% level.[6]

The different behaviour of the regions north and south of the Alps is further illustrated in Fig. 3.15, showing the correlation for successive 31-year periods with the northern Alps (NAO) and the south-eastern Alps (SEA) PC. The NOA PC exhibits significant positive correlations at the beginning of the century, but by the second half of the century the correlations are negative (and nonsignificant). The correlation of the SEA PC is less variable in sign, becoming gradually more significant in the second part of the century.

These findings indicate that interannual precipitation variations in the Alps exhibit marginal linear relationships with lower tropospheric circulation variations as cast by the univariate NAO index. The Alpine region is located between the main poles of enhanced NAOI-precipitation relationships (see Hurrell and van Loon, 1997) and is influenced by other prominent modes of the large-scale circulation (e.g. Quadrelli et al., 2001).

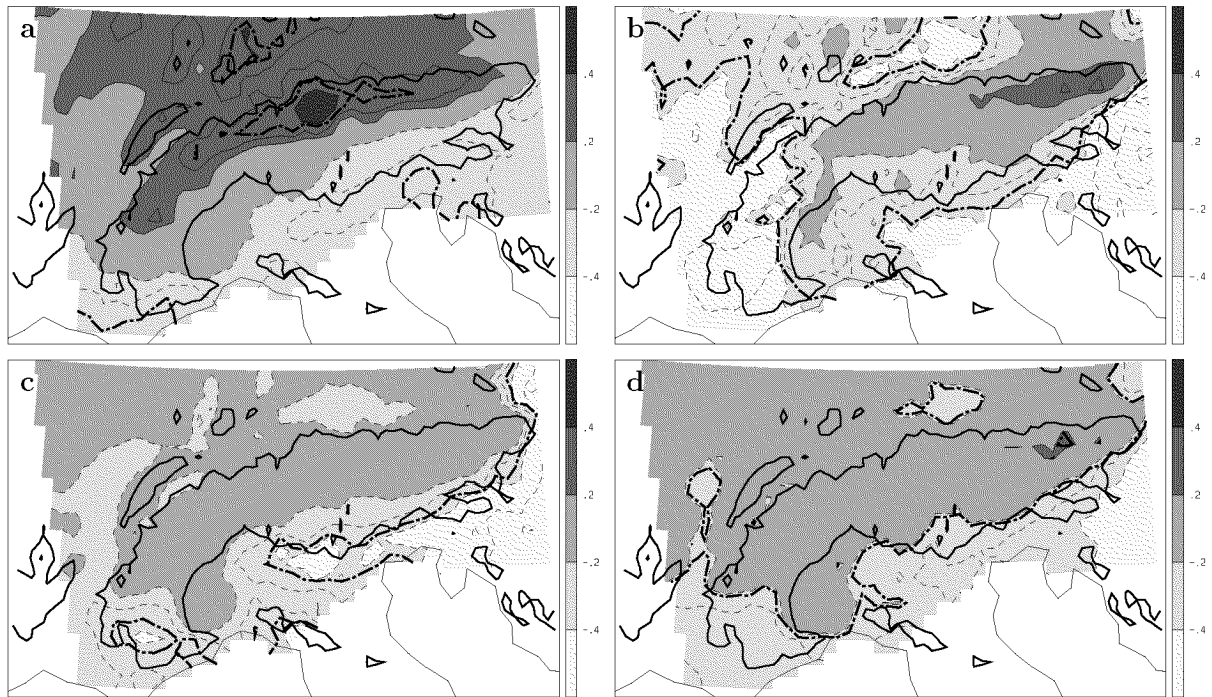[6]Further results are given in Appendix F.

FIG. 3.14: Correlation of mean winter (JFM) precipitation with the NAOI for the periods (a) 1901–30, (b) 1931–60, (c) 1961–90, and (d) 1901–90. The bold dashed line depicts the 10% significance level, of the correlation at the analysis grid points.

3.6   Comparison with the Alpine window of a global analysis

Here the reconstructed fields are compared to the Alpine section of the global dataset CRU05, which was briefly introduced in section 2c. It should be mentioned that the station dataset available for the CRU05 analysis in the Alpine region was coarser than that used for the present mesoscale reconstruction, but considerably denser compared to that for other mountainous regions of the world. To compensate for the coarser nominal resolution (about 50 km) and the more restricted station dataset in CRU05, this comparison is conducted for larger-scale subdomains which are adequately resolved by both analyses.

Time series of winter (DJF) and summer (JJA) precipitation totals, determined from the reconstruction and from CRU05 are displayed in Fig. 3.16 for three regions (subdomains in Fig. 3.1b). Also shown are results for the ANALYSIS after 1971. To first order, the two centennial analyses differ by a quasi-stationary offset which is due to differences in the respective climatologies and the available station data for its construction. With regard to the interannual variations the analyses agree fairly well in both seasons and for all three domains. Correlations (see Table 3.5) exceed 0.9 except for DJF of the northern Alps. Verification with the ANALYSIS for 1971–90, which is based on many thousand station records, indicates that the mesoscale reconstruction is slightly superior to CRU05 (see Fig. 3.16 and Table 3.5). The differences are particularly evident for the domain N-Alps, where for the present analysis the station sample is particularly dense. With regard to interdecadal variations (see low-pass filtered time series in Fig. 3.16) the two datasets exhibit very similar patterns of evolution, but some differences are evident in variations of the offset from its long-term mean value. Notice for instance that N-Alps exhibits an anomalously low (high) offset for 1980–90 (1905–15) in both seasons. These variations
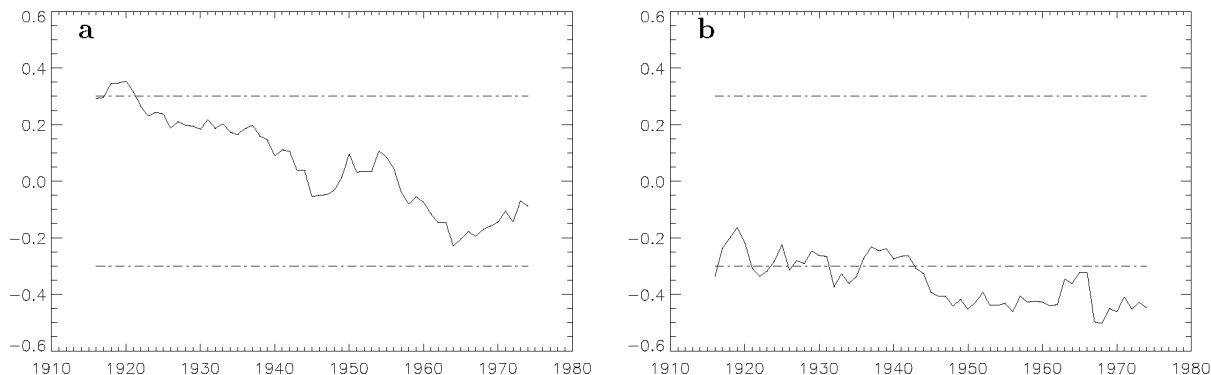
FIG. 3.15: Correlation of (a) the NOA PC and (b) the SEA PC with the NAOI during 31-year time windows for the winter season (JFM). The dash-dot lines depict the 10% significance level of the null hypothesis of no correlation.

reflect in differences of multidecadal trends. CRU05, for example, depicts a considerable decrease of N-Alps summer precipitation after 1965, whereas the present reconstruction is roughly stationary. The discrepancies between the datasets in the recent decades may be partly caused by the variations in station density for the CRU05 analysis. Prior to 1950 the analysis is based on about 50 stations, the number increases to approximately 100 during 1950–75 and finally drops to 40 by 1990 (M. New, personal communication).

Fig. 3.17 depicts the precipitation distribution for the wettest, in terms of domain-mean precipitation, autumn and summer month of the period 1901–90 for the mesoscale reconstruction and for CRU05. October 1907 is characterized by high precipitation values south of the Alpine crest and relatively dry conditions to the north, whereas June 1953 is distinguished by precipitation bands along the southern and northern Alpine rim. On the scale of the entire mountain range the two datasets give similar precipitation amounts for the two cases; on the regional scale, however, there are large differences. In June 1953, for instance, the precipitation maxima are centered over the top of the mountain range in CRU05, whereas in the mesoscale reconstruction, the maxima are located along the northern and southern Alpine rim. Based on the typical precipitation patterns found in the high-resolution ANALYSIS dataset and a high-resolution climatology (Schwarb et al., 2001), the mesoscale patterns of the reconstruction appear more plausible than the CRU05 patterns. As the patterns are of relatively large scale, the differences between the two analyses are not solely attributable to the different grid spacings. Possible causes for the differences include: the base climatology (see also Frei and Schär 1998), the number and distribution of the stations, the reconstruction method, and homogeneity issues.

3.7 Conclusion

A new gridded analysis of precipitation has been reconstructed: It covers the entire region of the European Alps, resolves the most prominent mesoscale patterns (grid spacing 25 km) and extends with a monthly time-resolution over most of the 20th century (1901–90). Special emphasis has been given to the temporal homogeneity of the new dataset in that the reconstruction comprises a constant number of quality-controlled, homogenized long-term records. To our knowledge, this is the first compound dataset describing long-term precipitation variability for the entire region of the European Alps which resolves

TABLE 3.5: Correlations of subdomain-mean monthly precipitation series from the reconstruction, the global dataset CRU05 (1901–90), and the ANALYSIS (1971–90) for three characteristic regions.

Region	1901–90 Rec/CRU		1971–90 Ana/Rec		Ana/CRU		Rec/CRU	
	DJF	JJA	DJF	JJA	DJF	JJA	DJF	JJA
Northern Alps	0.85	0.94	1.00	1.00	0.80	0.93	0.79	0.93
Southern Alps	0.96	0.93	0.98	0.97	0.96	0.92	0.96	0.91
Vosges	0.93	0.90	0.98	0.91	0.94	0.91	0.92	0.91

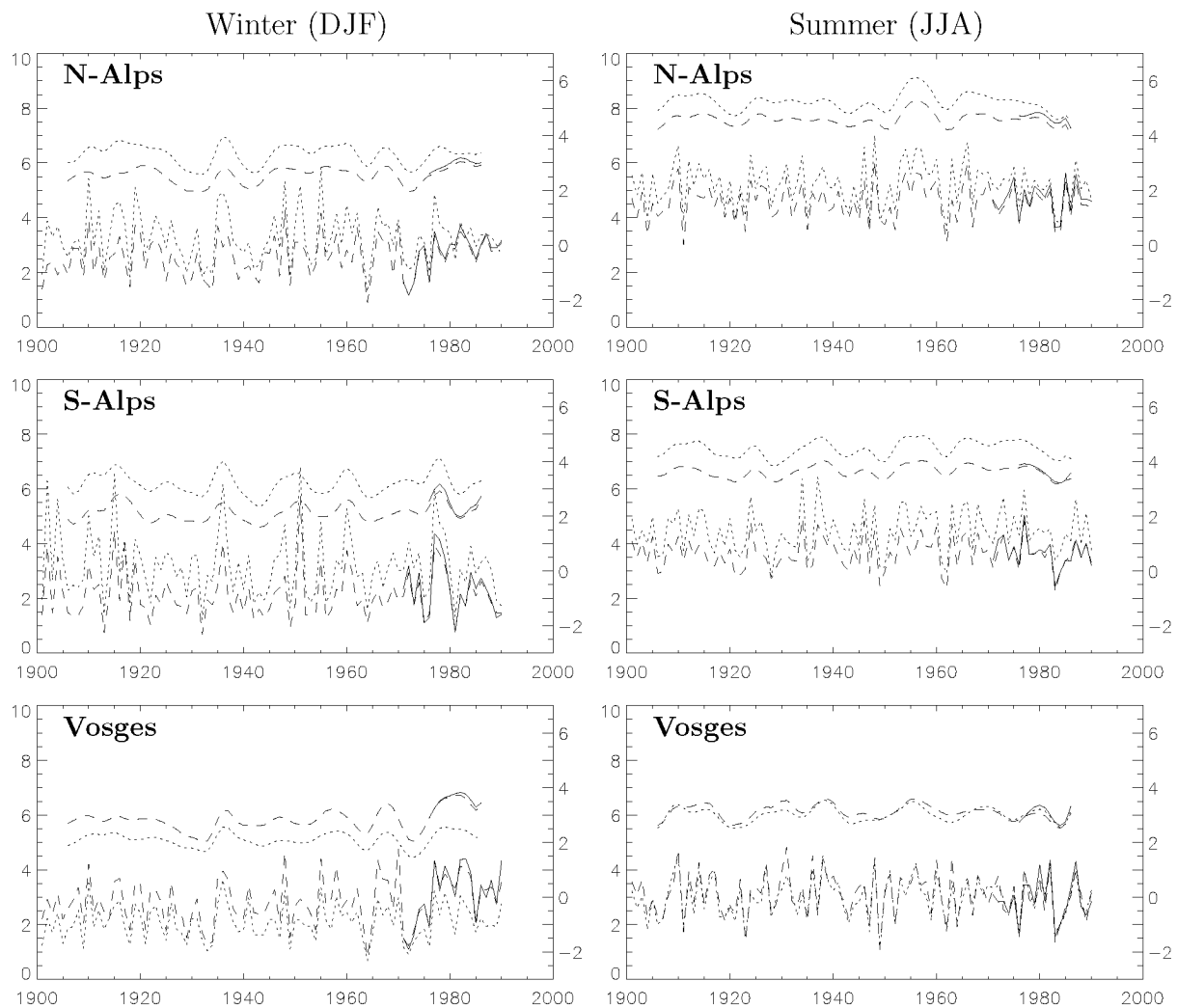Winter (DJF)   Summer (JJA)

FIG. 3.16: Time series of subdomain-mean precipitation calculated from the reconstruction (dashed), from a global precipitation dataset (CRU05, dotted), and from the Alpine dataset (ANALYSIS, solid). Depicted are seasonal mean values (lower curves, left-hand labels) and lowpass filtered values (11 point binomial filter, upper curves, right-hand labels). The subdomains are indicated by the boxes in Fig. 3.1b.
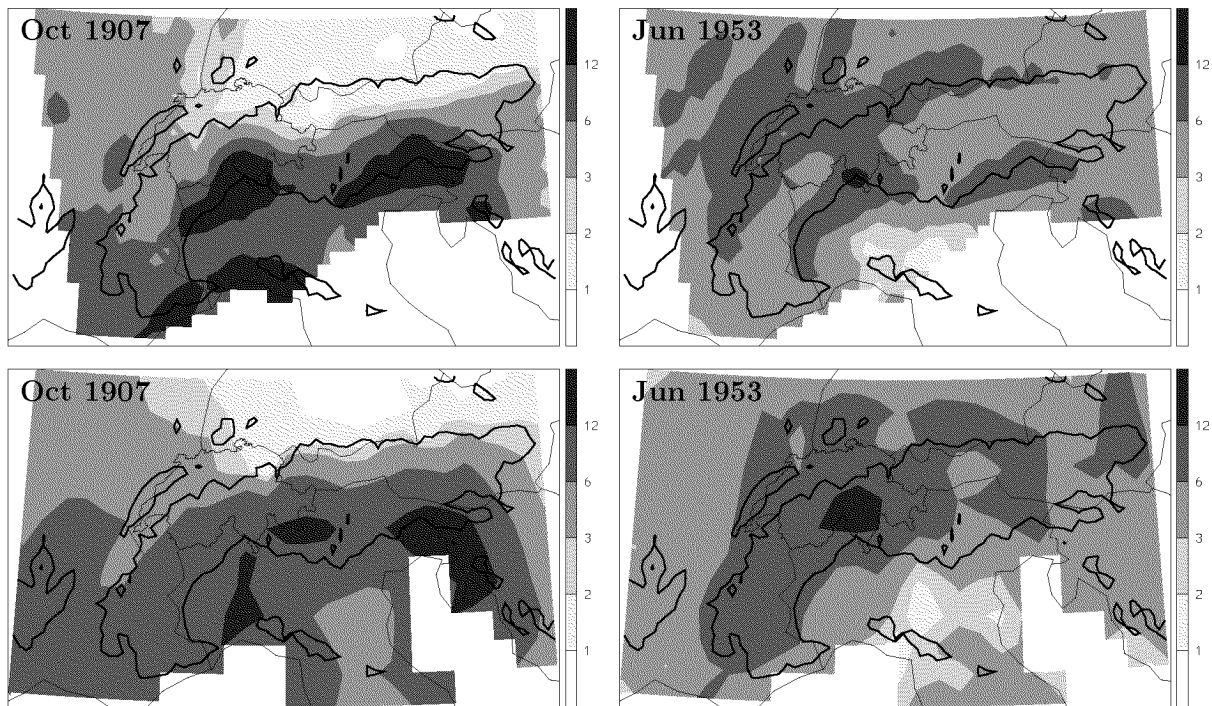
FIG. 3.17: Comparison of reconstructioned fields (upper panels) with CRU05 (lower panels). Wettest autumn and summer month of the period 1901–90.

the major subridge precipitation patterns, including those of the adjacent foreland and hill-ranges.

Validation for an independent period showed that the new dataset explains about 78% of the total variance of the gridded mesoscale analysis (ANALYSIS). At the level of individual grid points, the explained variance is 70–90% in the northern and eastern parts, but only 40–70% in the southern and western parts of the domain where the spatial sampling is very coarse. For averages over $100 \times 100 \, \text{km}^2$ subdomains, the explained variance increases to 90–99%. The accuracy of the reconstructed fields could be further improved by the processing and inclusion of additional long-term station records and the temporal extension of the ANALYSIS dataset.

The reconstructed dataset has been exploited to depict the precipitation variations during the 20th century and to study their relationship to the NAO. The main results are:

- A significant (at 10% level) increase of wintertime precipitation by 20–30% in a region extending from southern Germany to the south-western Alps, and a non-significant decrease by 20–30% in the south-eastern Alps. It is unlikely that the increasing trend is purely an artefact of variations in measurement biases.

- A significant decrease of autumn precipitation by 20–40% in Southern France, northern Italy, and the south-eastern Alps.

These results agree qualitatively with findings from previous regional trend studies (e.g. Buffoni et al., 1999; Schönwiese and Rapp, 1997; Widmann and Schär, 1997), however, the results of this study provide additional information on the main centers and mesoscale

demarcation of the trend patterns. They also yield more reliable trend estimates, given the comprehensiveness of the long-term records available for this study, and the use of a multivariate reconstruction technique that filters noise from individual records.

An increase of mean precipitation during the 20th century has been reported for a number of mid- and high-latitude regions of the world, see Folland et al. (2001) for a review. Possible explanations for trends include changes of the hemispheric circulation patterns (e.g. Hurrell, 1996) or changes in the hydrological cycle associated with the observed warming of the lower troposphere (see e.g. Trenberth, 1998; Stocker and et al. , 2001; Frei et al., 2000). As regards the Alpine region, the observation that precipitation changes in winter are primarily due to increasing precipitation activity rather than changes in the frequency of weather types (Widmann and Schär, 1997) and that the changes are associated with an increasing frequency of intense precipitation events (Frei and Schär, 2001) lend some support to the hypothesis of an intensified water cycle. Also, the weak and intermittent nature of the NAOI correlations, revealed in this study, imply that the increase of winter precipitation cannot be explained by the observed trend of the NAOI, at least in the framework of a simple linear regression model. More extensive analyses will be required, studying the relationship between Alpine precipitation and the atmospheric circulation, thermodynamics, and sea surface state, to isolate the physical mechanisms responsible for the observed centennial changes.

The present reconstruction offers a new opportunity for such studies due to its temporal extent and spatial resolution which was not available from previous analyses for the Alpine region. Further potential applications include the evaluation of regional climate models (e.g. Lüthi et al., 1996; Christensen et al., 1998; Murphy, 1999) and the development and calibration of statistical climate-change downscaling models (e.g. Gyalistras et al., 1994; Wilby et al., 1998; Biau et al., 1999). The availability of a long-term analysis will be beneficial to both of these applications, allowing for the evaluation of dynamical and statistical downscaling models with regard to their representation of interdecadal variability and permitting more robust calibration of the statistical models.

4 Summary

In this thesis, a new Alpine-wide dataset of monthly precipitation fields for the 20th century has been produced, and subsequently aspects of long-term (interannual to centennial) precipitation variability in the Alpine region have been investigated. A detailed discussion of the results has been presented in the concluding sections of each of the two papers forming the core of this thesis. Here we provide only a brief overview summary, together with some further considerations.

Monthly mean precipitation analyses have been reconstructed for the region of the European Alps, extending over the period 1901–90 and resolving the rich mesoscale structure in this area of complex topography. The EOF-based statistical method of reduced-space optimal interpolation was employed. It combines a low-resolution set of 140 homogenized long-term station records (1901–90) with gridded mesoscale analyses (ANALYSIS, 25 km, 6000 stations) over a subperiod (1971–90). Special emphasis has been given to the temporal homogeneity of the reconstructed dataset in that the sparse sample comprises a constant number of quality-controlled, homogenized records.

The reconstructions have been validated with respect to the mesoscale analyses. The accuracy of the reconstructions is high (rmse 10–30%) for most parts of the mountain range, but lower (rmse 30–60%) for the south-western Alps and some of the lowland regions. Months with comparatively poor skill are found mainly in summer. However, the seasonal variation of the mean skill is small. The pattern and magnitude of multi-annual precipitation anomalies is reproduced with good accuracy. Possible further inaccuracies not accounted for by this validation may result from systematic and random biases (i.e. rain-gauge measurement and representativity errors) of the mesoscale analysis (Frei and Schär, 1998).

The reconstructions have been applied to examine the long-term precipitation variability in the Alpine region. For the 1901–90 period, the following linear trends have been found: A significant (at 10% level) increase of wintertime precipitation by 20–30% in a region extending from southern Germany, through most of Switzerland, to the south-western Alps, and a non-significant decrease by the same amount in the south-eastern Alps. A significant decrease of autumn precipitation by 20–40% in Southern France, northern Italy, and the south-eastern Alps. For the 1961–90 period significant trends are also observed in the spring season. The preliminary study of the correlations between the Alpine precipitation and the NAO during the 20th century revealed weak and highly intermittent correlations for the regions north of the Alpine ridge, but stronger and more robust correlations for the regions to the south. The above results agree qualitatively well with the findings from previous studies. However, the results of this study provide additional information on the main centers and mesoscale demarcation of the trend and correlation patterns.

Furthermore, the new mesoscale dataset has been compared with the Alpine section of a coarser global dataset (CRU05). The examination of monthly subdomain (10000-50000 km^2) time series derived from the two datasets revealed consistently high correlations (usually above 0.9) throughout the 20th century. However, the two datasets exhibit noticeable differences in low-frequency (5–20 year) variations resulting in differing linear trends on these time scales. Also, the precipitation patterns of the new dataset reveal more spatial detail, resembling the patterns analyzed from high-resolution networks. This corroborates the benefit from exploiting the mesoscale covariance structure from the short-period, dense observations in the present reconstruction.

A crucial factor for the accuracy of the reconstruction for individual regions (and for the overall skill) is the number and distribution of the long-term station records. For the current reconstruction, the station density is high in the region of the northern Alps (Austria and Switzerland, 112 stations) and low in the southern Alps and the lowland areas to the south and west of the Alpine mountain range (France, Italy, Slovenia, Croatia, 28 stations). This very inhomogeneous distribution leads to the previously cited differences in the accuracy between the northern and southern regions. Unfortunately, this imbalance is in opposition to an ideal distribution for optimal overall representativity. This is evident from the sensitivity studies conducted in part B of this thesis. The reference sample SPARSE-REF (53 stations), obtained by a covariance-guided station selection procedure, for instance, contains about 35 stations in the south and only about 20 stations for the equally large region north of the Alpine ridge. Despite its much lower number of stations (53 compared to 140 stations) the reference sample achieves about the same overall skill as the current sample of long-term stations. The success of the reference sample is related to the near-to-optimal representation of regions with different precipitation variability, thus automatically taking into account the higher spatial variability of the precipitation field in the southern Alps and Mediterranean region.

There is the potential for a number of improvements to be made to future versions of the dataset. A better station coverage, especially in the sparsely sampled southern and western areas, would not only improve the accuracy of the reconstructions, but would also allow an extension of the reconstruction to include regions already covered by the ANALYSIS dataset (e.g. the Massif Central). However, the inclusion of additional long-term stations depends on the availability of and the access to data at services in the individual countries. Closely related to this point is the question of optimal balance between temporal homogeneity and spatial sampling density. Depending on the intented use of the data, a relaxation of the current homogeneity standards in exchange for a higher station density might be beneficial. For instance, if the focus is on a short period only, higher spatial density at the cost of reduced temporal homogeneity might be preferable. A further point related to the input data is the improvement of the accuracy and temporal extension of the gridded mesoscale dataset. The accuracy could be improved by a better station coverage in those parts of the domain where the station coverage for the ANALYSIS is coarser than the nominal grid resolution (cf. Frei and Schär, 1998). Also, an extension of the period covered by the ANALYSIS would be beneficial for the calibration of the reconstruction model. If the calibration period could be extended substantially (by 10–20 years), a seasonally stratified application of the reconstruction technique could be envisaged in order to better exploit the cyclostationary character of the precipitation data.

A possible application of the reconstruction method would be the production of mesoscale precipitation analyses in quasi real time. This is not possible with the standard interpolation methods, because most high-resolution datasets are only available several months after the observations are taken (a large fraction of the data has to be digitized from manual observations). The method presented in this thesis could be used to reconstruct the precipitation fields in real time using data from a set of selected observation sites (e.g. SYNOP stations). Furthermore, the covariance-guided station selection procedure could be used to define a network of automatic stations, representative for the area under consideration, which would yield real-time reconstructions with better quality. Clearly, this application would become even more attractive if it could be extended to the daily time scale.

Possible applications of the new dataset include the validation of regional climate models (RCMs) and general circulation models (GCMs), the development of regional precipitation scenarios from downscaling studies, the use for ecosystem and hydrological models, and a detailed analysis of the interannual and longer-term, mesoscale precipitation variability and its relation to the larger-scale forcings. For instance, use of the long-term data for a direct comparison of the skill of nonlinear, classification-based downscaling methods (e.g. Hewitson and Crane, 1996; Zorita and von Storch, 1999) with linear methods (e.g. Gyalistras et al., 1994; Widmann, 1996) to capture multidecadal variability could help to isolate those predictors of the continental atmospheric water cycle that are most relevant for the Alpine precipitation climate. A successful description of the link to the atmospheric circulation and the state of the neighbouring seas could serve to assess the consequences of an altered large-scale climate for regional precipitation and to understand the physical processes (e.g. Trenberth, 1998, 1999) which led to the observed 20th century precipitation changes. These important and open issues merit consideration using the mesoscale centennial precipitation dataset developed in this thesis.

A Mean precipitation and variability
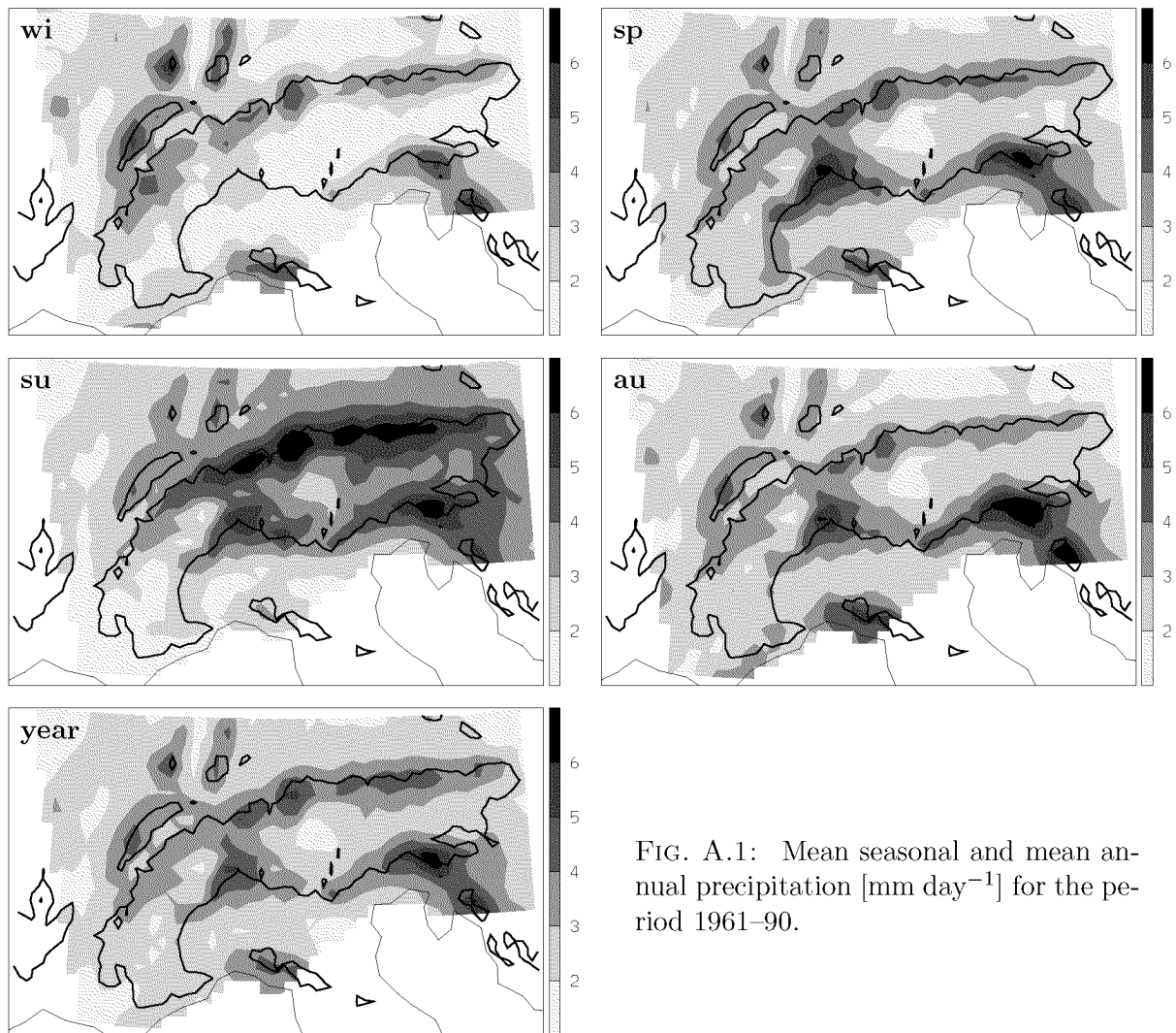
FIG. A.1: Mean seasonal and mean annual precipitation [mm day^{-1}] for the period 1961–90.
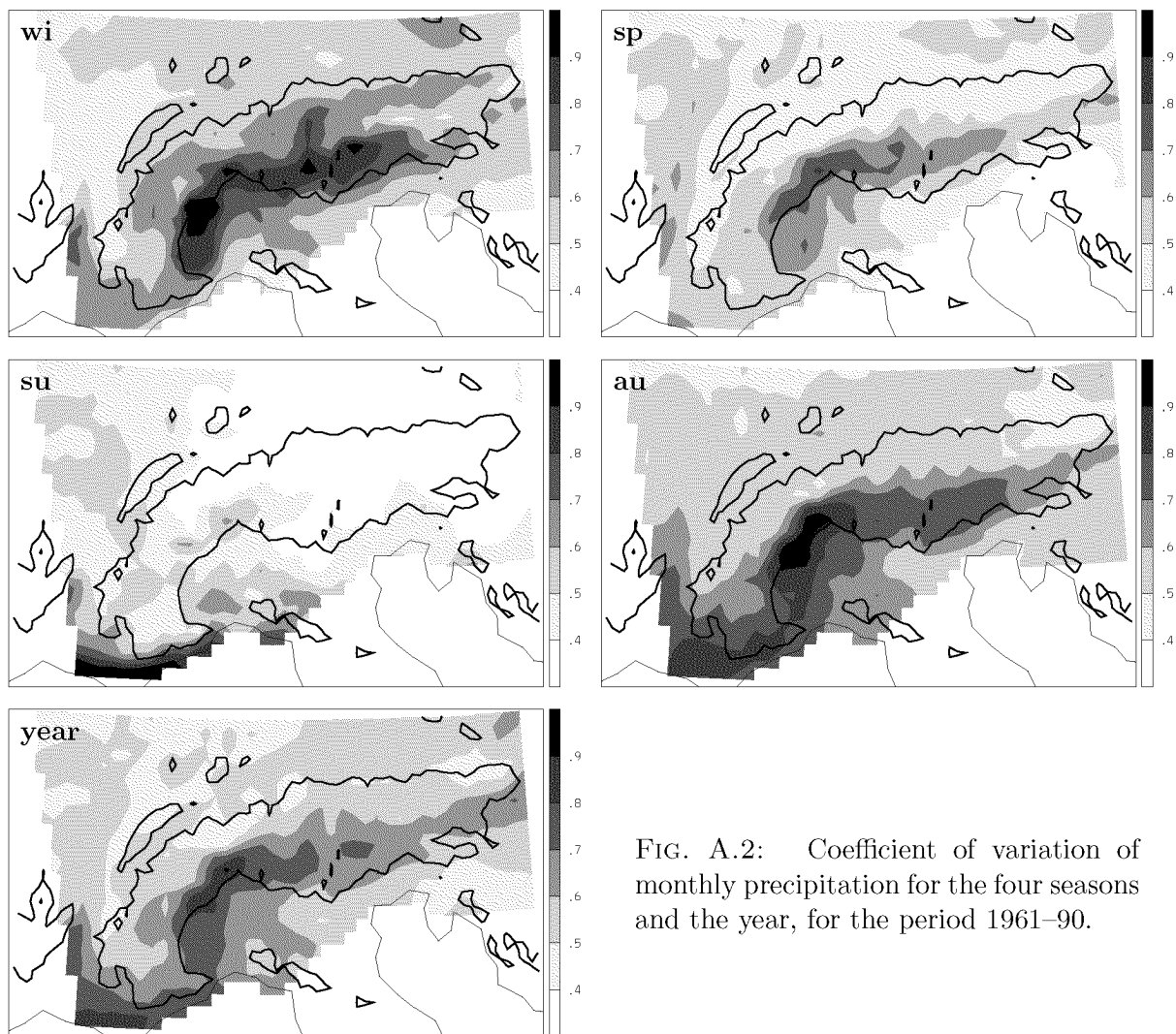
FIG. A.2: Coefficient of variation of monthly precipitation for the four seasons and the year, for the period 1961–90.

B   Decadal precipitation means
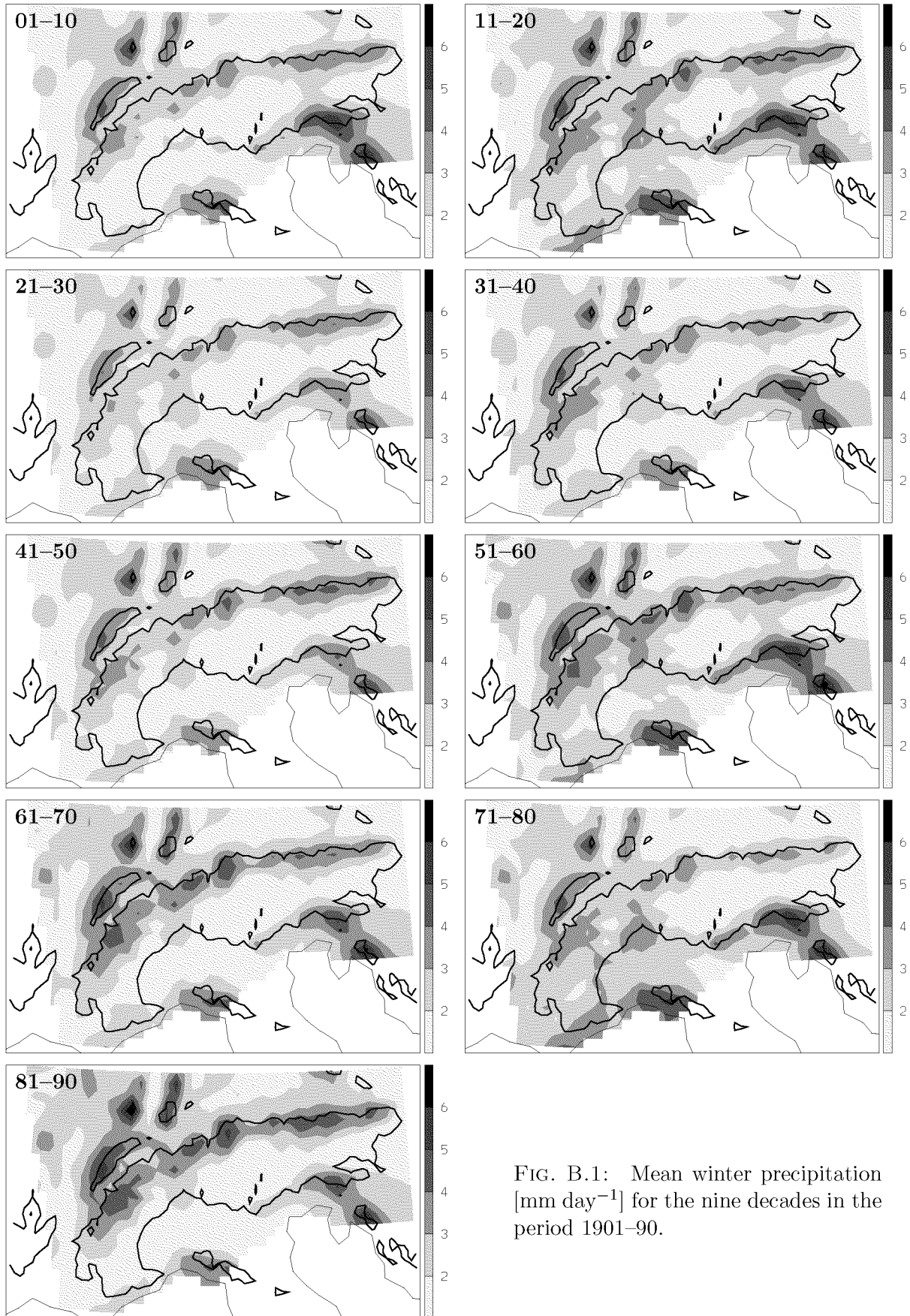
FIG. B.1: Mean winter precipitation [mm day^{-1}] for the nine decades in the period 1901–90.
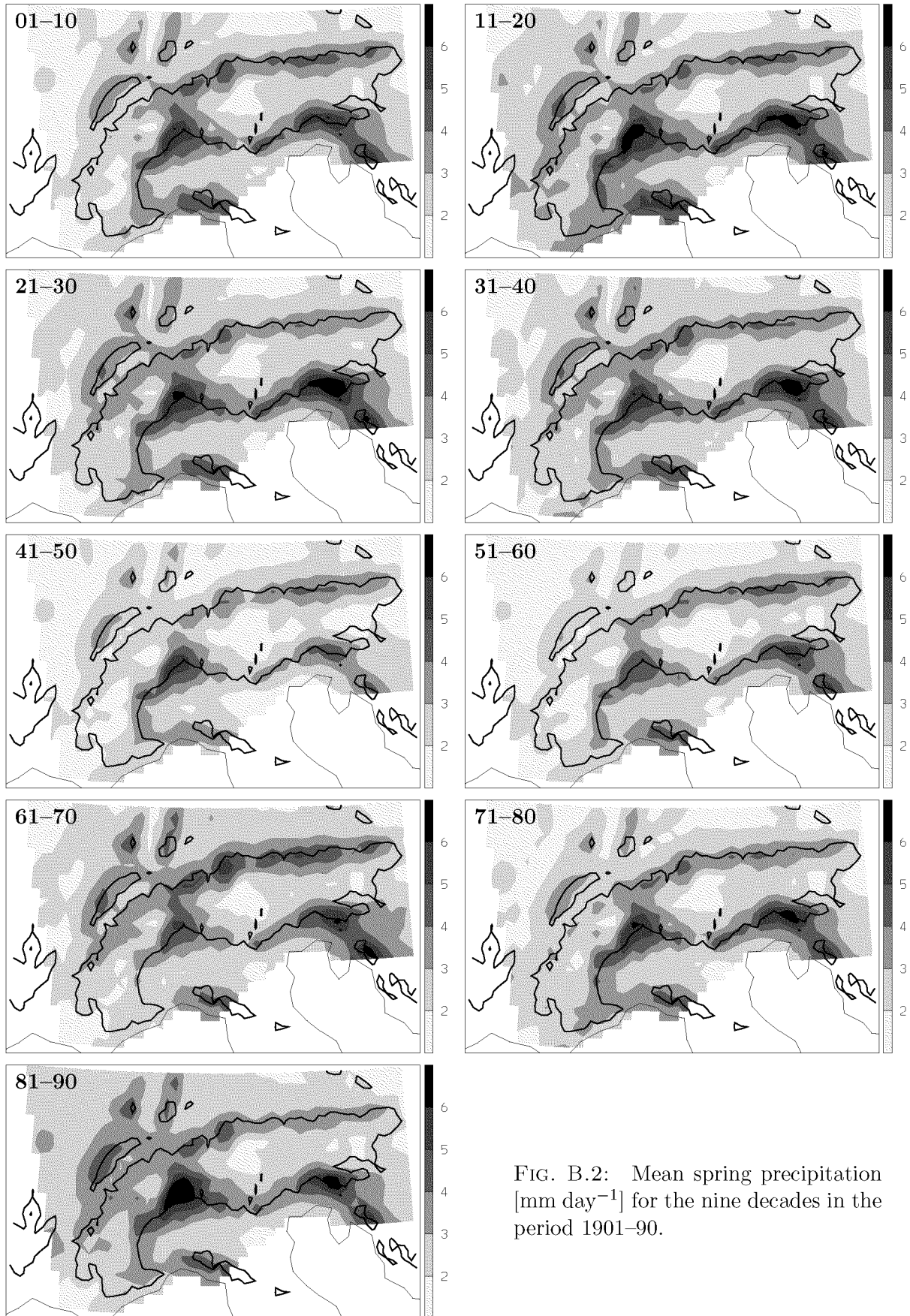
FIG. B.2: Mean spring precipitation [mm day^{-1}] for the nine decades in the period 1901–90.
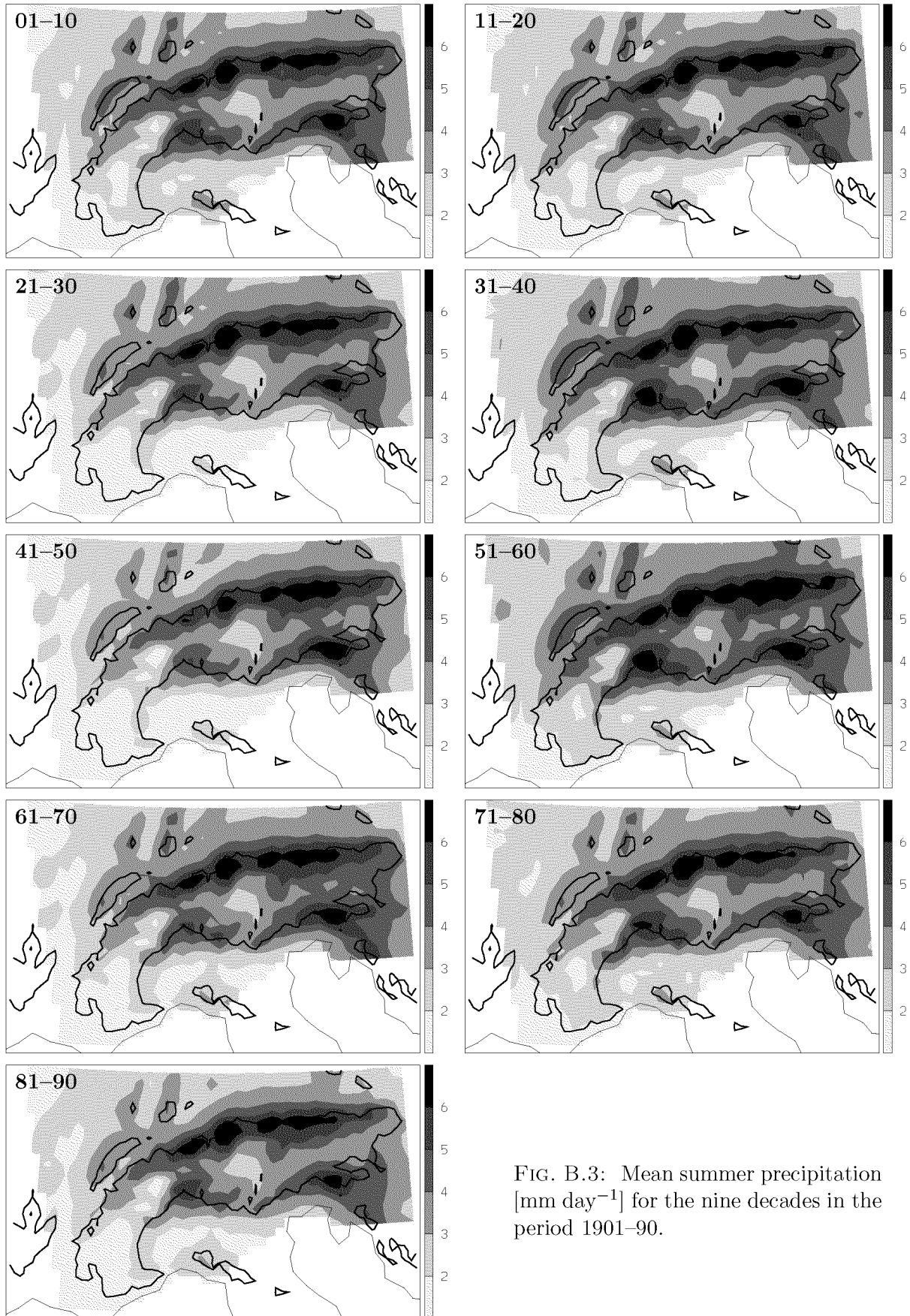
FIG. B.3: Mean summer precipitation [mm day^{-1}] for the nine decades in the period 1901–90.
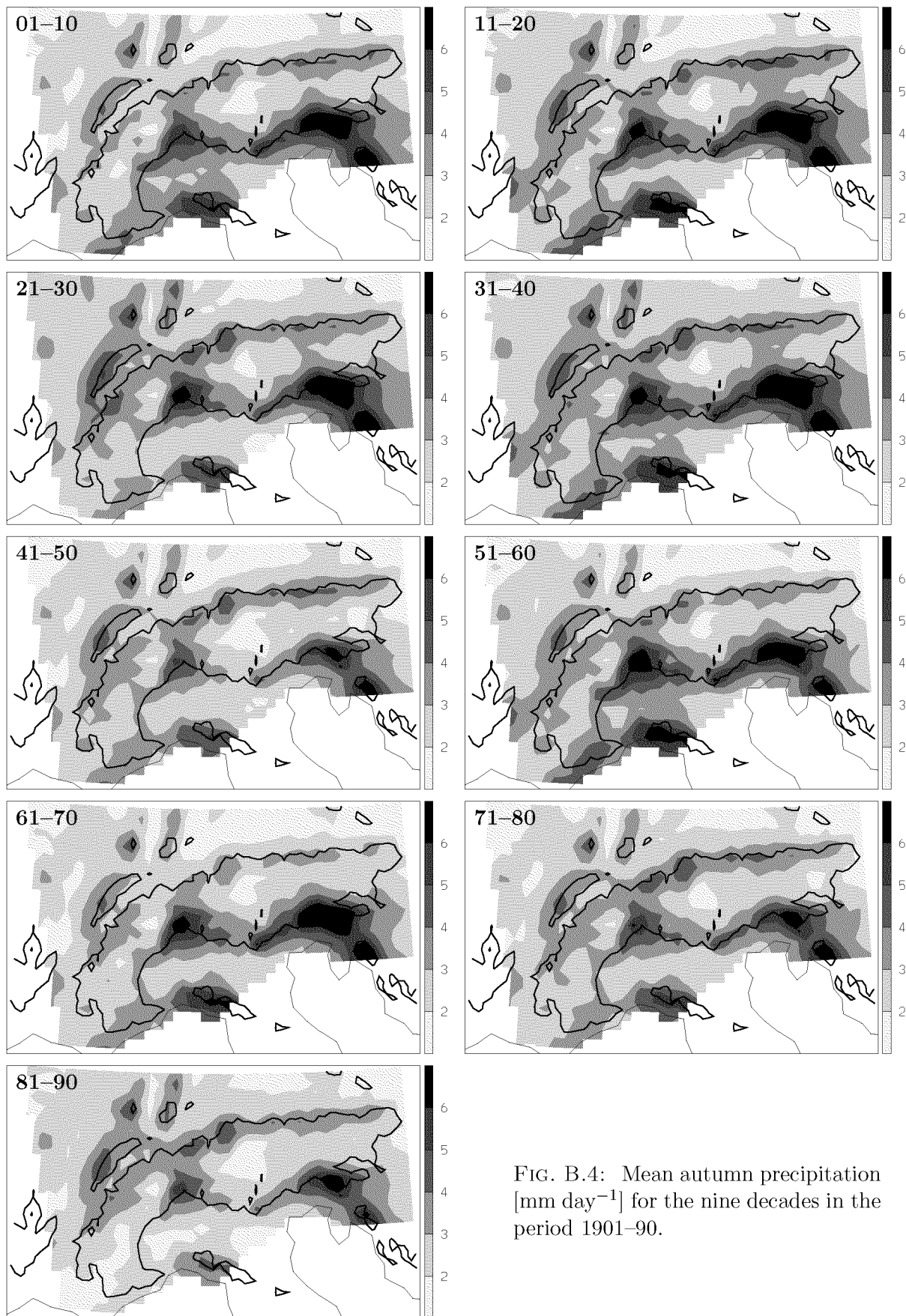
FIG. B.4: Mean autumn precipitation [mm day^{-1}] for the nine decades in the period 1901–90.

C Extreme cases
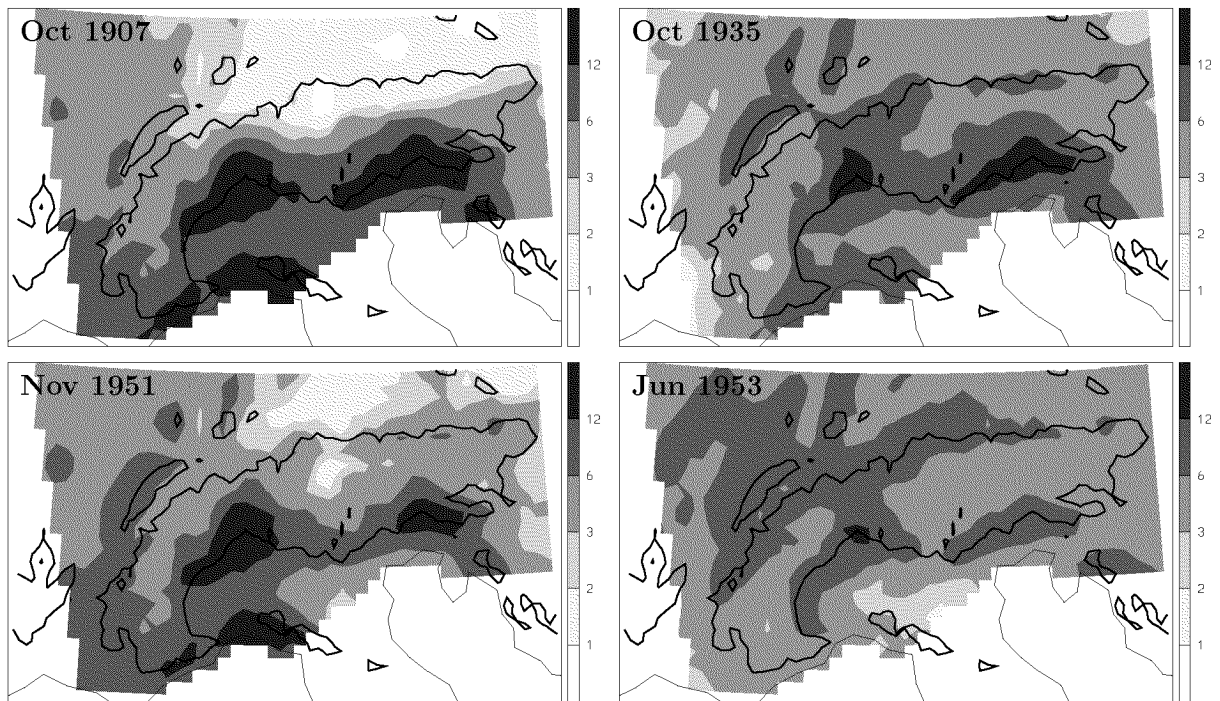
FIG. C.1:   Reconstructed precipitation [mm day^{-1}] for the four wettest months, in terms of domain-mean precipitation, in the period 1901–90. The domain-mean precipitation is about 5.5 mm day^{-1}.
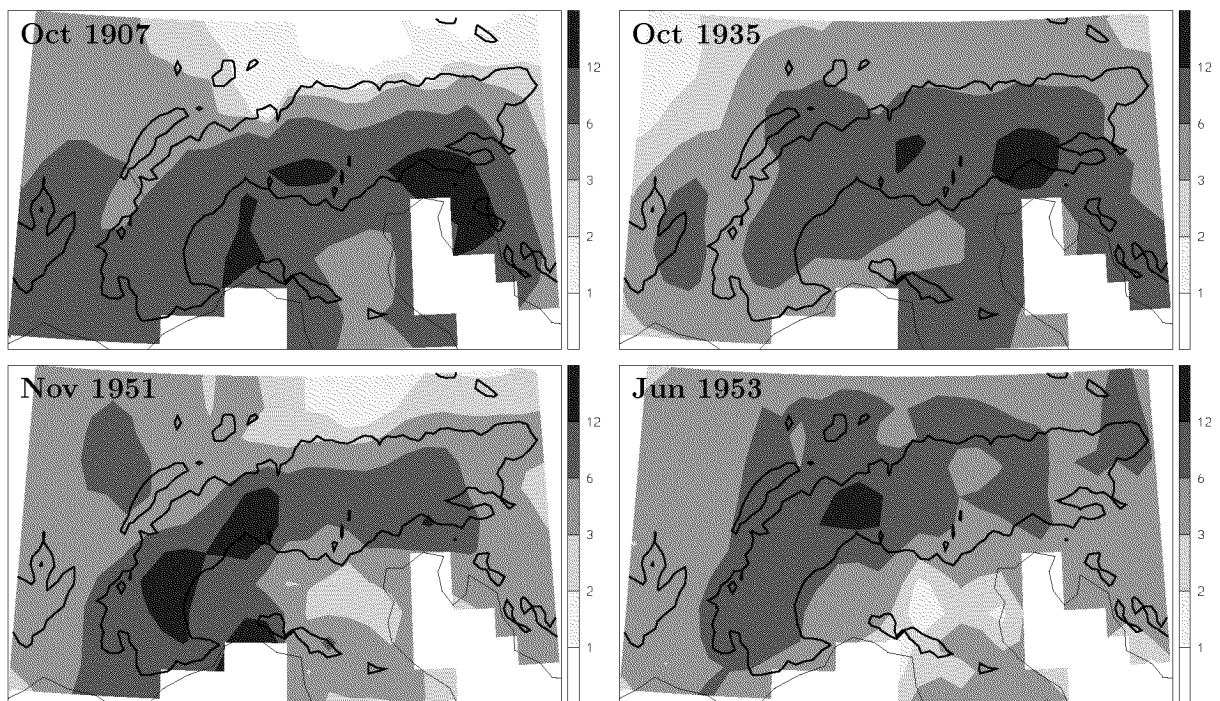
FIG. C.2:   As Fig. C.1, but for the global dataset CRU05.
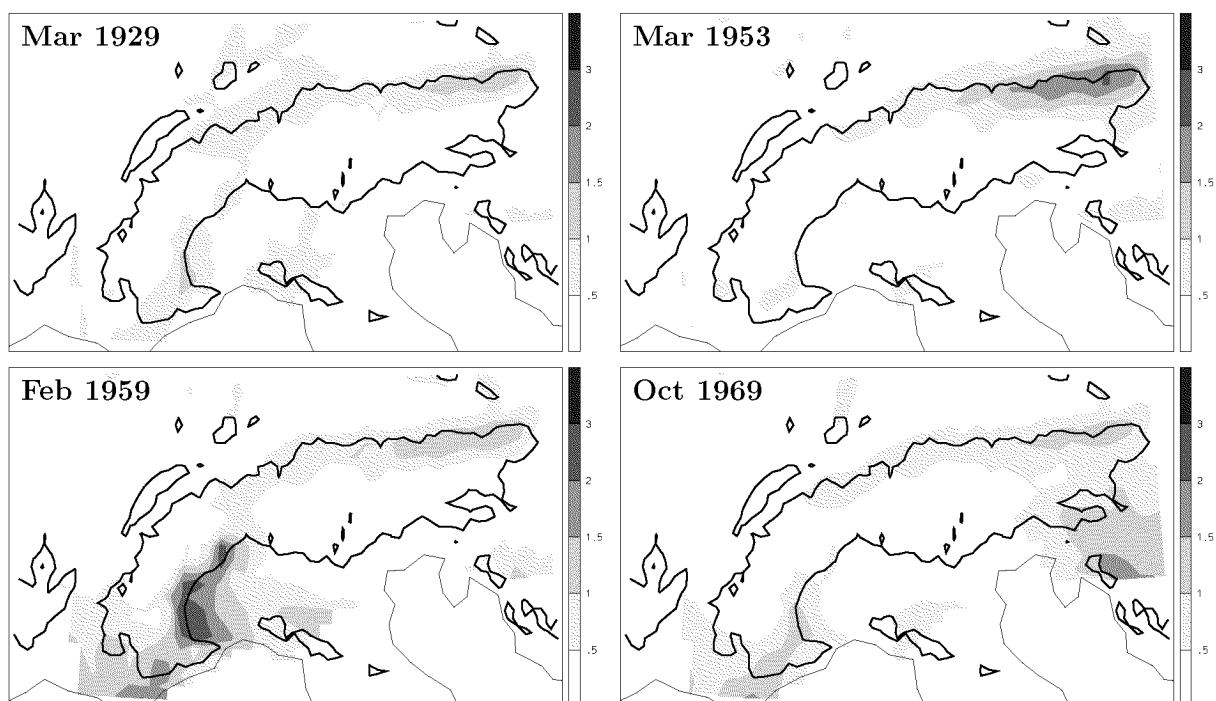
FIG. C.3: Reconstructed precipitation [mm day^{-1}] for the four driest months, in terms of domain mean precipitation, in the period 1901–90. The domain-mean precipitation is about 0.5 mm day^{-1}.
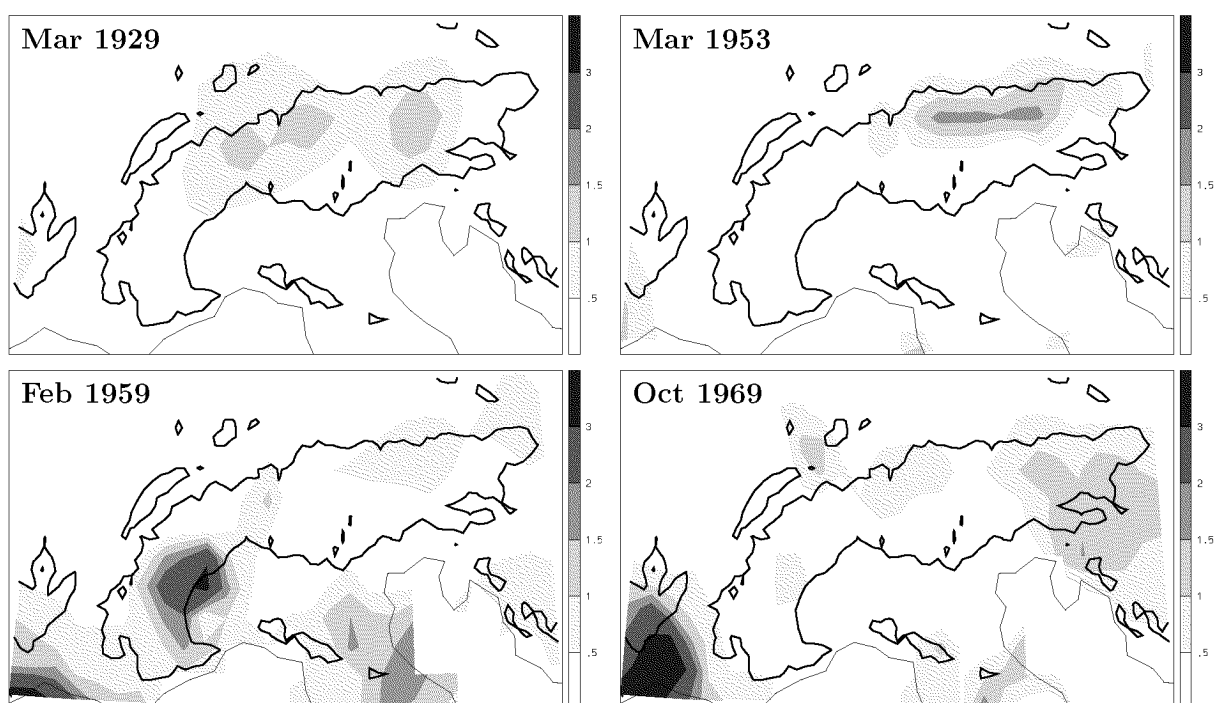
FIG. C.4: As Fig. C.3, but for the global dataset CRU05.

D Regionalization: REOF patterns
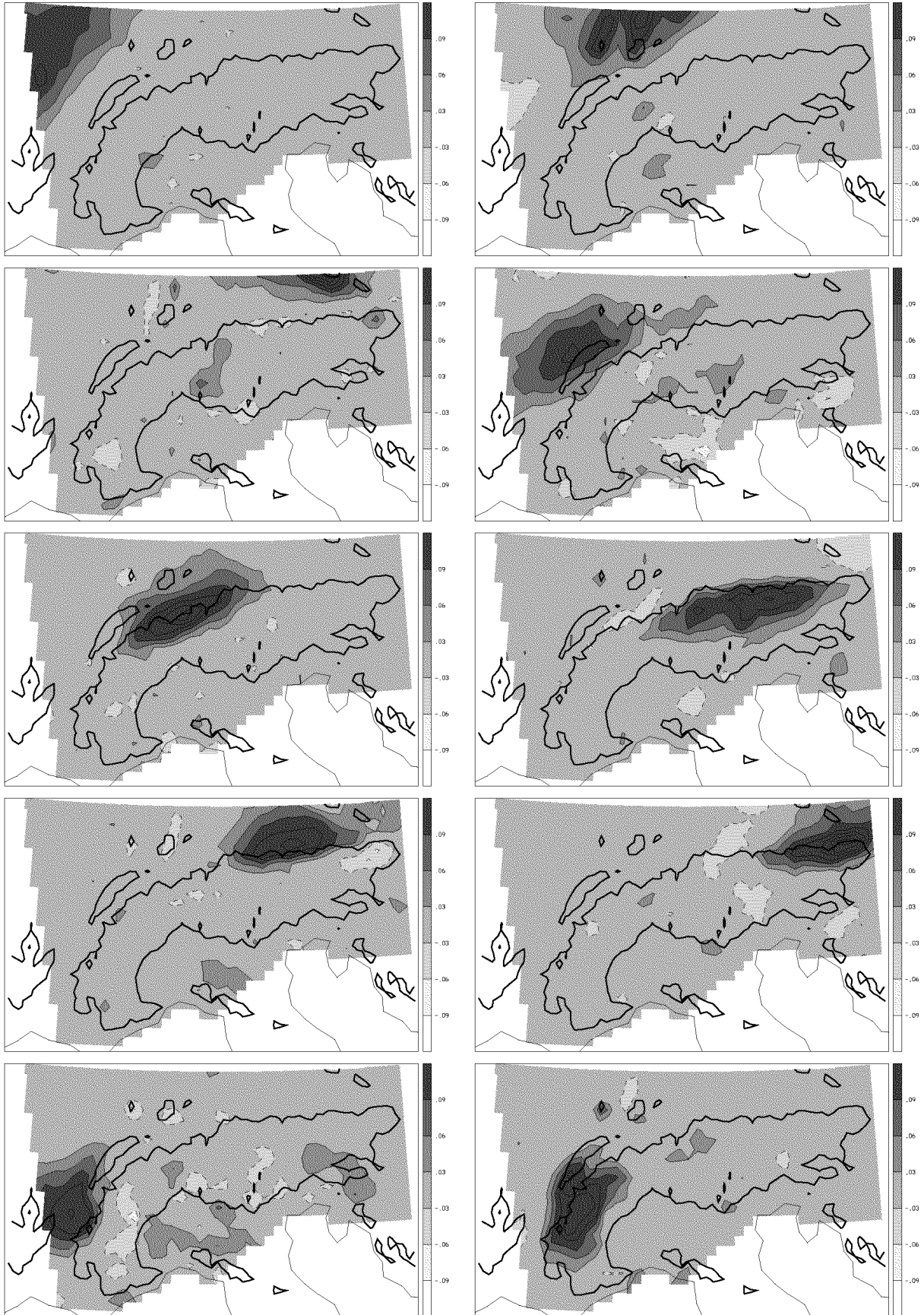
FIG. D.1: REOF patterns determined from the leading 28 EOFs of monthly precipitation for the years 1971–90.
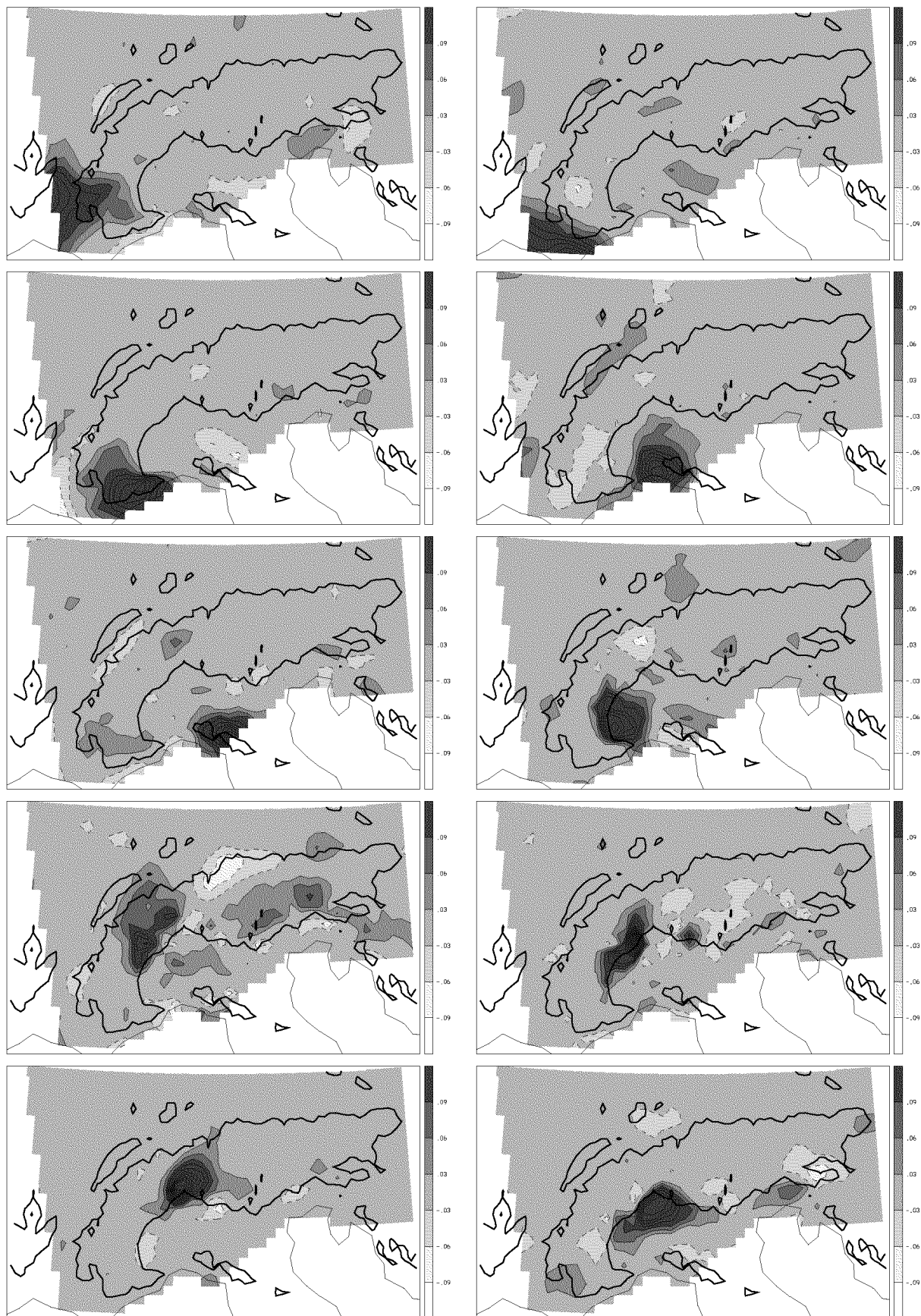
FIG. D.1: (cont.)
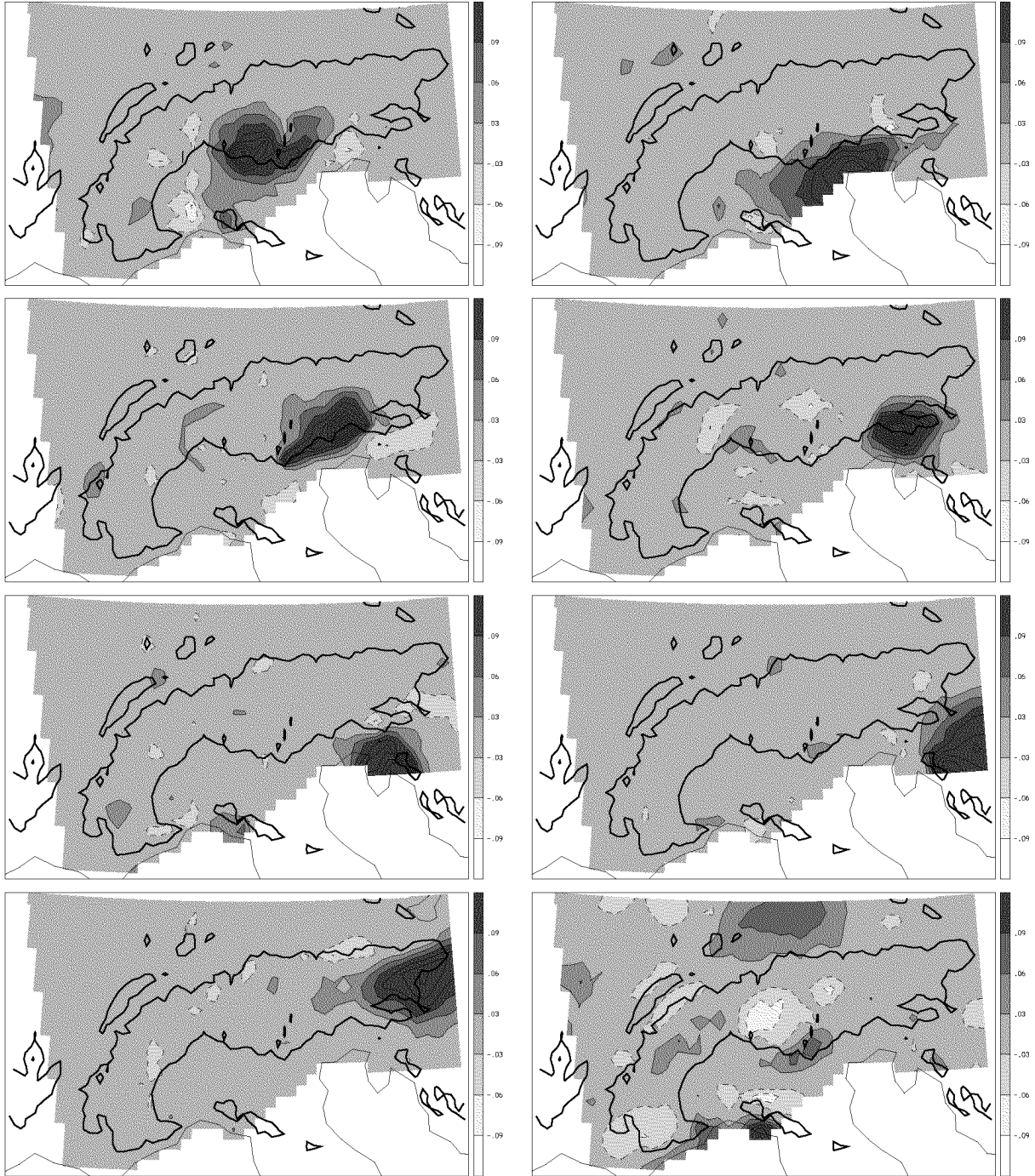
FIG. D.1: (cont.)

E Mean annual cycle of the five leadings RPCs

Western Alps (WEA)

Northern Alps (NOA)

Ticion (TIC)

Mediterranean (MED)

South-eastern Alps (SEA)
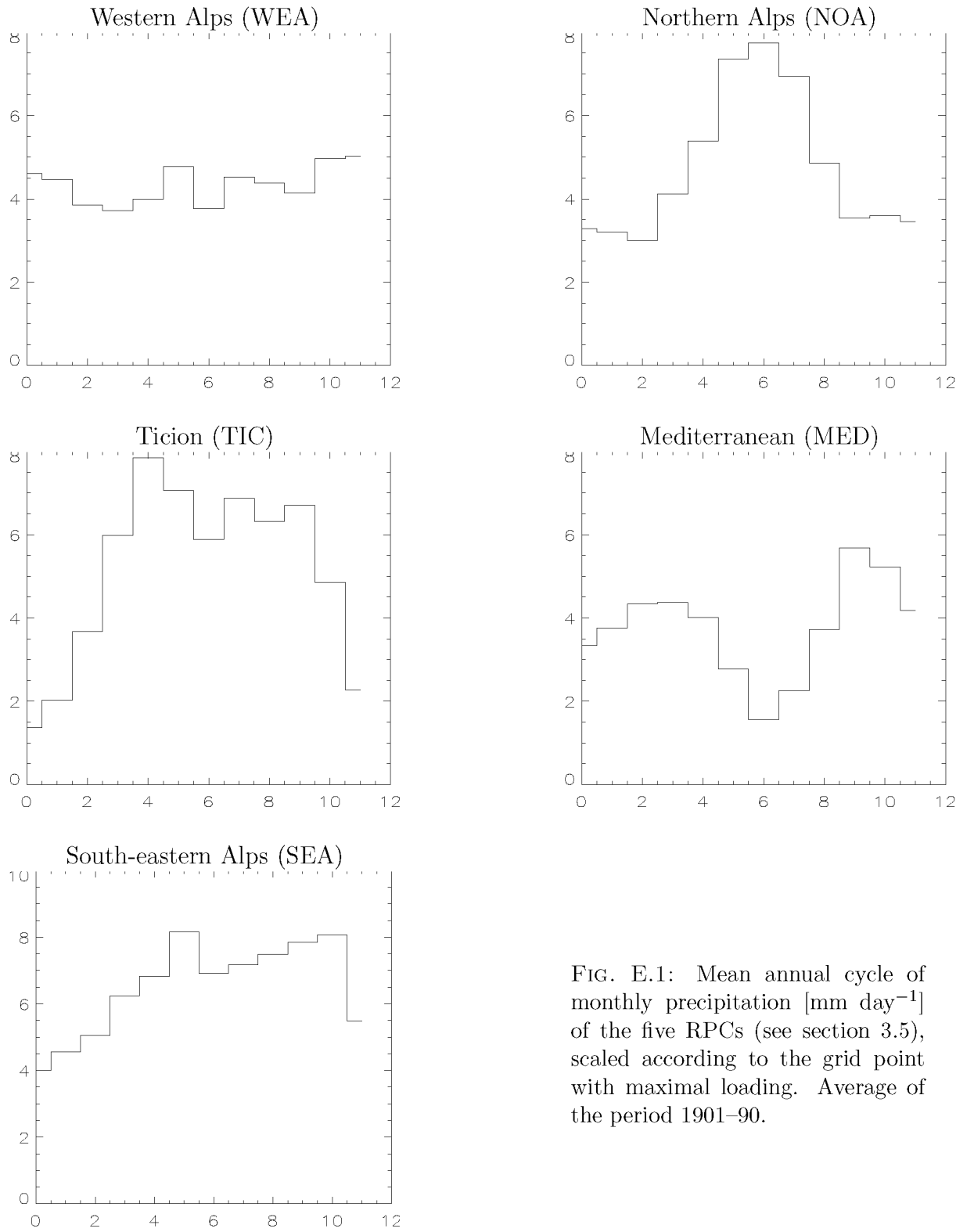
FIG. E.1: Mean annual cycle of monthly precipitation [mm day^{-1}] of the five RPCs (see section 3.5), scaled according to the grid point with maximal loading. Average of the period 1901–90.

F Precipitation anomalies associated with high-low NAO months
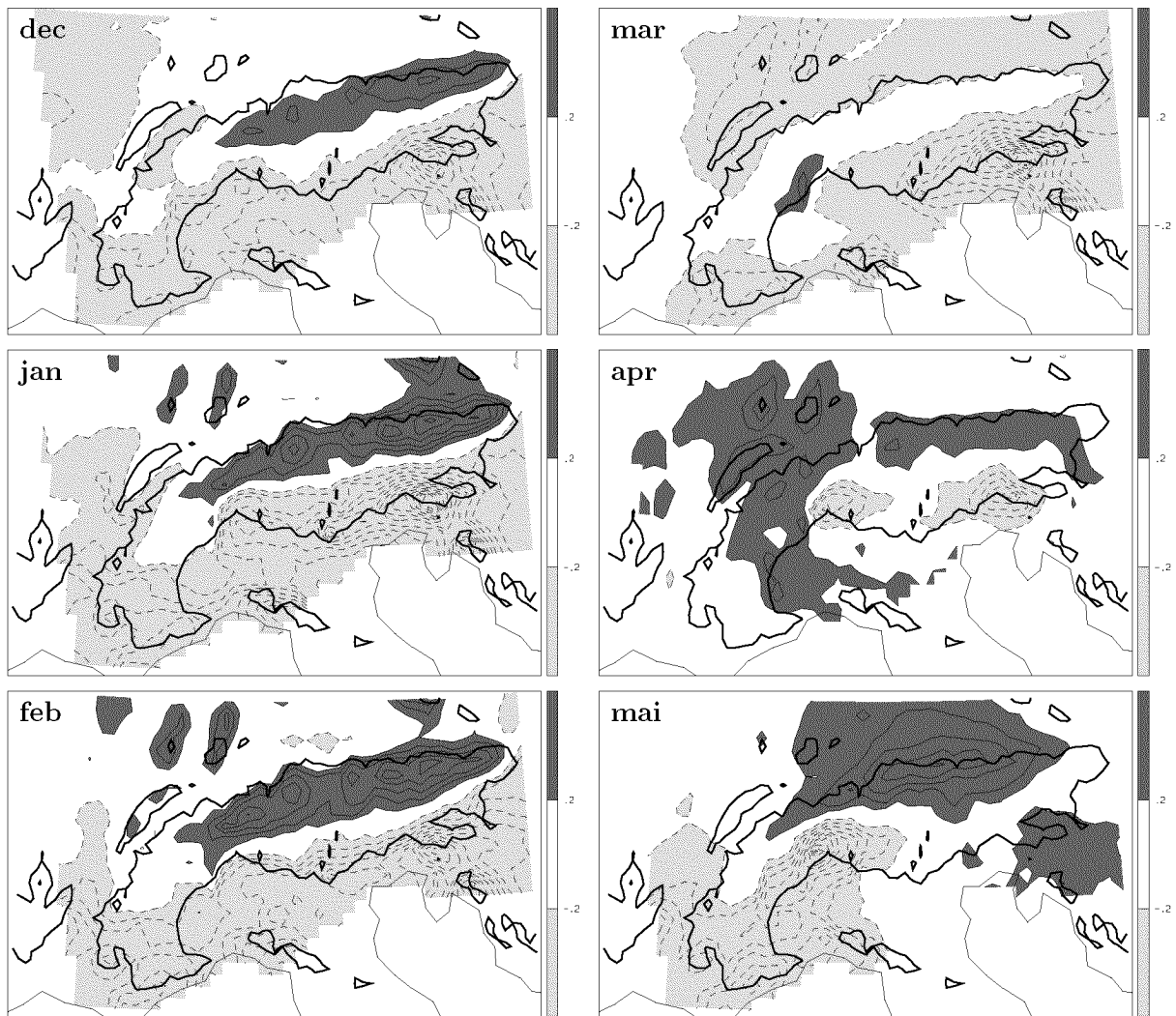
FIG. F.1: Mean precipitation anomalies [mm day^{-1}] associated with high-low NAO months expressed as departures from the 1901–90 mean. High (low) NAO months are those with the NAOI in the upper (lower) quartile. The contour increment is 0.2 mm day^{-1}.
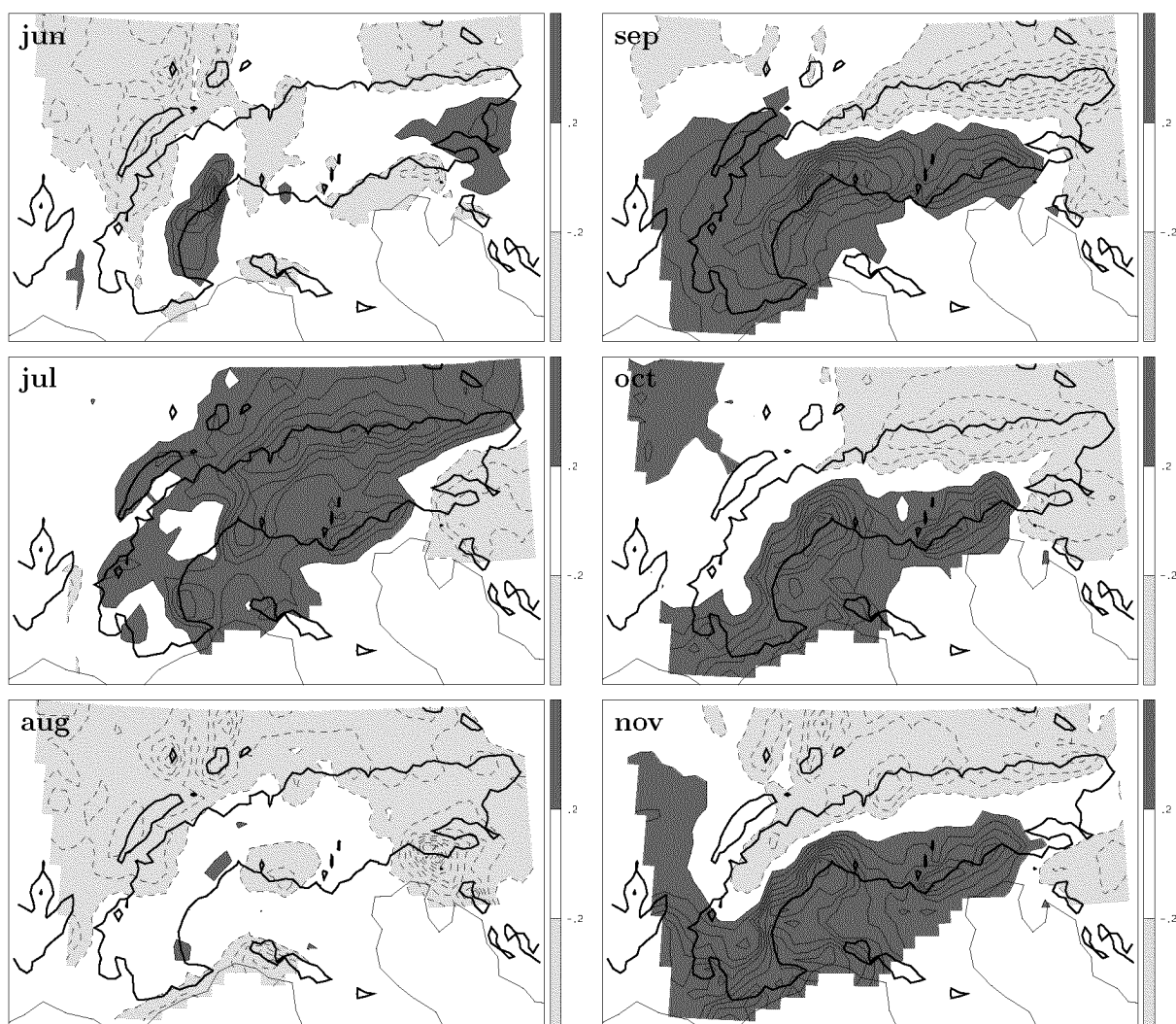
FIG. F.1: (cont.)

G Cross validation
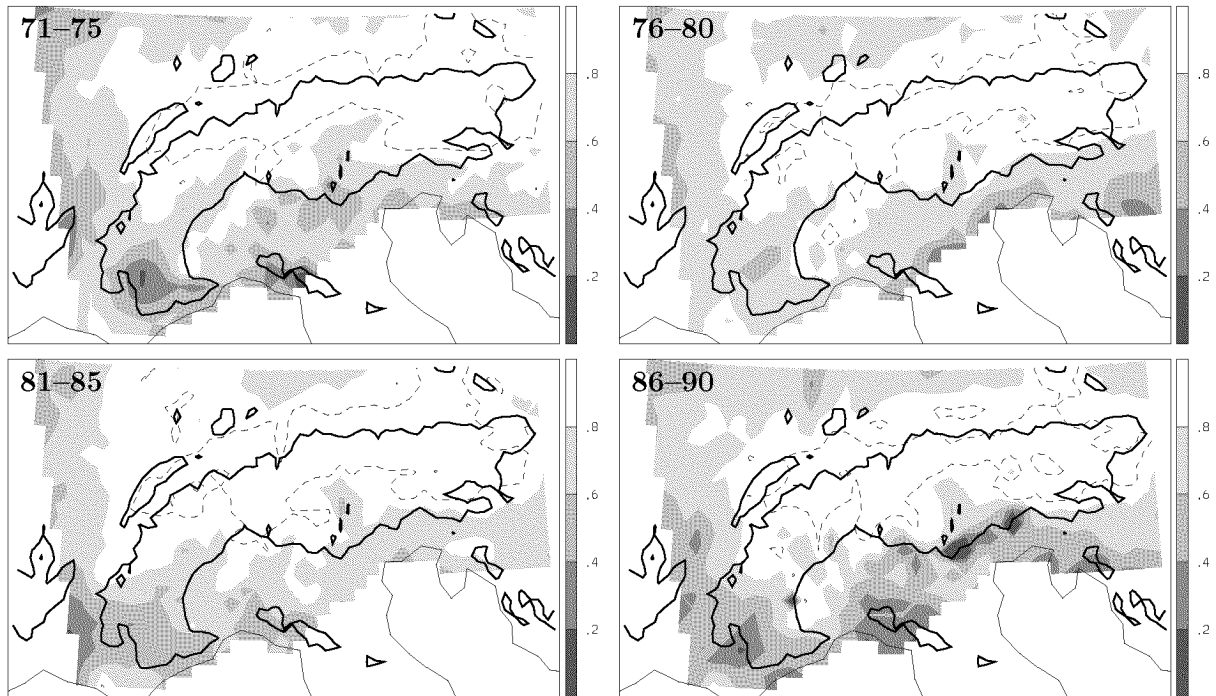
FIG. G.1:   Resolved variance skill β for four independent validation periods (see section 3.4). The dashed line depicts the 0.9 contour.
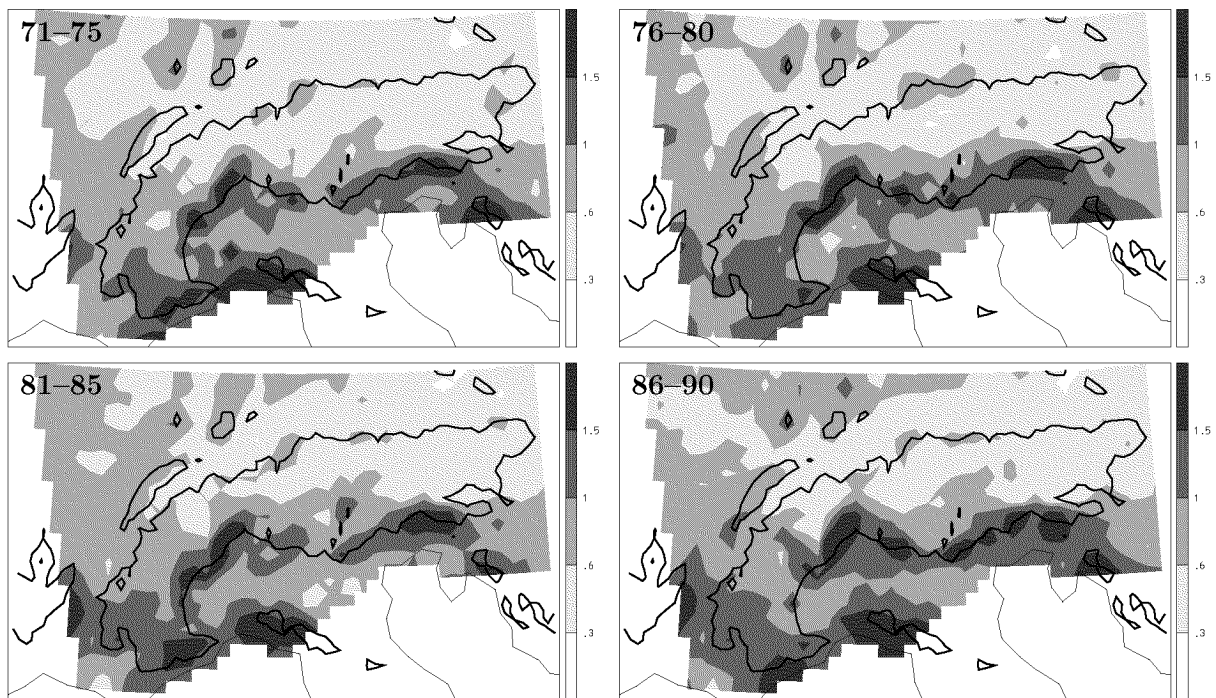
FIG. G.2:   As Fig. G.1, but for the root-mean-square error [mm day^{-1}].
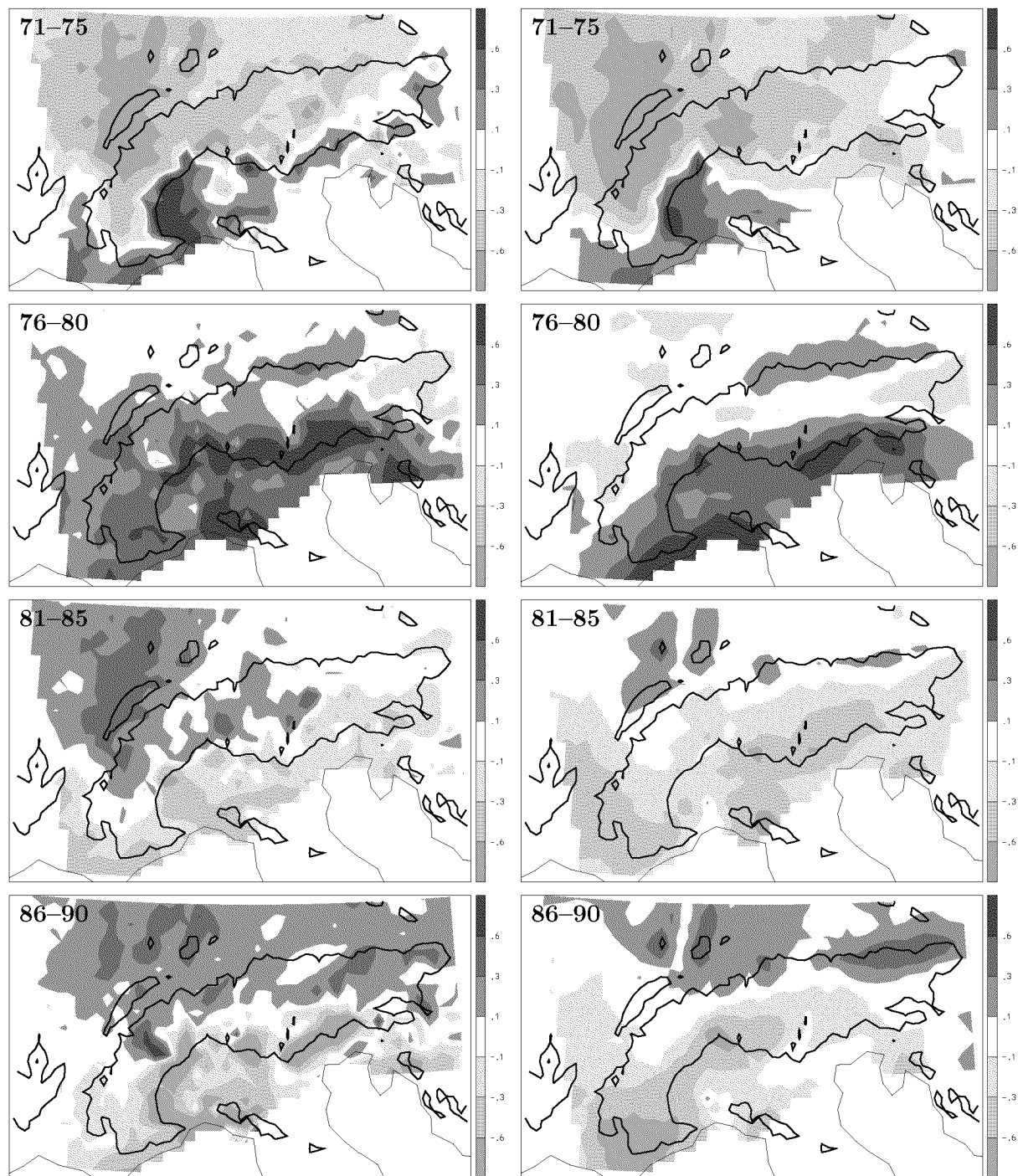
FIG. G.3: As Fig. G.1, but for the differences of mean annual precipitation [mm day^{-1}] between the validation and the calibration period: in the ANALYSIS (left panels), in the reconstruction (right panels).

H Station List

Station and related homogeneity list of the long-term records
(see section 3.2.b).

No	Name	Height	Lat	Long	Adjust	Qual
001	WienHoheWarte	203	16.35	48.24	yes	4
002	InnsbruckUni	578	11.39	47.25	no	1
003	GrazUni	366	15.45	47.08	no	3
004	Bildstein	730	9.78	47.47	no	1
005	Schroecken	1263	10.08	47.26	yes	2
006	Tannheim-Untergschwend	1090	10.50	47.50	yes	4
007	Scharnitz	960	11.26	47.39	yes	2
008	Hinterri	930	11.46	47.47	yes	2
009	Pertisau	935	11.70	47.44	no	1
010	Scuolschuls	1295	10.29	46.80	no	2
011	Ried	880	10.66	47.06	no	1
012	See	1040	10.47	47.09	no	1
013	Ritzenried	1120	10.79	47.12	no	1
014	Schwaz	535	11.71	47.35	yes	4
015	Rotholz	590	11.80	47.39	no	1
016	Kitzbuhel	763	12.40	47.45	no	1
017	Groarl	890	13.20	47.24	yes	2
018	St.Martin	970	13.38	47.47	yes	4
019	Huttau	730	13.31	47.41	no	1
020	Eugendorf	540	13.12	47.87	yes	4
021	Mattighofen	455	13.14	48.08	no	2
022	Vichtenstein	586	13.66	48.53	yes	2
023	Schwarzenberg	730	13.84	48.73	no	2
024	Schlaegl	555	13.96	48.64	yes	4
025	Haslach	526	14.04	48.59	yes	4
026	Goldwoerth	260	14.10	48.33	no	4
027	Neukirchen	555	13.78	48.41	yes	4
028	Bad	469	13.63	47.72	no	1
029	St.Gilgen	540	13.37	47.77	no	2
030	Fuschl	670	13.31	47.80	yes	4
031	Wolfsegg	585	13.68	48.11	yes	4
032	Lambach	360	13.87	48.10	yes	4
033	St.Florian	257	14.38	48.20	no	3
034	Hohentauern	1265	14.49	47.43	yes	4
035	Hieflau	492	14.74	47.61	yes	4
036	Weyer	410	14.67	47.86	yes	4
037	Reichraming	360	14.47	47.89	no	1
038	Spital	630	14.33	47.67	no	4
039	Klaus	458	14.16	47.83	yes	4
040	Gutau	610	14.61	48.42	no	2
041	Poeggstall	462	15.21	48.32	yes	4
042	Turnitz	460	15.49	47.93	yes	2
043	Maedihutte	380	16.13	48.27	yes	4
044	Wien-Mariabrunn	226	16.23	48.21	no	1
045	Weitra	580	14.89	48.70	no	4

No	Name	Height	Lat	Long	Adjust	Qual
046	Mailberg	220	16.19	48.68	no	2
047	Mariensee	780	15.97	47.54	no	1
048	Kirchberg	550	15.99	47.61	no	1
049	Deutsch	190	16.48	47.94	no	1
050	Weiz	480	15.64	47.22	no	1
051	Sinabelkirchen	330	15.83	47.10	no	1
052	Pinkafeld	389	16.12	47.37	no	1
053	St.Michael	1040	13.64	47.10	yes	4
054	Weipriach	1120	13.70	47.18	no	2
055	Tamsweg	1020	13.81	47.13	no	2
056	Murau	825	14.18	47.11	no	2
057	Noreia	1060	14.53	47.01	no	1
058	Oberwoelz	810	14.28	47.20	no	1
059	Kraubath	605	14.94	47.31	no	1
060	Frohnleiten	440	15.32	47.27	yes	2
061	Maria	530	15.07	47.07	yes	2
062	Deutschlandsberg	410	15.21	46.83	yes	4
063	Leibnitz	332	15.51	46.78	no	1
064	Kirchbach	350	15.67	46.93	yes	3
065	Bad	303	15.90	46.87	no	1
066	St.Johann	750	12.63	46.90	no	2
067	Oberdrauburg	620	12.98	46.75	yes	4
068	Greifenburg	610	13.18	46.75	no	1
069	Sachsenburg	550	13.35	46.83	yes	4
070	Obervellach	675	13.19	46.94	no	1
071	Afritz	715	13.80	46.73	no	1
072	Maria	1140	12.75	46.70	yes	4
073	Kornat	1025	12.89	46.69	no	1
074	Feistritz	590	13.61	46.57	yes	4
075	Latschach	610	13.93	46.56	no	2
076	Sirnitz	850	14.06	46.82	no	1
077	Klagenfurt(Flugplatz)	448	14.33	46.65	yes	2
078	Zagrebgric	157	15.98	45.82	no	1
079	Dijon	222	5.08	47.27	no	1
080	Grenoble	384	5.33	45.37	yes	2
081	Nancy	225	6.22	48.68	no	1
082	Marseille	75	5.40	43.31	no	2
083	Marignylecahouet	310	4.46	47.46	no	1
084	Besancon	307	5.99	47.25	no	1
085	Stuttgart	314	9.12	48.50	yes	2
086	Muenchen	529	11.42	48.07	no	1
087	Hohenpeissenberg	977	11.02	47.80	no	1
088	Kempten	705	10.20	47.43	yes	2
089	Weissenhorn	506	10.10	48.18	yes	3
090	Mindelheim	607	10.30	48.03	no	2
091	Metten	313	12.55	48.51	yes	4
092	Schneizlreuthweissbach	630	12.46	47.43	yes	4
093	Asti	158	8.18	44.91	no	2
094	Cuneo	567	7.55	44.38	yes	3

No	Name	Height	Lat	Long	Adjust	Qual
095	Moncalvo	297	8.27	45.05	no	1
096	Mondovi	416	7.82	44.40	no	4
097	Novara	181	8.62	45.45	yes	4
098	Noviligure	186	8.78	44.77	no	1
099	Torino	270	7.67	45.07	no	2
100	Varallo	454	8.25	45.81	yes	4
101	Parma	56	10.30	44.80	yes	2
102	Trento	312	11.10	46.10	no	1
103	Trieste	8	13.75	45.65	no	1
104	Mantova	55	10.75	45.15	no	1
105	Jlanz	707	9.21	46.77	yes	4
106	Arosa	1847	9.68	46.78	no	1
107	Churems	555	9.53	46.87	yes	2
108	Kilchbergbl	585	7.90	47.43	no	1
109	Delemont	416	7.35	47.36	no	1
110	Baselbinningen	317	7.58	47.54	no	3
111	Flawil	572	9.20	47.42	no	2
112	Niederneunforn	457	8.78	47.60	no	3
113	Grueningen	490	8.77	47.28	yes	4
114	Lachensz	426	8.86	47.19	yes	4
115	Kuesnachtzh	412	8.59	47.31	no	2
116	Zuerichsma	556	8.57	47.38	no	4
117	Baden	381	8.31	47.47	yes	4
118	Goeschenen	1111	8.59	46.67	yes	4
119	Engelberg	1018	8.41	46.82	no	4
120	Sarnen	479	8.25	46.89	yes	4
121	Meiringen	632	8.19	46.73	yes	4
122	Bernliebefeld	570	7.42	46.93	no	1
123	Chateaudoex	980	7.14	46.48	no	1
124	Aarberg	450	7.28	47.04	no	1
125	Valeyressousr	512	6.53	46.75	yes	4
126	Couvet	750	6.63	46.90	no	3
127	Langnauie	695	7.79	46.94	yes	4
128	Sturban	491	7.84	47.23	no	2
129	Aeschlu	450	8.23	47.26	yes	2
130	Beznau	327	8.24	47.56	yes	4
131	Zermatt	1638	7.75	46.03	no	1
132	Leukerbad	1285	7.62	46.38	yes	2
133	Grandstbernard	2479	7.17	45.87	yes	4
134	Bourgstpierre	1620	7.21	45.95	yes	2
135	Lausanne	618	6.64	46.53	no	1
136	Longirod	890	6.26	46.50	yes	4
137	Jussy	465	6.26	46.24	yes	2
138	Mesocco	815	9.23	46.39	no	1
139	Lugano	276	8.96	46.01	yes	2
140	Brusio	830	10.13	46.26	no	1

Definition of the quality flags in terms of the error probabilities α of the standard normal homogeneity test.

Qual	Adjust	Iteration		
		final	second	first
1	no	$\alpha > 5\%$	$\alpha > 5\%$	$\alpha > 1\%$
2	no/yes	$\alpha > 10\%$	$5\% \geq \alpha > 0.1\%$	$1\% \geq \alpha > 0.1\%$
3	no/yes	$10\% \geq \alpha > 5\%$	$5\% \geq \alpha > 0.1\%$	$1\% \geq \alpha > 0.1\%$
4	no/yes	$\alpha > 10\%$	$0.1\% > \alpha$	$0.1\% > \alpha$

References

Aebischer, U., and C. Schär, 1998: Low-level potential vorticity and cyclogenesis to the lee of the Alps. *J. Atmos. Sci.*, **55**, 186–207.

Airey, M., and M. Hulme, 1995: Evaluating climate model simulations of precipitation: Methods, problems and performance. *Prog. Phys. Geog.*, **19**, 427–448.

Alexandersson, H., 1986: A homogeneity test applied to precipitation data. *J. Climatol.*, **6**, 661–675.

Aschwanden, A., M. Beck, C. Haeberli, G. Haller, M. Kiene, A. Roesch, R. Sie, and M. Stutz, 1996: Bereinigte Zeitreihen. Die Ergebnisse des Projekts KLIMA90. Band 2: Methoden. Tech. Rep. 2.2, MeteoSwiss, 127 pp. [Available from MeteoSwiss, Krähbühlstrasse 58, CH-8044 Zürich, Switzerland].

Auer, I., and R. Böhm, 1994: Combined temperature-precipitation variations in Austria during the instrumental period. *Theor. Appl. Climatol.*, **49**, 161–174.

Auer, I., R. Böhm, and H. Mohnl, 1993: Climate change on Sonnblick - A multielemental approach to describe climate change using a centennial data set. *Proc., Eighth Conf. on Applied Climatology*, Boston, MA, Amer. Meteor. Soc., 249–251.

Auer, I., R. Böhm, and W. Schöner, 2001: Austrian long-term climate 1767–2000. Österreichische Beiträge zu Meteorologie und Geophysik 25, ZAMG, 147 pp. [Zentralanst. für Meteorologie und Geodynamik, Wien, Austria].

Barnston, A. G., and R. E. Livezey, 1987: Classification, seasonality and persistence of low-frequency atmospheric circulation patterns. *Mon. Wea. Rev.*, **115**, 1083–1126.

Beniston, M., M. Rebetez, F. Giorgi, and M. R. Marinucci, 1994: An analysis of regional climate change in Switzerland. *Theor. Appl. Climatol.*, **49**, 135–159.

Benteli, A., 1870: Die atmosphärischen Niederschläge in den 7 Hauptflussgebieten der Schweiz. *Schweiz. Meteorol. Beobachtungen*, **7**, 7–16.

Biau, G., E. Zorita, H. von Storch, and H. Wackernagel, 1999: Estimation of precipitation by kriging in the EOF space of the sea level pressure field. *J. Climate*, **12**, 1070–1085.

Bresch, D. N., and H. C. Davies, 2000: Covariation of the mid-tropospheric flow and the sea surface temperature of the North Atlantic: A statistical analysis. *Theor. Appl. Climatol.*, **65**, 197–214.

Briffa, K. R., P. D. Jones, and F. H. Schweingruber, 1992: Tree-ring density reconstructions of summer temperature patterns across western North-America since 1600. *J. Climate*, **5**, 735–754.

Browning, K. A., 1985: Conceptual models of precipitation systems. *ESA Journal*, **9**, 157–180.

Buffoni, L., M. Maugeri, and T. Nanni, 1999: Precipitation in Italy from 1833 to 1996. *Theor. Appl. Climatol.*, **63**, 33–40.

Cacciamani, C., F. Battaglia, P. Patruno, L. Pomi, A. Selvini, and S. Tibaldi, 1995: A climatological study of thunderstorm activity in the Po Valley. *Theor. Appl. Climatol.*, **50**, 185–203.

Christensen, O. B., J. H. Christensen, B. Machenhauer, and M. Botzet, 1998: Very high-resolution regional climate simulations over Scandinavia - Present climate. *J. Climate*, **11**, 3204–3229.

Cook, E. R., K. R. Briffa, and P. D. Jones, 1994: Spatial regression methods in dendroclimatology: A review and comparison of two techniques. *Int. J. Climatol.*, **14**, 379–402.

Craddock, J. M., and C. R. Flood, 1969: Eigenvectors for representing the 500 mb geopotential surface over the Northern Hemisphere. *Quart. J. Roy. Meteor. Soc.*, **99**, 576–593.

Cubasch, U., H. von Storch, J. Waszkewitz, and E. Zorita, 1996: Estimates of climate change in Southern Europe derived from dynamical model output. *Clim. Res.*, **7**, 129–149.

Dai, A., I. Y. Fung, and A. D. Del Genio, 1997: Surface observed global land precipitation variations during 1900–88. *J. Climate*, **10**, 2943–2962.

Daly, C., R. P. Neilson, and D. L. Philips, 1994: A statistical-topographic model for mapping climatological precipitation over mountainous terrain. *J. Appl. Meteorol.*, **33**, 140–158.

Easterling, D. R., and T. C. Peterson, 1995: A new method for detecting undocumented discontinuities in climatological time series. *Int. J. Climatol.*, **15**, 369–377.

Egger, J., and K. P. Hoinka, 1992: Fronts and Orography. *Meteorol. Atmos. Phys.*, **48**, 3–36.

Fliri, F., 1974: Niederschlag und Lufttemperatur im Alpenraum. *Wissensch. Alpenvereinshefte*, **24**, 110.

—, 1986: Synoptisch-klimatologische Niederschlagsanalyse zwischen Genfersee und Hohen Tauern. *Wetter Leben*, **38**, 140–149.

Folland, C. K., T. R. Karl, and et al. , 2001: Observed Climate Variability and Change. *IPCC WG I third assessment report*, 99–181.

Frei, C., H. C. Davies, J. Gurtz, and C. Schär, 2000: Climate dynamics and extreme precipitation and flood events in Central Europe. *Integrated Assessment*, **1**, 281–299.

Frei, C., and C. Schär, 1998: A precipitation climatology of the Alps from high-resolution rain-gauge observations. *Int. J. Climatol.*, **18**, 873–900.

—, 2001: Detection probability of trends in rare events: Theory and application of heavy precipitation in the Alpine region. *J. Climate*, **14**, 1568–1584.

Fritts, H. C., T. J. Blasing, B. P. Hayden, and J. E. Kutzbach, 1971: Multivariate techniques for specifying tree-growth and climate relationships and for reconstructing anomalies in palaeoclimate. *J. Appl. Meteorol.*, **10**, 845–864.

Fukutome, S., C. Frei, D. Lüthi, and C. Schär, 1997: The interannual variability as a test ground for regional climate simulations over Japan. *J. Met. Soc. Japan*, **77**, 649–672.

Gandin, L. S., R. Celnai, and V. E. Zakhariev, (Eds.) , 1976: *Statistical structure of meteorological fields*. Az Orszagos Meteorologiai Szolgalat, Budapest, 364 pp. [In Russian and Hungarian, resumes in German].

Glowienka-Hense, R., 1990: The North Atlantic Oscillation in the Atlantic-European SLP. *Tellus*, **42A**, 497–507.

Golubev, V. S., 1975: Results of the intercomparison of precipitation gages. *Transact. State Hydrolog. Instit.*, **224**, 38–46.

Grasso, L. D., 2000: The differentiation between grid spacing and resolution and their application to numerical modeling. *Bull. Amer. Meteor. Soc.*, **81**, 579–580.

Groisman, P. Y., and D. R. Legates, 1994: The accuracy of United States precipitation data. *Bull. Amer. Meteor. Soc.*, **75**, 215–227.

—, 1995: Documenting and detecting long-term precipitation trends: Where we are and what should be done. *Climatic Change*, **31**, 601–622.

Gutermann, T., 1974: Zur Niederschlagsmessung in der Schweiz: Aktuelle Beobachtungsnetze und grundsätzliche Messprobleme. Arbeitsber. Schweiz. Meteorol. Zentralanst. 45, MeteoSwiss, 33 pp. [Available from MeteoSwiss, Krähbühlstrasse 58, CH-8044 Zürich, Switzerland].

—, 1986: Das automatische Wetterbeobachtungsnetz der Schweiz (ANETZ). Tech. Rep., MeteoSwiss. [Available from MeteoSwiss, Krähbühlstrasse 58, CH-8044 Zürich, Switzerland].

Gyalistras, D. H., H. von Storch, A. Fischlin, and M. Beniston, 1994: Linking GCM-simulated climatic changes to ecosystem models: Case studies of statistical downscaling in the Alps. *Clim. Res.*, **4**, 167–189.

Haston, L., and J. Michaelsen, 1997: Spatial and temporal variability of Southern California precipitation over the last 400 yr and relationships to atmospheric circulation patterns. *J. Climate*, **10**, 1836–1852.

Hewitson, B. C., and R. G. Crane, 1996: Climate downscaling: Techniques and application. *Clim. Res.*, **7**, 85–95.

Houghton, J. T., L. G. M. Filho, B. A. Callander, N. Harris, A. Kattenberg, and K. Maskell, (Eds.) , 1996: *Climate Change 1996: The Science of Climate Change.* Cambridge University Press, 453 pp.

Huff, F. A., and W. L. Shipp, 1969: Spatial correlations of storms, monthly and seasonal precipitation. *J. Appl. Meteorol.*, **8**, 542–550.

Huntrieser, H. I. C., 1995: Zur Bildung, Verteilung und Vorhersage von Gewittern in der Schweiz. Ph.D. dissertation, Swiss Federal Institute of Technology (ETH), 246 pp. [Dissertation No. 11020].

Hurrell, J. W., 1995: Decadal trends in the Northern Atlantic Oscillation — Regional temperatures and precipitation. *Science*, **269**, 676–679.

—, 1996: Influence of variations in extratropical wintertime teleconnections on Northern Hemisphere temperature. *Geophys. Res. Letters*, **23**, 665–668.

—, 2000: North Atlantic Oscillation (NAO) Index — Seasonal. [Available on-line from: http://www.met.rdg.ac.uk/cag/NAO/index.html].

Hurrell, J. W., and H. van Loon, 1997: Decadal variations in climate associated with North Atlantic Oscillation. *Climatic Change*, **36**, 301–326.

Jolliffe, I. T., 1986: *Principal Component Analysis.* Springer-Verlag, 271 pp.

Jones, P. D., 1994: Hemispheric surface air temperature variations: A reanalysis and an update to 1993. *J. Climate*, **7**, 1794–1802.

Jones, P. D., and et al., 1999: Monthly mean pressure reconstructions for Europe for the 1780–1995 period. *Int. J. Climatol.*, **19**, 347–364.

Jones, P. D., and M. Hulme, 1996: Calculating regional climatic time series for temperature and precipitation: Methods and illustrations. *Int. J. Climatol.*, **16**, 361–377.

Jones, P. D., T. Jonsson, and D. Wheeler, 1997: Extension to the North Atlantic Oscillation using early instrumental pressure observations from Gibraltar and south-west Iceland. *Int. J. Climatol.*, **17**, 1433–1450.

Jones, R. G., J. M. Murphy, and M. Noguer, 1995: Simulation of climate change over Europe using a nested regional climate model. I: Assessment of control climate, including sensitivity to location of lateral boundaries. *Quart. J. Roy. Meteor. Soc.*, **123**, 265–292.

Jungo, P., and M. Beniston, 2001: Changes in the anomalies of extreme temperature anomalies in the 20th century at Swiss climatological stations located at different latitudes and altitudes. *Theor. Appl. Climatol.*, **69**, 1–12.

Kaplan, A., M. A. Cane, , Y. Kushnir, A. C. Clement, M. B. Blumenthal, and B. Rajagopalan, 1998: Analyses of global sea surface temperature 1856–1991. *J. Geophys. Res.*, **103**, 18 567–18 589.

Kaplan, A., Y. Kushnir, M. A. Cane, and M. B. Blumenthal, 1997: Reduced space optimal analysis for historical data sets: 136 years of Atlantic sea surface temperatures. *J. Geophys. Res.*, **102**, 27 835–27 860.

Kirchhofer, W., 1993: Mapping of corrected mean annual precipitation amount with respect to orography. *Analysis methods of precipitation on a global scale, GEWEX Workshop Koblenz*, Germany, WMO, WCRP-81, A87.

Legates, D. R., 1987: A climatology of global precipitation. *Publ. Climatol.*, **40**, 84.

Lüthi, D., A. Cress, H. C. Davies, C. Frei, and C. Schär, 1996: Interannual variability and regional climate simulations. *Theor. Appl. Climatol.*, **53**, 185–209.

Mann, M. E., R. S. Bradley, and M. K. Hughes, 1998: Global-scale temperature patterns and climate forcing over the past six centuries. *Nature*, **392**, 779–787.

Matheron, G., 1971: The theory of regionalised variables and its applications. *Cahiers du Centre de Morphologie Mathematiques*, Ecoles des Mines, Fountainebleau, 211.

McGregor, J. L., 1997: Regional climate modelling. *Meteorol. Atmos. Phys.*, **63**, 105–117.

Mearns, L. O., I. Bogardi, F. Giorgi, I. Matyasovszky, and M. Palecki, 1999: Comparison of climate change scenarios generated from regional climate model experiments and statistical downscaling. *J. Geophys. Res-Atmos.*, **104**, 6603–6621.

Mladek, R., J. Barckicke, P. Binder, P. Bougeault, N. Brzovic, C. Frei, J. F. Geleyn, J. Hoffmann, W. Ott, T. Paccagnella, P. Patruno, P. Pottier, and A. Rossa, 2000: Intercomparison and evaluation of precipitation forecasts for MAP seasons 1995 and 1996. *Meteorol. Atmos. Phys.*, **72**, 111–129.

Müller, G., and J. Joss, 1985: Messnetze und Instrumente. *Der Niederschlag in der Schweiz, Beitr. Z. Geol. Schweiz–Hydrologie*, No. 31, 17–47.

Murphy, A. H., and E. S. Epstein, 1989: Skill scores and correlation coefficients in model verification. *Mon. Wea. Rev.*, **117**, 572–581.

Murphy, J., 1999: An evaluation of statistical and dynamical techniques for downscaling local climate. *J. Climate*, **12**, 2256–2284.

Nespor, V., and B. Sevruk, 1999: Estimation of wind-induced error of rainfall gauge measurements using a numerical simulation. *J. Atmos. Oceanic Technol.*, **16**, 450–464.

New, M., M. Hulme, and P. Jones, 1999: Representing twentieth-century space-time climate variability. Part I: Development of a 1961–90 mean monthly terrestrial climatology. *J. Climate*, **12**, 829–856.

—, 2000: Representing twentieth-century space-time climate variability. Part II: Development of 1901–96 monthly grids of terrestrial surface climate. *J. Climate*, **13**, 2217–2238.

North, G. R., T. L. Bell, and R. F. Cahalan, 1982: Sampling errors in the estimation of empirical orthogonal functions. *Mon. Wea. Rev.*, **110**, 699–706.

O'Lenic, E. A., and R. E. Livezey, 1988: Practical considerations in the use of rotated principal component analysis (RPCA) in diagnostic studies of upper-air height fields. *Mon. Wea. Rev.*, **116**, 1682–1689.

Peterson, T. C., and et al., 1998: Homogeneity adjustments of in situ atmospheric climate data: A review. *Int. J. Climatol.*, **18**, 1493–1517.

Preisendorfer, R. W., 1988: *Principal Component Analysis in Meteorology and Oceanography*. Elsevier, 425 pp.

Quadrelli, R., Y. Pavan, and F. Molteni, 2001: Wintertime variability of Mediterranean precipitation and its links with large-scale circulation anomalies. *Clim. Dyn.*, **17**, 457–466.

Richman, M. B., 1986: Rotation of principal components. *J. Climatol.*, **6**, 29–35.

Richman, M. B., and P. J. Lamb, 1987: Pattern analysis of growing season precipitation in southern Canada. *Atmos.-Ocean*, **25**, 137–158.

Rogers, J. C., 1984: The association between the North Atlantic ocean and the Southern Oscillation in the northern hemisphere. *Mon. Wea. Rev.*, **112**, 1999–2015.

—, 1997: North Atlantic storm track variability and its association to the North Atlantic Oscillation and climate variability of northern Europe. *J. Climate*, **10**, 1635–1647.

Schär, C., T. D. Davies, C. Frei, H. Wanner, M. Widmann, M. Wild, and H. C. Davies, 1998: Current Alpine Climate. *A view from the Alps: Regional perspectives on climate change*, P. Cebon and et al., Eds., MIT Press, 21–72.

Schmidli, J., C. Frei, and C. Schär, 2001: Reconstruction of mesoscale precipitation fields from sparse observations in complex terrain. *J. Climate*, **14**, 3289–3306.

Schmidli, J., C. Schmutz, C. Frei, H. Wanner, and C. Schär, 2002: Mesoscale precipitation variability in the region of the European Alps during the 20th century. *Int. J. Climatol.*, **22**, 1049–1074.

Schmutz, C., 2001: A quality tested precipitation data base of monthly Alpine long-term (1901–1995) precipitation time series. *Theor. Appl. Climatol.*. [Submitted].

Schneidereit, M., and C. Schär, 2000: Idealised numerical experiments of Alpine flow regimes and southside precipitation events. *Meteorol. Atmos. Phys.*, **72**, 233–250.

Schönwiese, C.-D., and J. Rapp, 1997: *Climate trend atlas of Europe. Based on observations 1891–1990*. Kluwer Academic Publishers, 228 pp.

Schönwiese, C.-D., J. Rapp, T. Fuchs, and M. Denhard, 1994: Observed climate trends in Europe 1891–1990. *Meteorol. Z.*, **N. F. 3**, 22–28.

Schwarb, M., 2000: The Alpine precipitation climate: Evaluation of a high-resolution analysis scheme using comprehensive rain-gauge data. Ph.D. dissertation, Swiss Federal Institute of Technology (ETH). [Dissertation No. 13911].

Schwarb, M., C. Daly, C. Frei, and C. Schär, 2001: Mean annual and seasonal precipitation in the European Alps 1971–90. *Hydrological Atlas of Switzerland*, Landeshydrologie und Geologie, Bern, Switzerland, Plates 2.6 and 2.7.

Sevruk, B., 1985: Correction of precipitation measurements, summary report. *Proc., ETH/IAHS/WMO Workshop on the correction of precipitation data*, 13–23.

Shen, S. S., G. R. North, and K. Y. Kim, 1994: Spectral approach to optimal estimation of the global average temperature. *J. Climate*, **7**, 1999–2007.

Shen, S. S., T. M. Smith, C. F. Ropelewski, and R. E. Livezey, 1998: An optimal regional averaging method with error estimates and a test using tropical Pacific SST data. *J. Climate*, **11**, 2340–2350.

Shepard, D. S., 1984: Computer mapping: the SYMAP interpolation algorithm. *Spatial Statistics and Models*, G. L. Gaile and C. J. Willmott, Eds., D. Reidl Publishing, Dordrecht, 133–145.

SMI (Eds.), 1996: Klima90 Schlussbericht. Tech. Rep., MeteoSwiss. [Available from MeteoSwiss, Krähbühlstrasse 58, CH-8044 Zürich, Switzerland].

Smith, R. B., 1979: The influence of mountains on the atmosphere. *Adv. Geophys.*, **21**, 87–230.

Smith, T. M., R. E. Livezey, and S. S. Shen, 1998: An improved method for analyzing sparse and irregularly distributed SST data on a regular grid: The tropical Pacific ocean. *J. Climate*, **11**, 1717–1729.

Smith, T. M., R. W. Reynolds, R. E. Livezey, and D. C. Stokes, 1996: Reconstruction of historical sea surface temperatures using Empirical Orthogonal Functions. *J. Climate*, **9**, 1403–1420.

Stefanicki, G., P. Talkner, and R. O. Weber, 1998: Frequency changes of weather types in the Alpine region since 1945. *Theor. Appl. Climatol.*, **60**, 47–61.

Stocker, T. F., and et al. , 2001: Physical climate processes and feedbacks. *IPCC WG I third assessment report*. [417–470].

Tibaldi, S., A. Buzzi, and A. Speranza, 1990: Orographic cyclogenesis. *Extratropical cyclones: The Eric Palmen memorial volume*, C. W. Newton and E. O. Holopainen, Eds., Amer. Meteor. Soc., Boston, 107–127.

Trenberth, K. E., 1998: Atmospheric moisture residence times and cycling: Implications for rainfall rates and climate change. *Climatic Change*, **39**, 667–694.

—, 1999: Conceptual framework for changes of extemes of the hydrological cycle with climate change. *Climatic Change*, **42**, 327–339.

von Storch, H., 1995: Spatial patterns: EOFs and CCA. *Analysis of Climate Variability*, H. von Storch and A. Navarra, Eds., Springer, 227–257.

von Storch, H., and F. W. Zwiers, 1999: *Statistical Analysis in Climate Research*. Cambridge University Press, 513 pp.

Wanner, H., S. Brönnimann, C. Casty, D. Gyalistras, J. Luterbacher, C. Schmutz, D. B. Stephenson, and E. Xoplaki, 2001: North Atlantic Oscillation - Concepts and studies. *Surveys of Geophysics*. [Submitted].

Wanner, H., R. Rickli, E. Salvisberg, C. Schmutz, and M. Schüepp, 1997: Global climate change and variability and its influence on Alpine climate — Concepts and observations. *Theor. Appl. Climatol.*, **58**, 221–243.

Widmann, M. L., 1996: Mesoscale variability and long-term trends of Alpine precipitation and their relation to the synoptic-scale flow. Ph.D. dissertation, Swiss Federal Institute of Technology (ETH), 185 pp. [Dissertation No. 11769].

Widmann, M. L., and C. S. Bretherton, 2000: Validation of mesoscale precipitation in the NCEP reanalysis using a new gridcell dataset for the northwestern United States. *J. Climate*, **13**, 1936–1950.

Widmann, M. L., and C. Schär, 1997: A principal component and long-term trend analysis of daily precipitation in Switzerland. *Int. J. Climatol.*, **17**, 1333–1356.

Wilby, R. L., T. M. L. Wigley, D. Conway, P. D. Jones, B. C. Hewitson, J. Main, and D. S. Wilks, 1998: Statistical downscaling of general circulation model output: A comparison of methods. *Water Resour. Res.*, **34**, 2995–3008.

Willmott, C. J., C. M. Rowe, and W. D. Philpot, 1985: Small-scale climate maps: A sensitivity analysis of some common assumptions associated with grid-point interpolation and contouring. *Am. Cartogr.*, **12**, 5–16.

Xie, P., B. Rudolf, U. Schneider, and P. A. Arkin, 1996: Gauge-based monthly analysis of global land precipitation from 1971 to 1994. *J. Geophys. Res.*, **101**, 19 023–19 034.

Zorita, E., and H. von Storch, 1999: The analog method as a simple statistical downscaling technique: Comparison with more complicated methods. *J. Climate*, **12**, 2474–2489.

Curriculum Vitae

Jürg Schmidli, Allenmoosstr. 56, 8057 Zürich
born on 13 December 1971 in Zürich
citizen of Zürich and Dottikon (AG)

EDUCATION AND PROFESSIONAL TRAINING

1997–2000	Scientific collaborator and Ph. D. student in the group of Prof. C. Schär, at the Institue for Climate Research, ETH Zürich, and at the Institute for Atmospheric Physics, ETH Zürich
1991–1997	University study of environmental sciences at the Swiss Federal Institute of Technology (ETH) Zürich. Specialization in the field of atmospheric physics. Diploma thesis "The Effect of Barotropic Shear on Cyclones, Fronts, and Tropopause Structures — Numerical Simulations with a Primitive Equation Model" under the guidance of Prof. H. C. Davies and Dr. H. Wernli *Dipl. Natw. ETH*
1986–1990	Kantonsschule Zürich Oerlikon *Matura Type C*

INTERNATIONAL CONFERENCES AND WORKSHOPS
Workshop on Regional Numerical Weather Prediction, Deutscher Wetterdienst, Langen 2000; EGS General Assembly, Nice 2000; MAP Meeting, Appenzell 1999; Workshop on Computational Sciences and Engineering, Monte Verità, Ascona 1999; ACCORD (Atmospheric Circulation Classification and Regional Downscaling) meeting, Bologna 1999; SANW meeting, Special Symposium on MAP, Airolo 1998.